

Research

Internal dosimetry of radionuclides that can be released during an accident at the European Spallation Source (ESS)

2022:10

Author: Håkan Pettersson, Alexandr Malusek, Marie Karlsson
Linköpings universitet, Linköping
Report number: 2022:10
ISSN: 2000-0456
Available at: www.ssm.se

SSM perspective

Background

To strengthen the material science research in Europe, the European Spallation Source (ESS) is being built in Lund in the southern part of Sweden. In the spallation process, neutrons are generated when the accelerated protons hit the tungsten target. In addition, a broad range of radioactive by-products is produced that differs from the fission products produced in a nuclear reactor. In case of an accident scenario target material particles could be released to the atmosphere and contaminate the surroundings. From earlier studies, the alpha-emitting radionuclide ^{148}Gd (Gadolinium-148) has been found to be a major contributor to the total radiation dose at an ESS accident. Therefore, there is a need to enhance the knowledge about how to assess internal dose from radionuclides such as gadolinium in the presence of a mixture of other nuclides. The Swedish Radiation Safety Authority has found development of a method to determine the Committed Effective Dose (CED) resulting from inhalation of radionuclides that can be released during an accident at ESS of great importance to support.

Results

The method combines results from gamma spectrometry measurements using a whole-body counting (WBC) system and an analysis of bioassays. An automated method for calculating the minimum detectable activity was developed and results for the WBC system and a laboratory detector system were presented. The results showed that lung burden could be evaluated for a majority of the most prominent radionuclides in a release at CEDs around 1 mSv¹ and above. Furthermore, the results showed that the levels of radionuclide excretion in urine are low for most radionuclides and will not be quantitative for CEDs around 1 mSv.

In addition, the authors demonstrated that peaks of ^{146}Gd , ^{153}Gd and ^{146}Eu (Europium-146) are well shaped and could be used for the determination of the activity of these radionuclides in lungs. The activity of ^{148}Gd in the lungs could then be determined from fractions between activities of these radionuclides.

Relevance

The results of this project has generated some important conclusions regarding assessing internal dose after an accident at ESS:

- The WBC systems are essential for evaluating lung burden and CED evaluations at moderate exposures (1 mSv).
- The urine analysis has a limited value at moderate exposures and can complement lung burden measurements only at higher exposures (20 mSv²).

¹ 1 mSv is the size order of the allowed maximal annual effective dose to public

² 20 mSv is the size order of the allowed maximal annual effective dose to workers

- The method developed is designed for the WBC system at Westinghouse Electric AB in Västerås but can easily be modified for other radionuclide mixtures and WBC lung burden systems if the detector counting efficiencies are known.

Moreover, development of methods like this will help the assessment of internal dose from a potential accident at the ESS and therefore is an important piece of information related to the emergency preparedness around the ESS facility in Lund.

Need for further research

Today, the measuring techniques focuses on dominant fission products in the context of dose contribution such as radionuclides from iodine and cesium seen in large-scale accidents as Chernobyl and Fukushima Daiichi. While validated measurement techniques for determination of dominating radionuclides like gadolinium, tungsten and hafnium from an accident at ESS is missing. Future research should strive to fill those gaps to achieve more reliable dose assessments. The authors highlight the need of improvement of the estimation of the size-related attenuation by the person in WBC measurements. The authors also mention the need to further developing a separation method to radiochemically isolate gadolinium in different sample matrices for subsequent alpha spectrometric measurement.

Project information

Contact person SSM: Peter Frisk

Reference: SSM2019-4725/7030295-00



**Strål
säkerhets
myndigheten**

Swedish Radiation Safety Authority

Authors: Håkan Pettersson, Alexandr Malusek, Marie Karlsson
Linköpings universitet, Linköping

2022:10

Internal dosimetry of radionuclides
that can be released during an
accident at the European Spallation
Source (ESS)

Date: August 2022

Report number: 2022:10 ISSN: 2000-0456

Available at www.stralsakerhetemyndigheten.se

This report concerns a study which has been conducted for the Swedish Radiation Safety Authority, SSM. The conclusions and viewpoints presented in the report are those of the author/authors and do not necessarily coincide with those of the SSM.

Summary

Accidental aerial releases of radionuclides from the ESS facility may, if unmitigated, expose the public and workers to significant radiation doses, both from inhalation and from ground deposition of radionuclides. Such a release might contain a large and complex mixture of radionuclides, of which many are of exotic nature, i.e., are not studied in exposure and dosimetric situations, thus creating an analytical challenge for the dose assessment. The work presented here describes a method to calculate synthetic HPGe gamma spectra of (i) expected lung burden as a result of inhalation based on an existing HPGe whole-body counting (WBC) system and (ii) expected radionuclide excretion in the urine based on a laboratory HPGe counting system. The lung burden, i.e., the amount of radionuclides inhaled, is based on predicted radionuclide release mixtures and biokinetic calculations of radionuclide deposition in the lung followed by absorption, transport, dissolution, and further uptake to the systemic circulation and final excretion.

The results of the simulated WBC lung burden measurements confirm the expected complexity of the spectra composition, especially at counting periods close to the exposure event. However, spectra evaluation of the gamma peaks of the most prominent radionuclides regarding Committed Effective Dose (CED) shows great possibilities for quantification of the lung content of these radionuclides for measurements performed days to several weeks after inhalation intake, for CED levels down to about 1 mSv. Quantification also includes the Gd-isotopes ^{146}Gd and ^{153}Gd , which opens for evaluation of the lung burden of the α -emitter ^{148}Gd , which is a major contributor to the total radiation dose (CED).

The results of the simulated HPGe measurements of urine samples show that the levels of radionuclide excretion in urine are rather low for most of the radionuclides of interest, and therefore excretion analysis may not contribute to dose evaluations except for major exposures, CEDs of tens of mSv. Therefore, WBC systems are essential for evaluating lung burden and CED evaluations in this exposure context.

Sammanfattning

I händelse av allvarliga olyckor vid ESS anläggning kan omfattande luftburna utsläpp av radionuklidor ske, vilket kan exponera allmänheten och arbetare till betydande stråldoser, både från inhalation och från markdeponerad aktivitet. Ett sådant utsläpp kan innehålla en stor och komplex mix av radionuklidor, av vilka många är av exotisk natur, dvs. har inte tidigare studerats i exponerings- eller dosimetrisammanhang, vilket medför analytiska utmaningar för dosbestämning.

Arbetet som presenteras här beskriver en metod för beräkning av syntetiska HPGe gamma-spektra som resultat av (i) förväntad lungexponering genom inhalation baserat på ett HPGe helkroppsmätsystem (WBC) och (ii) förväntad utsöndring av radionuklidor i urin, baserat på ett HPGe laboratoriemätsystem. Lungintaget, dvs. mängden av inhalerade radionuklidor, baseras på förväntad utsläpps blandning av radionuklidor samt biokinetiska beräkningar av radionukliddeposition i lungan följt av absorption, transport, upplösning och vidare upptag genom systemisk cirkulation och utsöndring (urin, feces).

Resultatet av simulerade WBC-mätningar av lunginnehåll av radionuklidor bekräftar förväntad komplexitet i spektrumsammansättning, speciellt om mätningarna sker nära efter att exponering skett. Spektrumutvärdering av fullenergitoppar av de mest prominenta radionukliderna m a p dosinteckning (Committed Effective Dose; CED) visar på goda möjligheter till kvantifiering av lunginnehåll av dessa radionuklidor då mätningar utförs från några dagar upp till flera veckor efter intaget, för CED-nivåer ned till ca 1 mSv. Kvantifieringen inkluderar Gd-isotoperna ^{146}Gd och ^{153}Gd , vilket öppnar för evaluering av lunginnehåll av α -strålaren ^{148}Gd , vilken förväntas ge det enskilt största bidraget till totaldosen (CED).

Resultaten från simulerade HPGe-mätningar av urinprover visar att nivåerna av radionuklidaktivitet i urinutsöndring är förhållandvis låga för de flesta av de radionuklidor som är av betydelse m a p CED. Därför förväntas analys av utsöndring i urin endast kunna ge betydande information för dosutvärdering vid högre exponering, CED av storleksordning 10 mSv eller mer. Vid denna typ av olyckor är därför mätningar med WBC-system avgörande för att kunna utvärdera storlek på radionuklidintag via inhalation och för CED-bestämning.

Content

Summary.....	2
Sammanfattning.....	3
1. Background.....	6
1.1. ESS activity release scenario	6
1.2. IMBA and Taurus.....	7
2. Purpose and aims.....	7
3. Materials and Methods.....	8
3.1. Determination of committed effective dose (CED)	8
3.1.1. Acquisition of the gamma spectrum	9
3.1.2. Determination of activity in the lungs from the gamma spectrum	9
3.1.3. Determination of the intake activity from activity in the lungs	11
3.1.4. Determination of the committed effective dose from the intake activity.....	12
3.1.5. Collection of bioassays	12
3.1.6. Determination of intake activity from the bioassays	13
3.1.7. IMBA and Taurus.....	14
3.2. Simulation of gamma spectra.....	14
3.3. Calibration of the WBC system.....	19
3.3.1. Theory	19
3.3.2. Anthropomorphic phantom	20
3.3.3. Calibration sources	20
3.4. Simulation of the WBC system	20
3.4.1. CT scans.....	21
3.4.2. Monte Carlo simulations	21
3.5. Minimum detectable activity	22
3.5.1. Theory	22
3.5.2. Energy calibration of Nucleonica spectra	23
3.5.3. Energy resolution of Nucleonica spectra.....	24
3.5.4. The algorithm	24
4. Results	25
4.1. Retention of radionuclides in lungs	25
4.1.1. Bioassay calculations	25
4.2. Simulation of gamma spectra	29

4.2.1. Reduced vs. full list of radionuclides	31
4.3. Calibration of the WBC system.....	31
4.4. Simulation of the WBC system	35
4.5. Comparison of measured and simulated calibration spectra	36
4.6. Minimum detectable activity, MDA	37
4.6.1. Determination of MDA in lungs.....	38
4.6.2. Determination of MDA in urine	40
4.7. Expected lung activity vs. MDA	41
4.8. Bioassay analysis; expected daily urine excretion activity vs. MDA	42
5. Discussion.....	43
5.1. Minimum detectable activity	43
5.2. Accuracy of the CED measurement.....	43
5.3. Strategy for lung and urine measurements	43
6. Conclusions	44
7. Need for further research	45
7.1. Estimation of the size-related attenuation	45
7.2. Radiochemical method for ^{148}Gd analysis.....	46
References.....	47
8. Appendix.....	49
8.1. Decay radiation.....	49
8.1.1. Decay radiation for ^{146}Gd	49
8.1.2. Decay radiation for ^{148}Gd	50
8.1.3. Decay radiation for ^{153}Gd	50
8.2. Simulated gamma spectra.....	62
8.3. IMBA	68
8.4. CT scans.....	78
8.5. Minimum detectable activity	79
8.5.1. Urine.....	79
8.5.2. Lungs	80

1. Background

The European Spallation Source ERIC (ESS) research facility in Lund will be operating to produce slow neutrons by spallation when protons from a linear accelerator bombard a radiation target made of tungsten. The process will generate a suite of radionuclides (>900), of which most are not present in other operations in Sweden. This creates a complex analytical challenge in case of accidental releases, i.e., for measurements of samples (e.g., bioassay, filter) and dose assessments. For some of the radionuclides produced in this process that can significantly contribute to the internal dose, there are no validated methods for determination, for example, ^{148}Gd .

Internal radiation exposure can be assessed by estimating the amount of radioactive material that has entered the body. This is typically assessed by measuring the concentration of the radioactive materials in urine and/or by direct measurement of the radiation emitted by the body via a whole-body counter or calculated based on estimations of intake. The radiation dose can then be estimated by employing accepted biokinetic and dosimetry models. Though the transfer rate coefficients in ICRP models often represent the state of the art of the knowledge, they lack details in the systemic distribution for many of the “exotic” radionuclides present here and further uncertainties arise from incomplete knowledge about chemical forms of the radionuclides and in case of aerosols the sizes of dust particles to which the radionuclides are attached.

In the event of an accident or for monitoring of workers and eventually the public under normal operations, the following tasks need to be addressed to assess internal doses:

- measurement of the whole-body and lung contamination with HPGe detectors. Due to the vast number of gamma emitters present in an accidental release, whole body counting needs to utilize detectors with high energy resolution, e.g., HPGe.
- measurement of environmental samples to determine isotopic fractions, of particular importance for the determination of ^{148}Gd
- measurement of urine samples with HPGe to determine the excretion dynamics of gamma and alpha emitters
- determination of the chemical form of the nuclide compounds in the release
- for inhalation exposure, determination of activity size distribution (AMAD; Activity Median Aerosol Diameter) and its geometrical standard deviation (GSD)

The last two tasks are complex, and the parameters, which can have a large impact on the committed dose, should be assessed in advance and if feasible, confirmed with actual measurements during a release event. However, this part is not included in the proposed project.

1.1. ESS activity release scenario

Scenarios of uncontrolled major aerial releases of radionuclides at ESS have been simulated at ESS and SSM by modelling (ESS internal documents [1] [2]; SSM 2018:22 [3]). Release activities and corresponding inhalation doses to the public are given for 914 radionuclides (ESS internal documents). Of particular interest in this project are the corresponding isotopic ratios of Gd isotopes, in particular between ^{146}Gd , ^{148}Gd , and ^{153}Gd , and the dose coefficients that allow estimating the committed effective dose from the total intake activity.

During normal operations, ESS safety systems (e.g., HEPA filtration, waste treatment facilities) are designed to minimize effluents from the facility. Expected major effluents ^3H , ^{11}C , ^{13}V , ^{15}O , ^{41}Ar , ^{125}I , ^{179}Ta , and ^{181}W will be monitored on-site and are expected to give a very small contribution to the exposure of the public and workers. Therefore, it is not included for assessment in this project.

1.2. IMBA and Taurus

IMBA (Integrated Modules for Bioassay Analysis) is an internal dosimetry software that enables (i) internal dosimetry calculations based on specific oral or inhalation intakes, intakes from wounds or from the injection, (ii) estimated intakes based on bioassay measurements, and (iii) calculation of bioassay quantities from given intakes. Calculations can be made both for single and multiple intake regimes. It implements biokinetic and dosimetric models recommended by ICRP for the Reference Worker [4] (US 10 CFR 835). It allows for entering individual parameters apart from ICRP default input values.

In 2020, IMBA was superseded by the dosimetry software Taurus, implementing the latest ICRP dosimetry model data.

2. Purpose and aims

Specific goals of the project are

- Perform a detailed literature study of spallation source operations that includes accident and normal operations release scenarios, expected release compounds, dose assessment strategies, and models.
- Calculate the time-dependent synthetic HPGe gamma spectrum for the worst-case scenario of the instantaneous atmospheric release of the complete mixture of radionuclides to determine (i) which radionuclides can be quantified and (ii) detection limits for the whole-body and/or lung counting with HPGe. An operating whole-body HPGe system will serve as a model for this assessment, e.g., the system at Westinghouse Electric Sweden (WSE) in Västerås.
- Develop mathematical models (methods) to determine of intake activities from measurements (gamma spectrometry and biosamples). The models will utilize information from environmental samples and whole body and lung gamma spectroscopy. The model will incorporate existing software for biokinetic models, e.g., DCAL and IMBA.
- Develop a strategy for analyzing the HPGe body count measurement. For instance, we will answer whether collimated lung counting will suffice to estimate lung burden and intake and if repeated measurements are needed for dose assessment.

3. Materials and Methods

3.1. Determination of committed effective dose (CED)

The committed effective dose, $E(50)$, can be calculated as [5]

$$E(50) = \sum_j e_{j,\text{inh}}(50) \cdot I_{j,\text{inh}} + \sum_j e_{j,\text{ing}}(50) \cdot I_{j,\text{ing}} , \quad (1)$$

where $e_{j,\text{inh}}(50)$ and $e_{j,\text{ing}}(50)$ are the committed effective dose coefficients for activity intakes by inhalation and ingestion, respectively, of a radionuclide j , and $I_{j,\text{inh}}$ and $I_{j,\text{ing}}$ are corresponding activity intakes. The contribution to CED from ^{148}Gd is

$$E_{^{148}\text{Gd}}(50) = e_{^{148}\text{Gd},\text{inh}}(50) \cdot I_{^{148}\text{Gd,inh}} + e_{^{148}\text{Gd},\text{ing}}(50) \cdot I_{^{148}\text{Gd,ing}} . \quad (2)$$

Activity of a radionuclide j in the lungs at the time t , $A_{j,\text{lung}}(t)$, can be calculated as

$$A_{j,\text{lung}}(t) = R_{j,\text{lung}}(t) \cdot I_{j,\text{inh}} , \quad (3)$$

where $R_{j,\text{lung}}(t)$ is a corresponding retention factor.

In the proposed method, the committed effective dose coefficients $e_{j,\text{inh}}(50)$ and the retention factors $R_{j,\text{lung}}(t)$ are calculated with IMBA. The activity in the lungs $A_{j,\text{lung}}(t)$ for ^{148}Gd is measured using gamma spectroscopy. The corresponding intake by inhalation $I_{^{148}\text{Gd,inh}}$ is obtained from equation (3). Corresponding contribution to CED is obtained from equation (2).

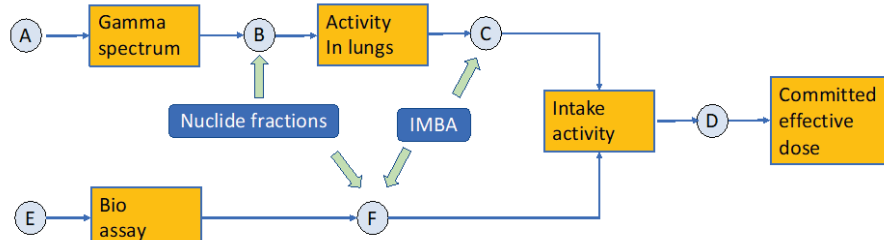


Figure 1. Workflow for the determination of the committed effective dose.

The proposed method consists of the following steps (Figure 1):

- Acquisition of the gamma spectrum
- Determination of activity in the lungs from the gamma spectrum
- Determination of the intake activity from activity in the lungs
- Determination of CED from the intake activity
- Collection of bioassays
- Determination of intake activity from the bioassays

Sections 3.1.1 – 3.1.7 describe these steps in more detail.

3.1.1. Acquisition of the gamma spectrum

The gamma spectrum is acquired for a whole-body counting system, see Figure 2(a). The detector system consists of three HPGe Ortec ACTINIDE-85 detectors optimized for lung burden measurements. Each detector has a height of 30 mm and a diameter of 85 mm, see Table 1. The detector endcap is made of an ultra-low background, high-strength carbon fibre composite, which provides greater than 85% transmission for photon energy above 15 keV and nearly 100% transmission for photon energy above 20 keV.

Table 1. Specifications of the detector. FWHM = Full Width at Half Maximum; FW0.1M = Full Width at One-tenth Maximum; FW.02M = Full Width at One-Fiftieth Maximum; total system resolution for a source at 1000 counts per second measured in accordance with ANSI/IEEE Std. 325-1996, using ORTEC standard electronics. P:C = peak to Compton ratio.

Model	Crystal Dimensions ¹		Energy Resolution (FWHM) ^{2,3}			Peak Shape ²			Nominal Relative Efficiency %	Endcap Diameter mm
	Diameter Nominal	Length Minimum (eV)	5.9 keV Warranted (eV)	@122 keV Warranted (eV)	@1.33 MeV Warranted (keV)	FW.1M/ FWHM Typical	FW.02M/ FWHM Typical	P:C Warranted		
ACT85	85	30	500	700	1.90	2.00	2.90	55	50	108

An example of a spectrum is shown in Figure 2(b).

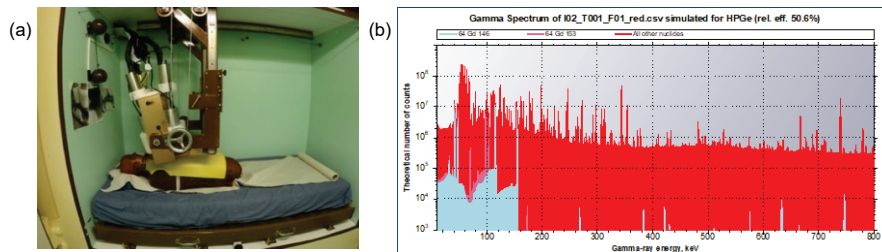


Figure 2. (a) Whole-body counting system for the measurement of radionuclide activity in the lungs. (b) Simulated gamma spectrum.

3.1.2. Determination of activity in the lungs from the gamma spectrum

The activity of the radionuclide is calculated as

$$A = \frac{\dot{N}_{\text{net}}}{\varepsilon(E, h)f}, \quad (4)$$

where \dot{N}_{net} is the net count rate in the peak of full absorption, f is the energy line intensity, $\varepsilon(E, h)$ is the full energy absorption detector efficiency, which depends on the photon energy E and the extra attenuation by the person characterized by the parameter h . In this work, we propose a simple method for the estimation of h , see below. A more elaborate method is described in section 7.1.

Consider an experimental setup in Figure 3 consisting of a point source, an absorbing layer, and a detector with spectrometric properties. In case (a), only the default layer is present. In case (b), an additional layer with a thickness of h is added to the default layer. Consider a radionuclide with two peaks, whose net areas are $N^*(E_1)$ and $N^*(E_2)$ in the calibration setup and $N(E_1)$ and $N(E_2)$ in the measurement setup;

E_1 and E_2 are corresponding photon energies. Consider an exponential attenuation only. Then

$$N(E_1) = N^*(E_1)e^{-\mu(E_1)h} \quad (5)$$

$$N(E_2) = N^*(E_2)e^{-\mu(E_2)h} , \quad (6)$$

where $\mu(E)$ is the energy-dependent linear attenuation coefficient of the additional absorbing layer. By dividing equation (6) by equation (5) we get

$$\frac{N(E_2)}{N(E_1)} = \frac{N^*(E_2)}{N^*(E_1)} e^{-[\mu(E_2)-\mu(E_1)]h} , \quad (7)$$

which can be written as

$$-\ln \left[\frac{N(E_2)}{N(E_1)} \frac{N^*(E_1)}{N^*(E_2)} \right] = [\mu(E_2) - \mu(E_1)]h , \quad (8)$$

Equation (8) can be solved for h .



Figure 3. Schematic view of an experimental setup consisting of a point source, an absorbing layer, and a detector. (a) Calibration configuration. (b) Measurement configuration. An additional layer with the thickness of h is added to the calibration configuration.

In practice, the second ratio on the left side can be determined from the energy calibration, see section 3.3. Let $\varepsilon(E_i)$ be the full energy absorption detector efficiency (equation (20)). Then

$$N^*(E_1) = \varepsilon(E_1)f_1A \quad (9)$$

$$N^*(E_2) = \varepsilon(E_2)f_2A \quad (10)$$

and the ratio is

$$\frac{N^*(E_1)}{N^*(E_2)} = \frac{\varepsilon(E_1)f_1A}{\varepsilon(E_2)f_2A} = \frac{\varepsilon(E_1)}{\varepsilon(E_2)} \frac{f_1}{f_2} . \quad (11)$$

Equation (8) can be written as

$$h = \frac{-1}{\mu(E_2)-\mu(E_1)} \ln \left[\frac{N(E_2)}{N(E_1)} \frac{\varepsilon(E_1)}{\varepsilon(E_2)} \frac{f_1}{f_2} \right] . \quad (12)$$

3.1.3. Determination of the intake activity from activity in the lungs

As discussed in section 3.2, the activity of a radionuclide X_i in the lungs at the time t can be calculated as

$$A_{X_i}(t) = A_{X_i}(0) \sum_j f_{(X_i,j)} R_{(X_i,j)}(t) , \quad (13)$$

where $R_{(X_i,j)}(t)$ is the retention fraction calculated with IMBA, and $f_{(X_i,j)}$ is the fraction of the chemical form j . In the case of a measurement of a contaminated person, activity $A_{X_i}(t)$ in the lungs is determined in the previous step (section 3.1.2), and the activity intake $A_{X_i}(0)$ is then calculated as

$$A_{X_i}(0) = \frac{A_{X_i}(t)}{\sum_j f_{(X_i,j)} R_{(X_i,j)}(t)} . \quad (14)$$

AMAD

If the Activity Median Aerosol Diameter, AMAD, of the particles is not known, ICRP publication 66 [6] recommends using the AMAD of $5\text{ }\mu\text{m}$ for workplace exposure and $1\text{ }\mu\text{m}$ for indoor or outdoor exposure of the public. We used the AMAD of $1\text{ }\mu\text{m}$ for all nuclides in the IMBA calculations and geometric standard deviation $\sigma_g = 2.47$ (SSM 2018)[3].

Parameters, Absorption type & Chemical compounds of the nuclide

The values of the absorption parameter f_1 , s_r , s_s , f_b , s_b , and f_A , were retrieved from ICRP publications. The lanthanide parameters were published in ICRP 141 [7], iodine parameters in ICRP 137 [8], and cobalt and yttrium in ICRP 134 [9]. The remaining nuclide parameters were retrieved from ICRP 119 [10] (f_1) and ICRP 130 [11] (s_r , s_s , f_b , s_b , and f_A), and the chemical compound from ICRPs supporting guidance 3 [12].

Regarding parameters for the particles transport, GI tract model, and bioassay model, the IMBA and Taurus default values were used.

The ICRP uses four absorption types according to rates of absorption into the blood from the respiratory tract; F (fast rate, with almost instantaneous absorption (gases and vapours)), M (medium/intermediate absorption rate), S (slow absorption rate, i.e., for deposited material that are relatively insoluble in the respiratory tract) and V (Vapour) for reactive gases, where immediate 100% absorption to blood is assumed. However, IMBA/Taurus does not include alternative type V. Depending on the chemical form, some elements/nuclides have more than one absorption type. Therefore, if the chemical compound of the nuclide is not established, calculations of more than one absorption type need to be done. For lanthanoids, ICRP recommends using type M if the chemical compound is unspecified.

Table 2. This table shows the parameters that were used for the calculations in IMBA and Taurus respectively. The parameters were taken from different ICRP publications (see the color code under the columns “ICRP”). The table shows data for the more prominent nuclides of the release regarding CED. AMAD=1 µm, GSD=2,474 was used.

Radio-nuclide							fraction dissolved				Model used	ICRP-del		
	Absorption type			fraction	$F_A=f_r \cdot f_1$	f_r	rapid rate	compounds	s_s/dag					
	F	M	S											
¹⁴⁸ Gd		M		0.0005	0.0001	0.2	1	oxides	0.005	Taurus	141			
¹⁸² Ta			S	0.001	0.00001	0.01	3	oxides	0.0001	IMBA	130	guide 3		
¹⁸⁷ W	F			0.3	0.3	1	30	all compounds	-	IMBA	130	guide 3		
¹⁷² Hf		M		0.002	0.0004	0.2	3	oxides	0.005	IMBA	130	guide 3		
¹⁸⁵ W	F			0.3	0.3	1	30	all compounds	-	IMBA	130	guide 3		
¹⁸¹ W	F			0.3	0.3	1	30	all compounds	-	IMBA	130	guide 3		
¹⁷⁵ Hf		M		0.002	0.0004	0.2	3	oxides	0.005	IMBA	130	guide 3		
¹²⁵ I	F			1	1,0	1	100	methyl/ethyl I		Taurus	137			
¹⁷³ Lu		M		0.0005	0.0001	0.2	1	unspecified	0.005	Taurus	141			
¹⁷⁹ Ta			S	0.001	0.00001	0,01	3	oxides	0.0001	IMBA	130	guide 3		
¹⁶⁹ Yb		M		0.0005	0.0001	0,2	1	unspecified	0,005	Taurus	141			
¹⁸³ Ta		S		0.001	0.00001	0,01	3	oxides	0.0001	IMBA	130	guide 3		

All of the 49 radionuclides from the list from report [3], except ¹²²I, were included in the Taurus/IMBA-calculation.

3.1.4. Determination of the committed effective dose from the intake activity

Estimates of CED can be made when the data on the radionuclide inhalation intake are evaluated, based on WBC-lung analyses and IMBA/Taurus calculations. However, in order to estimate CED for the complete set of radionuclides released/inhaled, assumptions have to be made since not all radionuclides will be detected by WBC-lung analyses, i.e., pure α- and β-emitters or γ-emitters with low γ-energies. WBC analyses, bioassay analyses and analyses of environmental samples (e.g. air filters), will together, depending on concentrations, supply data to either support the nuclide vectors used in the release models [2], [3] or suggest significant deviation from these. If the former applies the CED can readily be estimated from the WBC-lung data and IMBA/Taurus calculations, including radionuclides having no gamma emissions. If the latter applies laborious work is needed to reconstruct the release radionuclide vectors, presumably based on analysis of air filter samples.

Since the alpha emitter ¹⁴⁸Gd is expected to give the single highest contribution to the inhalation dose, radiochemical analyses are needed to verify the Gd isotope activity ratios. It is expected that environmental samples, e.g., air filters and wet fallout will be analysed but also analyses of urine samples of exposed individuals will be made.

3.1.5. Collection of bioassays

Normally 24 h urine sampling is preferred since the concentration of radionuclides in urine for an individual may vary during the day. If 24 h urine sampling cannot be provided, the daily excretion of the activity needs to be based on spot samples. This can be done by converting spot sample data by using the creatinine method.

Creatinine method

Creatinine is produced in the muscles and released at a fairly constant rate by the body.

$$Q_{RN,I} = F_{urine,RN,24h} * \left(\frac{KRE_{24h}}{Kre_I} \right) * \text{CONC}_{urine,RN,I}, \quad (15)$$

where $F_{urine,RN,24h}$ is the fraction between 24 h excretion and whole body or specific organ content for radionuclide RN, KRE_{24h} is the standard value for daily excretion of creatinine [mmol d⁻¹], Kre_I is the amount of creatinine that is in the urine sample [mmol], and $\text{CONC}_{urine,RN,I}$ is the concentration of the radionuclide in the spot sample.

3.1.6. Determination of intake activity from the bioassays

The method for calculating the intake from bioassay analyses is described in the Appendix 8.3.

Urine samples will preferably be analysed with low background HPGe detector systems using standard methods. The alpha emitter ¹⁴⁸Gd will be analysed via radiochemical separation and alpha spectrometry [13]. A whole-body counter with HPGe detectors designed for lung measurements is best suited to measure the uptake in the lungs.

More than 900 radionuclides are expected to be produced in the ESS-target. In case of major accidents and subsequent atmospheric releases there are several radionuclides that could result in significant internal exposure to the public, e.g. (in order of significance) ¹⁴⁸Gd, ¹⁸⁷W, ¹⁷²Hf, ¹⁸²Ta, ¹⁸⁵W, ¹⁷⁸ⁿHf, ¹⁸³Ta, ¹⁷³Lu. Of particular interest for the dose assessment is knowledge about ¹⁴⁸Gd, since this radionuclide is a pure alpha emitter, with a long physical half-life (71.1 y) and released in significant quantities. The ESS estimate in their assessment that from a major target meltdown and unmitigated release about 53% of the inhalation dose to representative person of the public will arrive from ¹⁴⁸Gd (ESS 2016 [2]). In order to quantify the lung intake of ¹⁴⁸Gd by WBC the gamma emitting Gd isotopes ¹⁴⁶Gd and ¹⁵³Gd together with the ¹⁴⁶Gd daughter ¹⁴⁶Eu will be used. However, the activity ratios of the Gd-isotopes in a major release are not known in detail. Assessment made by ESS (ESS 2016 [2]) show the following activity ratios; ¹⁴⁸Gd/¹⁴⁶Gd: 0.036, ¹⁴⁸Gd/¹⁵³Gd: 0.044, whereas MC-simulations made by Barkauskas et al. [14], show an ¹⁴⁸Gd/¹⁵³Gd activity ratio of 0.53. The estimates are made for inventories after maximum target use, 5 years. SSM 2018:22 [3] base their estimates on the same activity ratios as the ESS-estimates (see Table 3.). In our work we base our evaluations on the SSM 2018 [3] report.

Table 3. Gd isotope release activities given in the SSM 2018:22 report [3]. The activities are from 0-20 min after the release.

Nuclide	Activity 0-20 min after the release. [Bq]
¹⁴⁶ Gd	9.7E+11
¹⁴⁸ Gd	3.5E+10
¹⁵³ Gd	8.1E+11

3.1.7. IMBA and Taurus

As an add-on, IMBA enables input of 8 different bioassay quantities; whole body, lung, urinary and faecal excretion, blood, thyroid, liver, and user defined. This opens for using HPGe lung and urine measurements for intake assessment.

The latest version of IMBA includes 740 radionuclides. Of the 100 most prominent radionuclides listed in the simulated accidental ESS-release, i.e., in terms of inhalation dose, 69 radionuclides are included in IMBA (^{148}Gd is included). Of the list of radionuclides used here in the IMBA- and Taurus calculations, SSM 2018:22 [3], 48 of the 49 radionuclides are included, only ^{122}I was missing. For this project our IMBA-version was updated to this latest version.

It should be noted that IMBA implements biokinetic and dosimetric models recommended by ICRP for the reference worker and methodology described in ICRP 60 [15]. Therefore, in order to comply with the latest knowledge; model adjustments and changes in model input parameters found in recent ICRP publications (e.g. ICRP 130 [11], 134 [9], 137 [8], 141 [7]) need to be applied to IMBA. Thus, instead of using the IMBA ICRP default settings, manual editing is needed. Also, for dose calculations the most recent tissue weighting factors, ICRP 103 [16], need to be entered manually. During 2020 the IMBA was superseded with the Taurus, which incorporates the latest ICRP-methodology and dosimetric data. However, the present version allows for calculations for a rather limited number of radionuclides, e.g., only 22 of the 49 radionuclides considered in this report, based on the SSM 2018:22 report [3], are included. Therefore, we decided to base our evaluation on (i) Taurus-calculations for radionuclides available in the Taurus library, and (ii) otherwise use data provided by IMBA, keeping in mind that changes in the HRTM-model regarding lung clearance and longer retention in parts of the lung may somewhat affect the retentions obtain by IMBA-calculations.

3.2. Simulation of gamma spectra

Nucleonica was used to calculate gamma-ray spectra for two activity releases:

- model 1 with 914 nuclides provided in an ESS internal document and
- model 2 with 49 nuclides provided in SSM Report 2018:22 [3]; see Table 4.

The standard web-based version of Nucleonica can calculate spectra for no more than 20 nuclides in the mixture in one run. Web-based test servers with Nucleonica can process all 914 nuclides. In this case, however, it is not possible to generate some output reports owing to large memory demands. When these output reports were needed (like in the calculation of the MDA), model 1 with 49 nuclides was used.

Table 4. Activity release model 02.

Nuclide	A (Bq)	Nuclide	A(Bq)	Nuclide	A (Bq)
¹⁰⁹ Cd	3.8e+11	¹⁶⁶ Yb	3.4e+12	¹⁷⁶ Ta	1.6e+13
¹¹⁸ Te	8.8e+11	¹⁶⁹ Yb	7.0e+12	¹⁷⁷ Ta	2.2e+13
¹²⁰ I	5.8e+11	¹⁶⁹ Lu	5.9e+12	¹⁷⁹ Ta	2.2e+13
¹²¹ I	6.9e+11	¹⁷⁰ Lu	7.8e+12	¹⁸⁰ Ta	7.2e+12
¹²² I	6.5e+11	¹⁷¹ Lu	9.3e+12	¹⁸² Ta	7.4e+12
¹²³ I	8.4e+11	¹⁷² Lu	5.2e+12	¹⁸³ Ta	1.1e+13
¹²⁴ I	1.1e+11	¹⁷³ Lu	6.7e+12	¹⁸⁴ Ta	4.0e+12
¹²⁵ I	7.5e+11	¹⁷⁰ Hf	5.8e+12	¹⁷⁷ W	1.3e+13
¹²⁶ I	2.9e+10	¹⁷² Hf	4.1e+12	¹⁷⁸ W	2.2e+13
¹³⁹ Ce	8.8e+11	¹⁷³ Hf	1.1e+13	¹⁸¹ W	8.6e+13
¹⁴⁷ Eu	1.2e+12	¹⁷⁵ Hf	1.1e+13	¹⁸⁵ W	2.6e+14
¹⁴⁶ Gd	9.7e+11	¹⁷⁸ⁿ Hf	2.5e+11	¹⁸⁷ W	6.7e+14
¹⁴⁸ Gd	3.5e+10	¹⁸¹ Hf	9.5e+11	¹⁸² Re	9.3e+11
¹⁵³ Gd	8.2e+11	¹⁷³ Ta	8.4e+12	¹⁸⁴ Re	6.8e+11
¹⁴⁹ Tb	8.1e+11	¹⁷⁴ Ta	8.9e+12	¹⁸⁶ Re	1.1e+13
¹⁶⁶ Tm	3.6e+12	¹⁷⁵ Ta	1.3e+13	¹⁸⁸ Re	8.3e+12
¹⁶⁷ Tm	4.3e+12				

Two detector configurations were simulated:

- HPGe model 3 for lung measurement (Figure 4) and
- HPGe model 2 for urine measurement (Figure 5).

In both cases, the isotropic point source-detector distance of 100 mm, and the filtration of 50 mm of polyethylene were used. For the lung measurement, the polyethylene simulated absorption of photons in the chest. For the urine measurement, it simulated self-absorption in the 1 litre of urine.

The input mixture of radionuclides in lungs or urine was obtained using the biokinetic models of IMBA as follows. A radionuclide X_i , for instance ^{60}Co , can be found in different physical and chemical forms, which may affect the dispersion of the radionuclide but more importantly the absorption/retention rate at inhalation. A specific form is denoted (X_i, j) , where $j=1,\dots,n$. Activity in lungs at time t is then calculated as

$$A_{X_i}(t) = \sum_j A_{X_i}(0)f_{(X_i,j)}R_{(X_i,j)}(t) , \quad (16)$$

where $R_{(X_i,j)}(t)$ is the retention fraction calculated with IMBA, and $f_{(X_i,j)}$ is the fraction of form j . The fractions are normalized so that $\sum_j f_{(X_i,j)} = 1$.

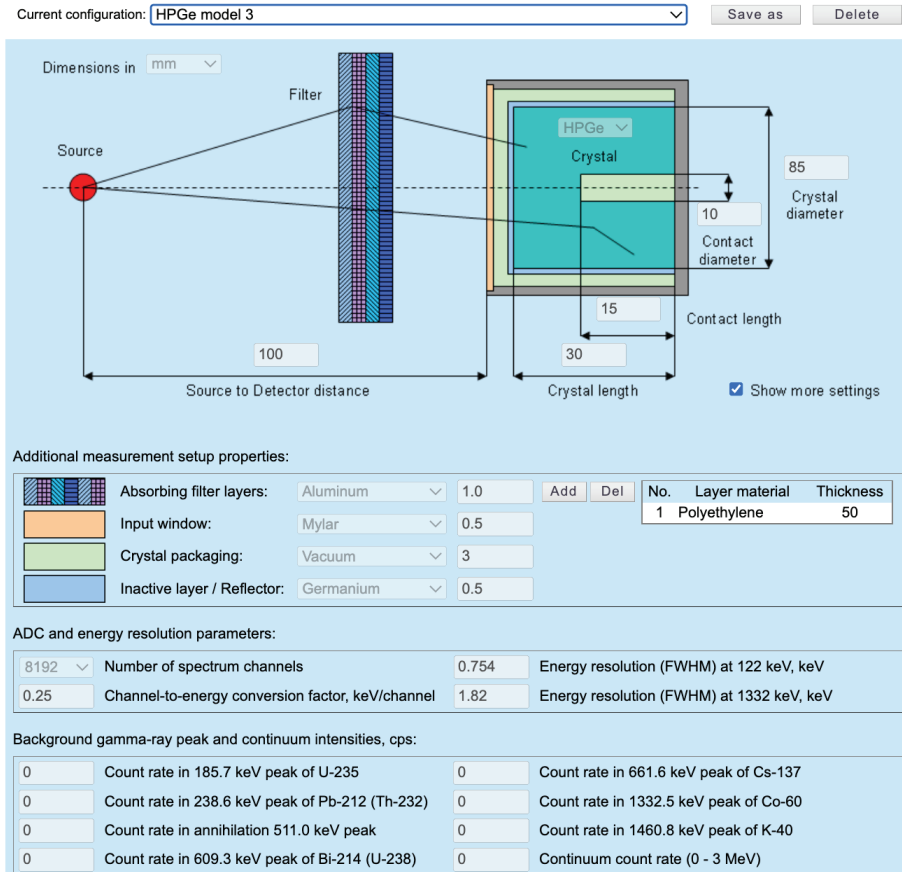


Figure 4. Simulation parameters used in Nucleonica for the lung measurements. A source-detector distance of 100 mm, crystal length of 30 mm, and crystal diameter of 85 mm were used. Energy resolution (FWHM) was set to 0.7 keV at 122 keV and 1.9 keV at 1332 keV, see Table 1. Material of the input window was set to Mylar.

This approach does not account for radionuclides created by radioactive decay in the contaminated person; the algorithm does not add them to the list of radionuclides (the “mixture” of radionuclides in Nucleonica terms) for which the gamma spectrum is simulated. While this does not seem to be a problem for most of such radionuclides, there is one exception. ^{146}Eu is the daughter product of ^{146}Gd with a half-life of 4.6 day. It means that an activity equilibrium between these two radionuclides will be reached in about two weeks. This period is most likely shorter as ^{146}Eu is expected to be present in the activity intake. In the calculations of lung burden the *in-situ* ingrowth was included.

In this work, chemical forms were denoted for instance $^{109}\text{Cd_L_F_V0}$ (see Table 5) where ^{109}Cd , L, F, and V0 stand for the radionuclide, lung, fast absorption, and version 0. Corresponding fractions $f_{(X_i,j)}$ were specified by the user in a spreadsheet shown in Table 5.

Intake activities, $A_{X_i}(0)$, were modified using equation (16) to give activities in lungs at the time t . Such a vector of activities was then used to define a mixture in Nucleonica and calculate corresponding gamma spectrum

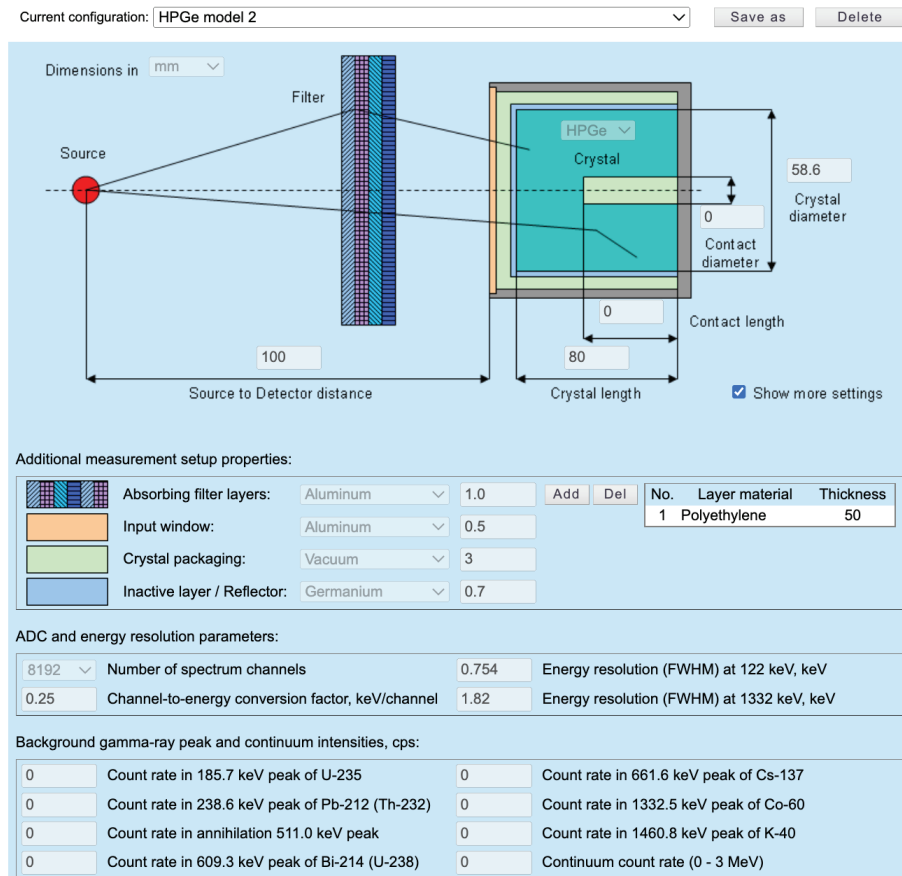


Figure 5. Simulation parameters used in Nucleonica for urine measurements. A source-detector distance of 100 mm, crystal length of 30 mm, and crystal diameter of 85 mm were used. Energy resolution (FWHM) was set to 0.7 keV at 122 keV and 1.9 keV at 1332 keV, see Table 1. Material of the input window was set to Mylar.

Table 5. Nuclide form fractions

nuclide	nuclideForm1	fr1	nuclideForm2	fr2	nuclideForm3	fr3
Cd-109	Cd-109_L_F_V0	0.4	Cd-109_L_M_V0	0.3	Cd-109_L_S_V0	0.3
Ce-139	Ce-139_L_M_V0	1.0				
Co-58	Co-58_L_M_V0	0.4	Co-58_L_S_V0	0.3	Co-58_L_S_V1	0.3
Co-60	Co-60_L_M_V0	0.4	Co-60_L_S_V0	0.3	Co-60_L_S_V1	0.3
Eu-146	Eu-146_L_M_V0	1.0				
Eu-147	Eu-147_L_M_V0	1.0				
Eu-154	Eu-154_L_M_V0	1.0				
Gd-145	Gd-145_L_M_V0	1.0				
Gd-146	Gd-146_L_M_V0	1.0				
Gd-147	Gd-147_L_M_V0	1.0				
Gd-149	Gd-149_L_M_V0	1.0				
Gd-151	Gd-151_L_M_V0	1.0				
Gd-152	Gd-152_L_M_V0	1.0				

Gd-153	Gd-153_L_M_V0	1.0				
Gd-159	Gd-159_L_M_V0	1.0				
H-3	H-3_L_F_V0	0.5	H-3_L_M_V0	0.5		
Hf-170	Hf-170_L_F_V0	0.5	Hf-170_L_M_V0	0.5		
Hf-172	Hf-172_L_F_V0	0.5	Hf-172_L_M_V0	0.5		
Hf-173	Hf-173_L_F_V0	0.5	Hf-173_L_M_V0	0.5		
Hf-175	Hf-175_L_F_V0	0.5	Hf-175_L_M_V0	0.5		
Hf-178n	Hf-178n_L_F_V0	0.5	Hf-178n_L_M_V0	0.5		
Hf-181	Hf-181_L_F_V0	0.5	Hf-181_L_M_V0	0.5		
I-120	I-120_L_F_V0	1.0				
I-121	I-121_L_F_V0	1.0				
I-123	I-123_L_F_V0	1.0				
I-124	I-124_L_F_V0	1.0				
I-125	I-125_L_F_V0	1.0				
I-126	I-126_L_F_V0	1.0				
Lu-169	Lu-169_L_M_V0	1.0				
Lu-170	Lu-170_L_M_V1	0.5	Lu-170_L_M_V0	0.5		
Lu-171	Lu-171_L_M_V0	1.0				
Lu-172	Lu-172_L_M_V0	1.0				
Lu-173	Lu-173_L_M_V0	1.0				
Mn-54	Mn-54_L_F_V0	0.5	Mn-54_L_M_V0	0.5		
Re-182	Re-182_L_F_V0	0.5	Re-182_L_M_V0	0.5		
Re-184	Re-184_L_M_V0	0.5	Re-184_L_F_V0	0.5		
Re-186	Re-186_L_F_V0	0.5	Re-186_L_M_V0	0.5		
Re-188	Re-188_L_F_V0	0.5	Re-188_L_M_V0	0.5		
Rh-102	Rh-102_L_F_V0	0.4	Rh-102_L_M_V0	0.3	Rh-102_L_S_V0	0.3
Ta-173	Ta-173_L_M_V0	0.5	Ta-173_L_S_V0	0.5		
Ta-174	Ta-174_L_M_V0	0.5	Ta-174_L_S_V0	0.5		
Ta-175	Ta-175_L_M_V0	0.5	Ta-175_L_S_V0	0.5		
Ta-176	Ta-176_L_M_V0	0.5	Ta-176_L_S_V0	0.5		
Ta-177	Ta-177_L_M_V0	0.5	Ta-177_L_S_V0	0.5		
Ta-179	Ta-179_L_M_V0	0.5	Ta-179_L_S_V0	0.5		
Ta-180	Ta-180_L_M_V0	0.5	Ta-180_L_S_V0	0.5		
Ta-182	Ta-182_L_M_V0	0.5	Ta-182_L_S_V0	0.5		
Ta-183	Ta-183_L_M_V0	0.5	Ta-183_L_S_V0	0.5		
Ta-184	Ta-184_L_M_V0	0.5	Ta-184_L_S_V0	0.5		
Tb-149	Tb-149_L_M_V0	1.0				
Tm-166	Tm-166_L_M_V0	1.0				
Tm-167	Tm-167_L_M_V0	1.0				
W-177	W-177_L_F_V0	1.0				
W-178	W-178_L_F_V0	1.0				

W-181	W-181_L_F_V0	1.0			
W-185	W-185_L_F_V0	1.0			
W-187	W-187_L_F_V0	1.0			
Y-88	Y-88_L_M_V0	0.5	Y-88_L_S_V0	0.5	
Yb-166	Yb-166_L_M_V0	1.0			
Yb-169	Yb-169_L_M_V0	1.0			

3.3. Calibration of the WBC system

3.3.1. Theory

Consider a radioactive decay leading to an emission of a photon with an energy E_i , where the probability of the emission is $f(E_i)$. For a radioactive source with the activity $A(t)$, the average number, $N_e(E_i)$, of emitted photons in the time interval (t_1, t_2) is

$$N_e(E_i) = f(E_i) \int_{t_1}^{t_2} A(t) dt . \quad (17)$$

In the case of energy calibration sources, the half-life of the nuclide is much larger than the considered time interval $\Delta t = t_2 - t_1$ and therefore equation (17) can be approximated as

$$N_e(E_i) = f(E_i)A(t)\Delta t . \quad (18)$$

The net number of detected photons (net count in a photopeak), $N_n(E_i)$ can formally be written as

$$N_n(E_i) = \frac{N_n(E_i)}{N_e(E_i)} N_e(E_i) = \varepsilon(E_i) N_e(E_i) , \quad (19)$$

where $\varepsilon(E_i)$ is full energy absorption detector efficiency. For the calibration sources, the efficiency can be estimated as

$$\varepsilon(E_i) = \frac{N_n(E_i)}{N_e(E_i)} = \frac{N_n(E_i)}{f(E_i)A(t)\Delta t} = \frac{\dot{N}_n(E_i)}{f(E_i)A(t)} , \quad (20)$$

where $\dot{N}_n(E_i) = N_n(E_i)/\Delta t$ is the net count rate.

Consider an experimental setup where the activity of the left and right lungs is measured separately. Let A_L and A_R be the activities of the left and right lungs, respectively. We assume that the activity per unit volume is a homogeneous function inside the lungs. Then the total net count is $N_n(E_i) = N_{n,L}(E_i) + N_{n,R}(E_i)$. The full energy absorption detector efficiency can then be calculated as

$$\varepsilon(E_i) = \frac{N_{n,L}(E_i) + N_{n,R}(E_i)}{f(E_i)[A_L(t)\Delta t_L + A_R(t)\Delta t_R]} , \quad (21)$$

where Δt_L and Δt_R are the acquisition times for the left and right lungs, respectively.

In the case of the measurement at the WBC with calibration sources, the acquisition times were $\Delta t_L = \Delta t_R = 1800$ s. Equation (21) was evaluated as

$$\varepsilon(E_i) = \frac{\dot{N}_{n,L}(E_i) + \dot{N}_{n,R}(E_i)}{f(E_i)[A_L(t) + A_R(t)]} , \quad (22)$$

where $\dot{N}_{n,L}(E_i)$ and $\dot{N}_{n,R}(E_i)$ are the net count rates for the left and right lungs, respectively.

3.3.2. Anthropomorphic phantom

The phantom used for WBC calibration is an anthropomorphic phantom developed by RDS (Radiology Support Devices) (<http://rsdphantoms.com/health-physics/the-fission-product-phantom/>) and provided for loan by NKS via STUK, Finland. The phantom consists of head and torso made of tissue equivalent materials, closely matching the ICRU Report No. 44 [17] standard for tissue substitutes, see Figure 6(a). However, some internal organs are hollow to allow for filling with liquid sources. The head interior is made from a human skull. The lungs are made from lung equivalent materials and provided with medial-lateral ducts in a 4 cm x 4 cm grid array, 8 mm diameter. The left lung contains 13 holes and the right lung 15 holes, the difference reflects the different size of the left and right lung, or more relevant the difference in ventilation capacity. The phantom also contains 4 chest overlay plates of different thickness, made of fat equivalent material, to calibrate for different body fat content. Two plate thicknesses were used in the calibration in addition to no plates attached.

3.3.3. Calibration sources

The calibration sources were made from a certified reference multi-gamma standard solution; Eckert & Ziegler MIX-8700. The mixed standard contains 11 radionuclides providing gamma emissions covering photon energies from 59 to 1400 keV. Aliquots of known weight were transferred from the standard solution to 15 Poly(methyl methacrylate) (PMMA) cylinders (8 mm outer diameter, 25 mm length), see Figure 6(b). The solution was evaporated in air and the cylinders then hermetically sealed. The cylinders were then used to fill the ducts of the anthropomorphic phantom.



Figure 6. (a) The disassembled anthropomorphic phantom. (b) The set of 15 cylindrical inserts containing calibration sources.

3.4. Simulation of the WBC system

An alternative to the simplified simulations via Nucleonica is a simulation using the Monte Carlo method that uses CT scans of the anthropomorphic phantom. This work had begun but the results were not available for this report. Nevertheless, the methodology and the work performed are described here.

The full energy absorption detector efficiency, which is used in equation (11) to convert net area of the peak to the activity of the radionuclide, depends on the size of the measured person. Calibrations using a physical phantom with layers of additional fat showed that the efficiency varied by a factor larger than 2. An uncertainty in this factor directly affects the uncertainty in the committed effective dose by the radionuclide mixture. A mathematical model of the whole-body counting system can address this problem. A common approach is to simulate the energy imparted to

each detector via a Monte Carlo method. In this work, we used a simulation geometry where attenuation properties of the person were represented by a voxel array derived from a CT scan. The detector system was modelled as 3 independent detectors. Such approach allows to more accurately determine, (i) the detector efficiency for a specific person, and (ii) uncertainties associated with the calculation of the activity. More information on this mathematical model is in the following sections.

3.4.1. CT scans

A Siemens SOMATOM Force scanner was used to scan the anthropomorphic phantom. A clinical-like, helical, dual-energy protocol with 80 and Sn150 kV was used. Images were reconstructed with the ADMIRE algorithm (Br44d kernel, strength 3) in the Siemens' syngo.via 5.1 software. Voxel size was $0.8203 \times 0.8203 \times 1.0$ mm³. Virtual monoenergetic images at 70 keV were obtained from the reconstructed images using the Monoenergetic Plus (version VB30) application profile of the Siemens' CT Dual Energy software.

3.4.2. Monte Carlo simulations

DICOM images were saved in Analyze 5 format, re-binned from the 512×512 resolution to 128×128 resolution and segmented using ImageJ. Energy imparted to each detector was simulated using the penEasy code. Model of the detector system consisting of detector probes, metallic collimator, and plastic shielding is plotted in Figure 7.

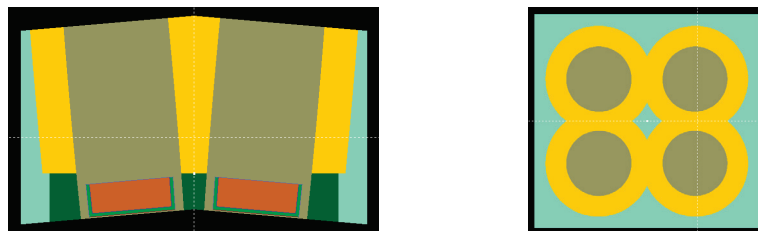


Figure 7. Cross sectional views of the WBC detector system visualised via the gview.exe code. The detector probes are plotted in brown colour. Only three detector probes were positioned in the collimator system.

A 3D view of the same detector system is plotted in Figure 8.

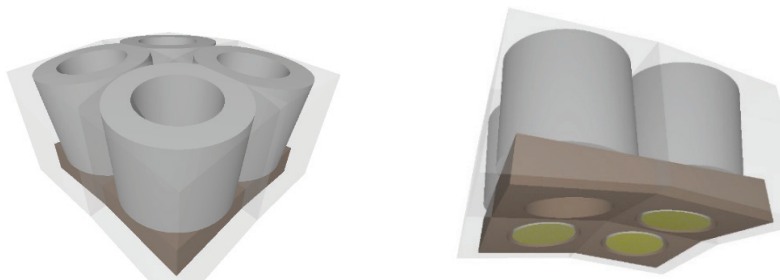


Figure 8. Model of the WBC detector system visualised in 3D via POV-Ray. The entrance windows of the HPGe detector probes and the metallic collimator are plotted in green and brown colours, respectively. Note that one of the collimator tubes did not contain the detector probe.

Views of the detector system positioned above the chest of the phantom can be seen in Figure 9.

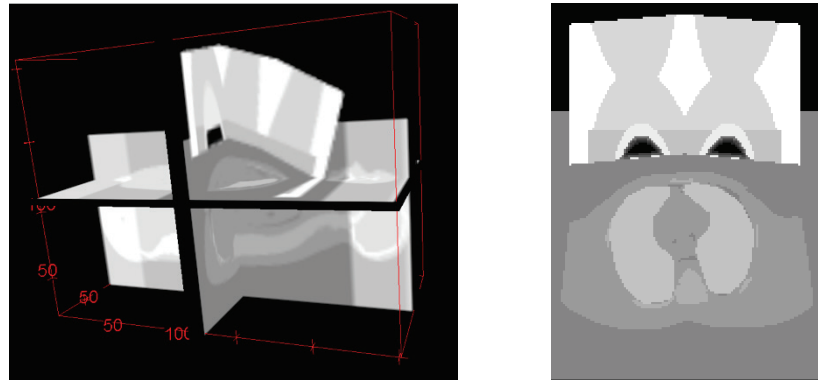


Figure 9. Visualization of the detector system positioned above the chest of the phantom.

3.5. Minimum detectable activity

3.5.1. Theory

Measurements in gamma-ray spectroscopy are affected by random fluctuations in the number of detected photons. Consequently, claims about the presence or absence of a specific radionuclide in the measured sample must be based on statistical theory.

The *detection limit* indicates the smallest true value of the measurand which can still be detected with the applied measurement procedure; this gives a decision on whether or not the measurement procedure satisfies the requirements and is therefore suitable for the intended measurement purpose [18].

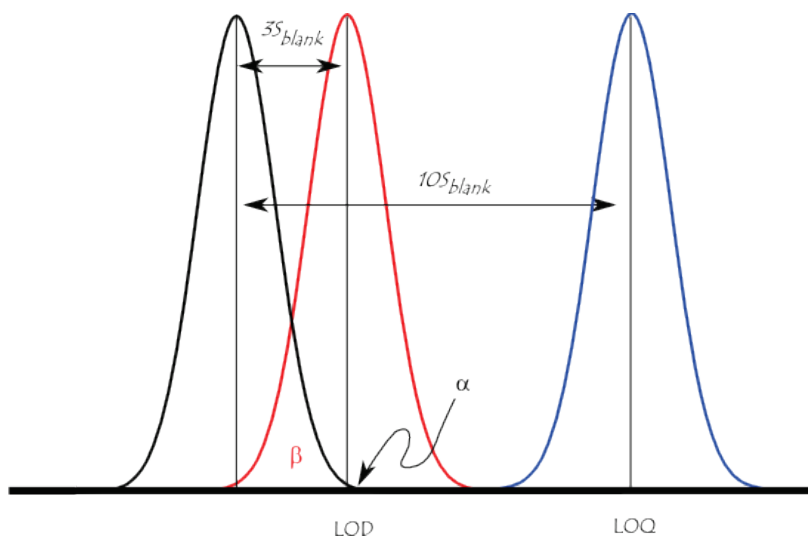


Figure 10. The relation between the detection limit, LOD, and the probabilities α and β . Source: Wikipedia.

The *minimum detectable activity* (MDA) is the activity of a sample that corresponds to the limit of detection, L_D , for a measured number of counts [19].

Assume that the background number of counts, N_B , and the total number of counts, N_{B+S} , are Poisson distributed random quantities. The subscripts indicate that the background number of counts is measured directly and contains contributions from the background B only, while the total number of counts contains contributions from both the background B and the signal S . In this case, the number of counts corresponding to the detection limit L_D can be calculated as [20]

$$L_D = 2.71 + 4.65\sqrt{N_B} , \quad (23)$$

where N_B is the mean number of background counts when signal S is not present.

The background N_B of a well-defined isolated peak can be defined as the sum of channels in a region of interest (ROI) covering the $(E - k\sigma, E + k\sigma)$ interval of the gamma-ray spectrum, where E stands for the peak centroid, σ is a parameter describing the width of the peak, and the parameter k is related to the fraction of detection events covered by the ROI. In practice the ROI is often set to cover the whole peak, which has a gaussian shape. This corresponds to $k = 2$. The probability that the measured pulse falls into $(E - 2\sigma, E + 2\sigma)$ is then 95%. The parameters σ (standard deviation) of the normal distribution is related to the full width at half maximum (FWHM) of the peak as $\text{FWHM} = 2\sqrt{2 \ln 2}\sigma \approx 2.35\sigma$ (Wikipedia, 2022). Other option is $k = 2$ corresponding to the 95% coverage.

The peak may be superimposed on one or more other peaks. The background N_B of a peak is then more difficult to determine. For measured spectra, possible methods range from treating the other peaks as a part of the background to fitting the peaks with a sum of gaussian functions. For computer simulated spectra, the software may provide the mean number of counts in each channel for the Compton continuum. This Compton continuum then can be used for the determination of N_B .

For a known detection limit L_D , the MDA can be calculated as [19]

$$\text{MDA} = \frac{L_D}{t\varepsilon P_\gamma} , \quad (24)$$

where t is the acquisition time, ε is the full energy absorption detector efficiency, and P_γ is the gamma-line intensity.

The MDA was calculated for simulated spectra modified with the experimentally determined correction factor for the energy-dependent efficiency of the detector. The simulated spectra for selected committed effective dose (CED) levels were obtained by rescaling spectra produced by Nucleonica.

3.5.2. Energy calibration of Nucleonica spectra

Nucleonica uses a linear relation between the channel number, c , and corresponding photon energy, E . The first energy channel is defined as the interval $(0, \Delta E)$, where ΔE is the channel width. The i -th energy channel is defined as $((i-1)\Delta E, i\Delta E)$, where $i = 1, \dots, N$. Nucleonica reports the energy of the bin center:

$$E = \frac{\Delta E}{2} + \Delta E c , \quad (25)$$

where $c = 1, \dots, N$ is the channel number. In this work, the bin width was set to 0.25 keV and the number of energy channels of the gamma ray spectrum was set to 8192. The relation between the energy of the bin center E and the channel c is then

$$E = 0.125 \text{ keV} + c \cdot 0.25 \text{ keV} . \quad (26)$$

3.5.3. Energy resolution of Nucleonica spectra

For HPGe detectors, Nucleonica sets the energy resolution, $\Delta_{1/2}(E)$, of the detector (defined as the full width at half maximum) as¹

$$\Delta_{1/2}(E) = a + b\sqrt{E} . \quad (27)$$

For scintillation detectors, the relation is linear, $\Delta_{1/2}(E) = a + bE$. The coefficients a and b in equation (27) were determined from the resolution at the energies of $E_1 = 122.0$ keV and $E = 1332.5$ keV corresponding to ⁵⁷Co and ⁶⁰Co, respectively:

$$\Delta_{1/2}(E_1) = 0.754 \text{ keV} , \quad (28)$$

$$\Delta_{1/2}(E_2) = 1.82 \text{ keV} . \quad (29)$$

The resulting formulas were

$$b = \frac{\Delta_{1/2}(E_2) - \Delta_{1/2}(E_1)}{\sqrt{E_2} - \sqrt{E_1}} , \quad (30)$$

$$a = \Delta_{1/2}(E_1) - b\sqrt{E_1} . \quad (31)$$

3.5.4. The algorithm

The algorithm computing MDA for a gamma line E_X of radionuclide X at the committed effective dose level $E(50)$ consists of the following steps:

1. Compute $S_{M_i,0}$ spectra using Nucleonica for a mixture M_i of selected radionuclides. Activities of these radionuclides correspond to the activity release by ESS scaled so that the total activity (sum of activities of the radionuclides) equals 1 MBq at day 0. Computation of $S_{M_i,0}$ spectra is described in section 3.2.
2. Compute Compton continuum spectrum $S_{M_i,1,c}$ from spectra $S_{M_i,0}$ produced by Nucleonica for the mixture M_i without radionuclide X .
3. Determine the committed effective dose $E_{S_{M_i,1,c}}(50)$ for $S_{M_i,1,c}$.
4. Compute $S_{M_i,2,c}$ by rescaling $S_{M_i,1,c}$ with the factor $E(50)/E_{S_{M_i,1,c}}(50)$.
5. Compute $S_{M_i,3,G,c}$ by applying the energy dependent detector-efficiency correction factor $k_{\varepsilon,G}(E) = \varepsilon_G(E)/\varepsilon_N(E)$, where $\varepsilon_N(E)$ and $\varepsilon_G(E)$ are the detector efficiencies for Nucleonica and the measurement in configuration G , respectively, on the spectrum $S_{M_i,2,c}$.
6. Compute the number of counts for the background $N_{B,S_{M_i,3,G,c}}$ as the number of counts in the $(E_X - 2\sigma(E_X), E_X + 2\sigma(E_X))$ interval of the $S_{M_i,3,G,c}$ spectrum. The parameter $\sigma(E_X)$ is obtained as $\sigma(E_X) = \Delta_{1/2}(E_X)/2.35$.
7. Compute $L_{D,S_{X,3,G,c}} = 2.71 + 4.65 \sqrt{N_{B,S_{X,3,G,c}}}$
8. Compute $A_{MDA,X,G}$ from $L_{D,S_{X,3,G,c}}$ using equation (24).

Note that the resulting $L_{D,S_{M_i,3,G,c}}$ depends on the gamma line of the radionuclide X and the geometry G of the detector efficiency measurement; that is the detector probe of the WBC system and the fat layer thickness of the anthropomorphic phantom.

¹ https://nucleonica.com/wiki/index.php?title=Help:Gamma_Spectrum_Generator%2B%2B

4. Results

4.1. Retention of radionuclides in lungs

Figure 11 shows activities in lungs as a function of time corresponding to the intake of 1 Bq for the 49 most prominent radionuclides released. Data were calculated using IMBA and Taurus. The latest biokinetic data from ICRP publications 130 [11], 134 [9], 137 [8], 141 [7] were used. These functions were used for the calculation of simulated spectra.

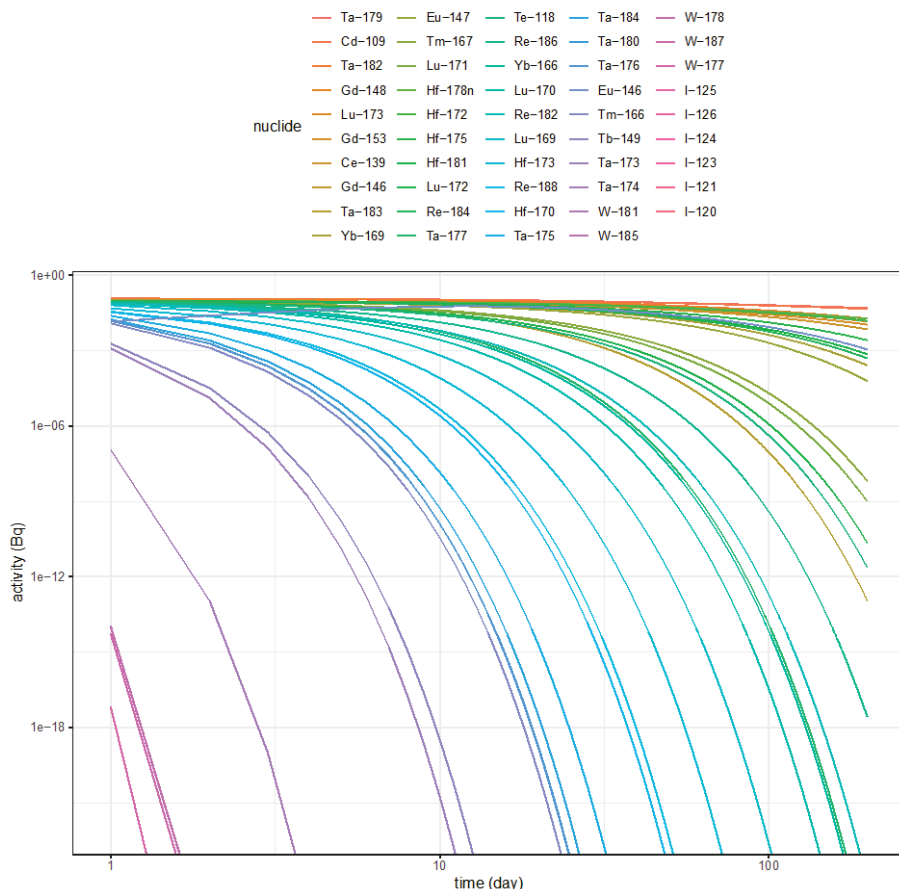


Figure 11. Activities in lungs corresponding to the intake of 1 Bq for the most prominent radionuclides available in IMBA.

4.1.1. Bioassay calculations

Figure 12 shows activities in urine as a function of time corresponding to the intake of 1 Bq for 49 most prominent radionuclides released. Data were computed with IMBA and Taurus.

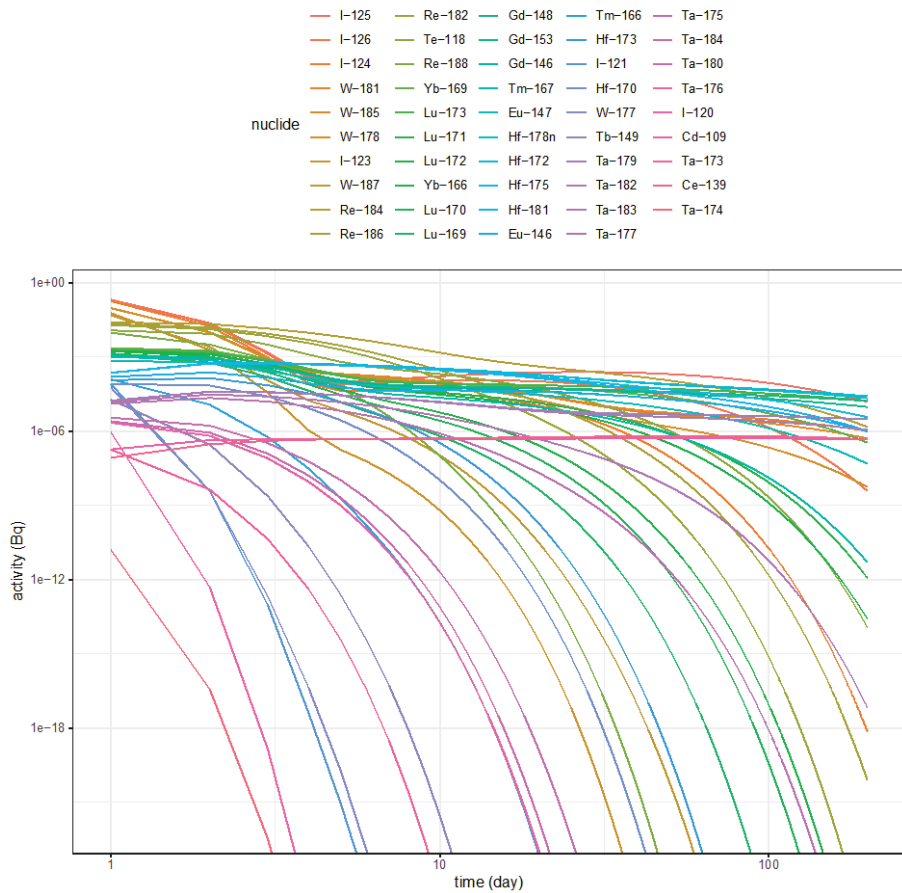


Figure 12. Activities in urine corresponding to the intake of 1 Bq for the most prominent radionuclides available in IMBA.

Figure 13 shows the excretion curve for urine samples for radionuclides ^{148}Gd , ^{146}Gd , ^{153}Gd type M and ^{172}Hf type M and F, for the 10 first days after intake. Figure 14 shows the same retention curve as in Figure 13 but with ^{187}W (type F) added. Day zero is the time of intake, the urine sample was collected for 24 h, and the intake was set to 1 Bq.

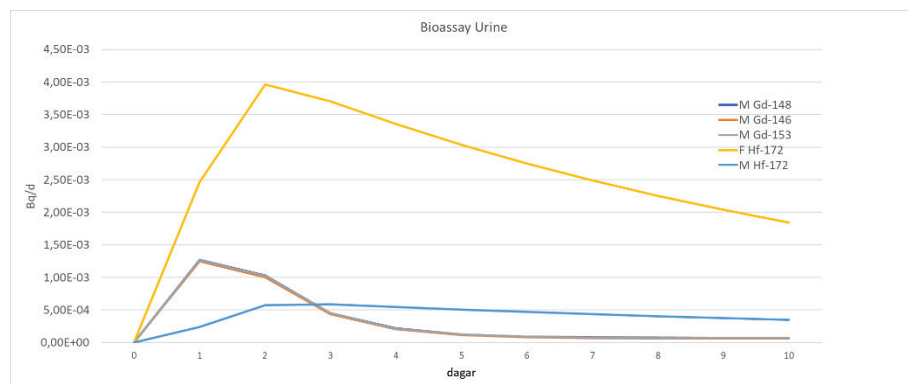


Figure 13. The excretion curve for ^{148}Gd , ^{146}Gd , ^{153}Gd (type M) and ^{172}Hf (type F and M) for urine samples, unit intake of 1 Bq.

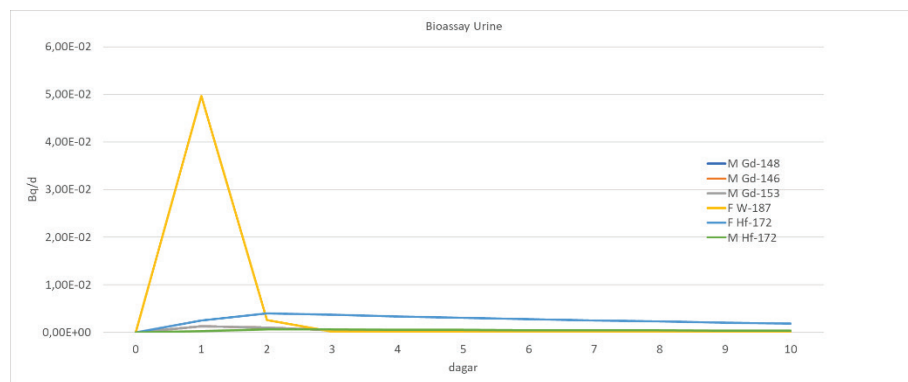


Figure 14. The same excretion curve as in Figure 13 with ^{187}W added.

The Table 6 shows the activity in the lungs and in the urine per day from day 0 to day 10, for the isotopes ^{146}Gd , ^{148}Gd , and ^{153}Gd , all with absorption type M.

The Table 7 shows the activity in the lungs and in the urine per day from day 0 to day 10, for the isotopes ^{187}W (absorption type F), ^{172}Hf (absorption type F) ^{172}Hf (absorption type M).

Table 6. The activity in the lungs and in the urine per day, from day 0 to day 10 for the isotopes ^{146}Gd , ^{148}Gd and ^{153}Gd with absorption type M. Unit intake 1 Bq.

Day	^{146}Gd type M		^{148}Gd type M		^{153}Gd type M	
	Activity lungs [Bq]	Activity urine [Bq]	Activity lungs [Bq]	Activity urine [Bq]	Activity lungs [Bq]	Activity urine [Bq]
0	1.36E-01	0.00E+00	1.36E-01	0.00E+00	1.36E-01	0.00E+00
1	1.04E-01	1.25E-03	1.06E-01	1.27E-03	1.05E-01	1.26E-03
2	9.49E-02	1.00E-03	9.76E-02	1.03E-03	9.71E-02	1.02E-03
3	9.02E-02	4.35E-04	9.41E-02	4.54E-04	9.33E-02	4.50E-04
4	8.69E-02	2.03E-04	9.21E-02	2.15E-04	9.10E-02	2.13E-04
5	8.43E-02	1.17E-04	9.05E-02	1.26E-04	8.93E-02	1.24E-04
6	8.19E-02	8.46E-05	8.92E-02	9.22E-05	8.77E-02	9.06E-05
7	7.96E-02	7.13E-05	8.80E-02	7.88E-05	8.62E-02	7.73E-05
8	7.74E-02	6.51E-05	8.68E-02	7.30E-05	8.48E-02	7.14E-05
9	7.53E-02	6.15E-05	8.56E-02	6.99E-05	8.35E-02	6.82E-05
10	7.32E-02	5.88E-05	8.45E-02	6.79E-05	8.21E-02	6.60E-05

Table 7. The activity in the lungs and in the urine per day, from day 0 to day 10 for the isotopes ^{187}W (absorption type M), ^{172}Hf (absorption type F) and ^{172}Hf (absorption type M). Unit intake 1 Bq.

Day	^{187}W type F		^{172}Hf type F		^{172}Hf type M	
	Activity lungs [Bq]	Activity urine [Bq]	Activity lungs [Bq]	Activity urine [Bq]	Activity lungs [Bq]	Activity urine [Bq]
0	1.36E-01	0.00E+00	1.36E-01	0.00E+00	1.36E-01	0.00E+00
1	5.67E-15	4.97E-02	1.14E-14	2.46E-03	9.78E-02	2.37E-04
2	2.59E-28	2.61E-03	1.04E-27	3.96E-03	9.43E-02	5.71E-04
3	1.20E-41	1.14E-04	9.64E-41	3.70E-03	9.27E-02	5.85E-04
4	5.54E-55	1.78E-05	8.93E-54	3.36E-03	9.13E-02	5.45E-04
5	2.56E-68	6.78E-06	8.27E-67	3.04E-03	8.99E-02	5.05E-04
6	1.18E-81	2.93E-06	7.66E-80	2.75E-03	8.86E-02	4.67E-04
7	5.48E-95	1.28E-06	7.10E-93	2.49E-03	8.73E-02	4.34E-04
8	0.00E+00	5.59E-07	0.00E+00	2.25E-03	8.61E-02	4.03E-04
9	0.00E+00	2.45E-07	0.00E+00	2.04E-03	8.49E-02	3.75E-04
10	0.00E+00	1.07E-07	0.00E+00	1.84E-03	8.37E-02	3.49E-04

4.2. Simulation of gamma spectra

As described in section 3.2, gamma spectra were simulated with Nucleonica in a simplified geometry comprising a point source and a detector, the point source was located on the detector axis at the distance of 100 mm from the front cap of the detector. Figure 15 shows that the full energy peaks of ^{153}Gd at 97.4 and 103.2 keV, the peak of ^{146}Gd at 154.6 keV, and the peak of ^{146}Eu at 747.2 keV are well shaped and can be used for the determination of the net area. It should be noted that since Gd and Eu show a very similar retention in lung, the ^{146}Eu levels found by lung counting will correspond to the ^{146}Gd levels in the lung after a sufficient *in-situ* in-growth period.

Table 8. Net peak areas for peaks in Figure 15 obtained using the Web Spectrum Analyzer module of Nucleonica. The quantity $c_A = A/\dot{N}$ is also shown.

Nuclide	Energy (keV)	Channel (chn)	FWHM	Peak Area	Net count rate (1/s)	Activity (Bq)	c_A
Gd-153	97.5	487	3.17	2.02E+12	5.61E+08	7.07E+10	1.26E+02
Gd-153	103.1	515	3.24	1.52E+12	4.22E+08	7.07E+10	1.67E+02
Gd-146	154.7	773	3.97	3.69E+12	1.03E+09	7.72E+10	7.53E+01

Activity of the radionuclide can be calculated as

$$A = \frac{\dot{N}_{\text{net}}}{\varepsilon(E)f} , \quad (32)$$

where \dot{N}_{net} is the net count rate, $\varepsilon(E)$ is the energy dependent full energy absorption detector efficiency, and f is the energy line intensity.

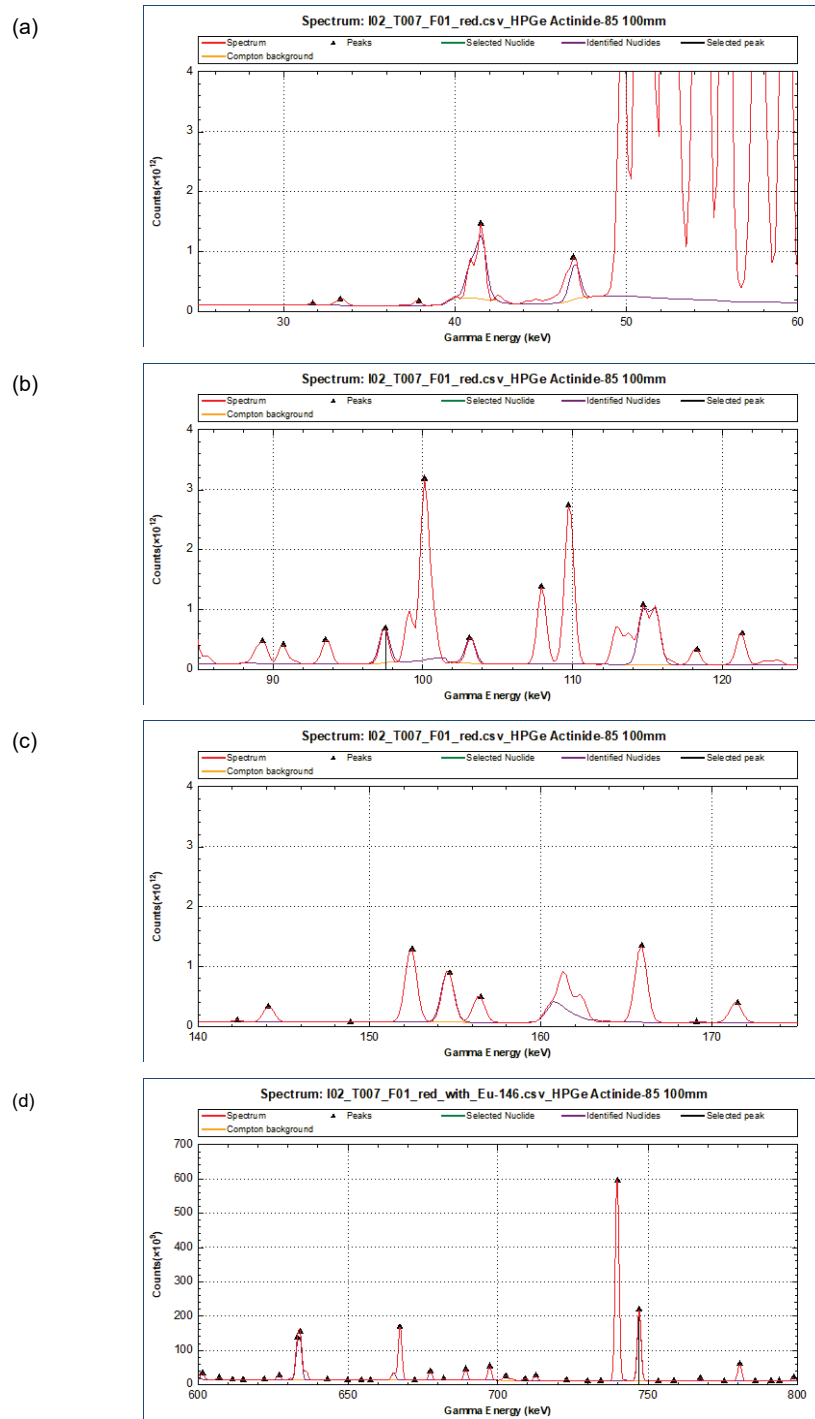


Figure 15. Simulated peaks of ^{146}Gd , ^{153}Gd and ^{146}Eu . (a) X-rays in the energy range 40-48 keV. Note that both isotopes have the same characteristic lines and so these peaks cannot be directly used for the determination of activity. (b) Well-shaped 97.4 and 103.2 keV peaks of ^{153}Gd and the composite 114.7 and 115.5 keV peak of ^{146}Gd . The net area of the latter peak is difficult to determine. (c) The well-shaped 154.6 keV peak of ^{146}Gd . (d) Composite 633.1 and 634.1 keV peak of ^{146}Eu and a well-shaped 747.2 keV peak of the same radionuclide.

4.2.1. Reduced vs. full list of radionuclides

The full list of released radionuclides contains about 1000 entries. The standard version of Nucleonica cannot simulate spectra for such a long list; the maximum number is 20. Fortunately, it was possible to perform the simulations on Nucleonica's test servers. Figure 16 shows a spectrum generated for the full list of released radionuclides and the spectrum corresponding to the 49 most prominent radionuclides according to the release mixture [3]. Unfortunately, a spectrum analysis presented in Figure 16(a) could not be performed since the system crashed during the computations due to large memory demands of the code. Note that the number of peaks is larger for the full list, nevertheless the main peaks are the same in both spectra. In the ideal situation, none of the additional radionuclides in the full list will disturb the shape of the peaks of interest.

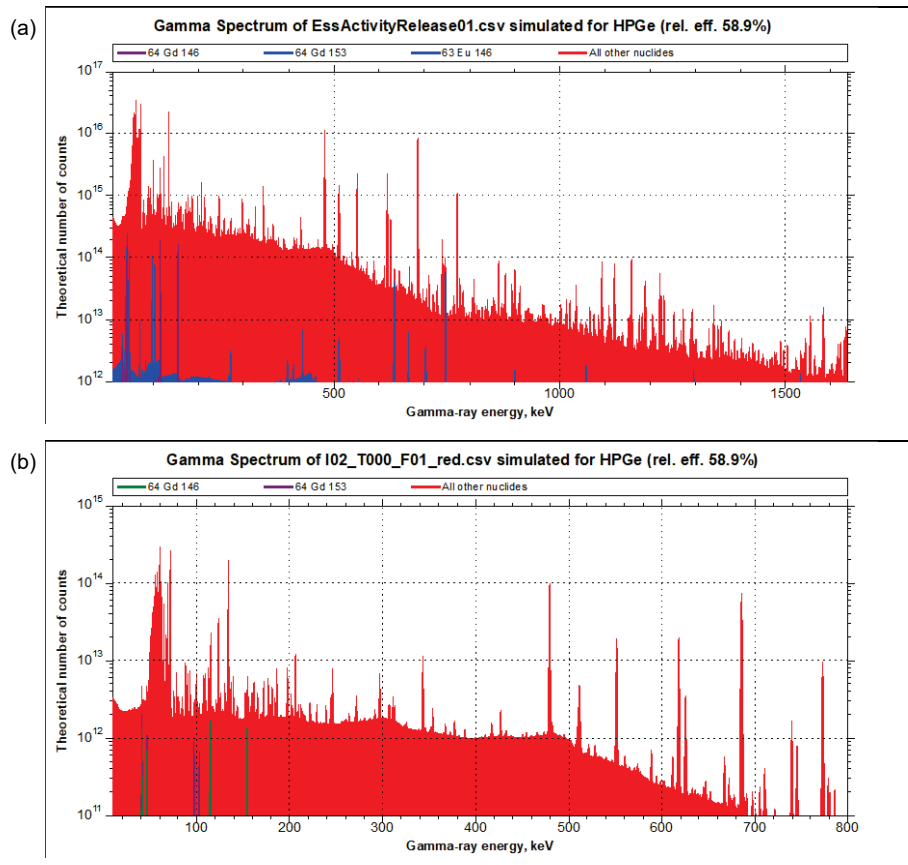


Figure 16. Simulated gamma spectrum for (a) full list of released radionuclides, and (b) 49 most prominent radionuclides according to the release mixture.

4.3. Calibration of the WBC system

Figure 17 and Table 9 show the results of the calibration of the WBC-system (detector 1-3) using the phantom described in section 4.3.2 and calibration sources described in section 4.3.3. Detector efficiency curves are shown for standard bare phantom and for phantom with 2 sets of fat torso plates of different thickness.

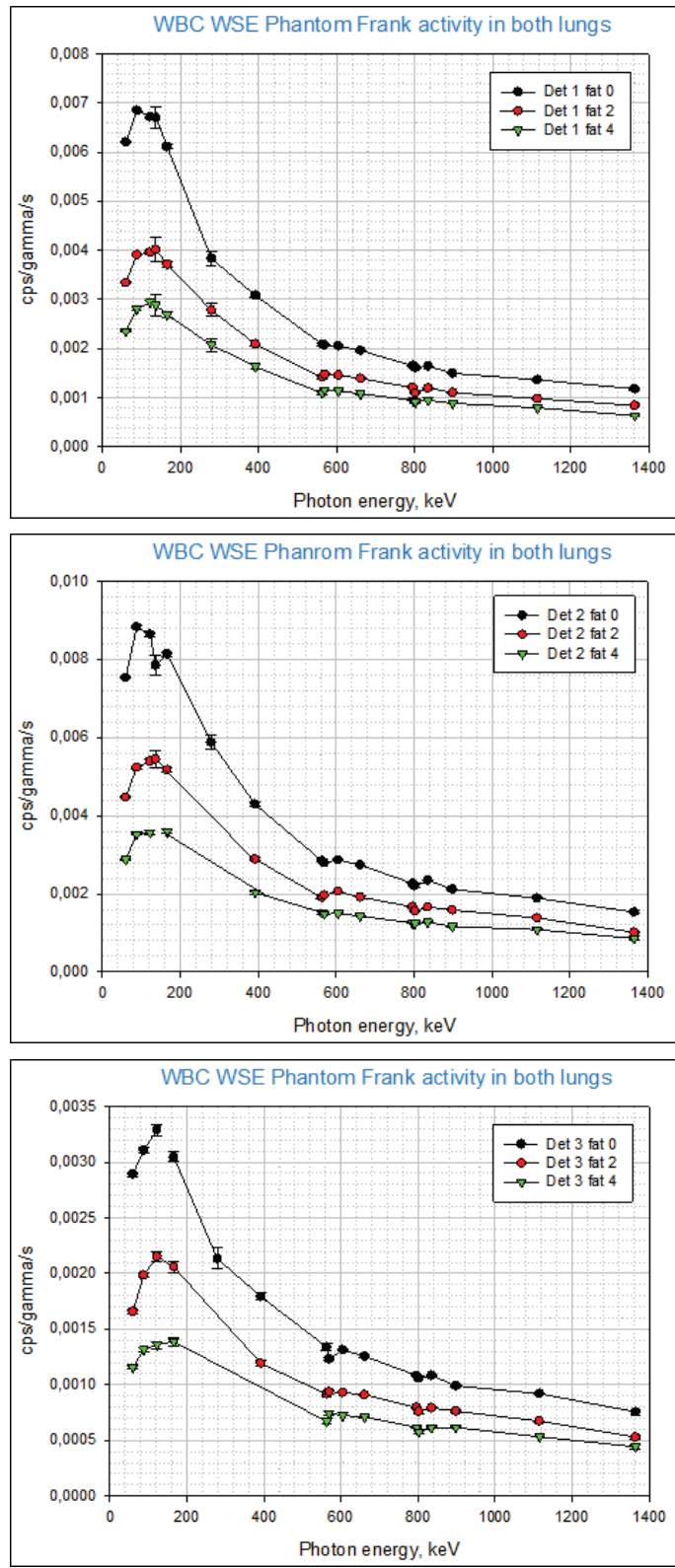


Figure 17. The detector efficiency for the 3 HPGe detectors as a function of energy for the calibration sources and the phantom, for 3 different torso fat layers.

Table 9. Detector efficiency ε_D [cps/g/s] and associated standard uncertainty $u(\varepsilon_D)$ for the detectors D₁, D₂ and D₃ and the fat layer 0.

Nuclide	E (keV)	ε_{D_1}	$u(\varepsilon_{D_1})$	ε_{D_2}	$u(\varepsilon_{D_2})$	ε_{D_3}	$u(\varepsilon_{D_3})$
Am-241	59.54	6.20E-03	1.92E-05	7.53E-03	2.03E-05	2.89E-03	1.68E-05
Cd-109	88.03	6.85E-03	2.42E-05	8.82E-03	2.64E-05	3.11E-03	2.02E-05
Co-57	122.06	6.72E-03	4.09E-05	8.64E-03	4.40E-05	3.29E-03	5.03E-05
Co-57	136.47	6.70E-03	2.30E-04	7.84E-03	2.56E-04		
Ce-139	165.86	6.11E-03	4.72E-05	8.13E-03	5.87E-05	3.04E-03	4.46E-05
Hg-203	279.20	3.83E-03	1.51E-04	5.87E-03	1.77E-04	2.13E-03	9.67E-05
Sn-113	392.00	3.08E-03	3.50E-05	4.29E-03	4.27E-05	1.79E-03	3.15E-05
Cs-134	563.20	2.09E-03	3.02E-05	2.84E-03	3.47E-05	1.34E-03	2.83E-05
Cs-134	569.30	2.08E-03	1.83E-05	2.80E-03	2.23E-05	1.23E-03	1.60E-05
Cs-134	604.70	2.05E-03	5.73E-06	2.87E-03	6.96E-06	1.31E-03	4.70E-06
Cs-137	661.70	1.96E-03	1.20E-05	2.74E-03	1.48E-05	1.26E-03	1.04E-05
Cs-134	795.90	1.65E-03	5.35E-06	2.26E-03	6.68E-06	1.08E-03	4.40E-06
Cs-134	802.00	1.62E-03	2.01E-05	2.21E-03	2.90E-05	1.06E-03	1.80E-05
Mn-54	834.80	1.64E-03	7.94E-06	2.35E-03	1.06E-05	1.08E-03	6.47E-06
Y-88	898.00	1.50E-03	1.06E-05	2.12E-03	1.35E-05	9.91E-04	9.03E-06
Zn-65	1115.50	1.37E-03	6.58E-06	1.89E-03	8.27E-06	9.19E-04	5.44E-06
Cs-134	1365.00	1.18E-03	2.84E-05	1.53E-03	3.79E-05	7.55E-04	2.50E-05

Table 10. The same as Table 9 for the fat layer 2.

Nuclide	E (keV)	ε_{D_1}	$u(\varepsilon_{D_1})$	ε_{D_2}	$u(\varepsilon_{D_2})$	ε_{D_3}	$u(\varepsilon_{D_3})$
Am-241	59.54	3.34E-03	1.62E-05	4.47E-03	1.95E-05	1.66E-03	1.82E-05
Cd-109	88.03	3.91E-03	2.26E-05	5.23E-03	2.35E-05	1.98E-03	1.93E-05
Co-57	122.06	3.96E-03	3.65E-05	5.39E-03	5.05E-05	2.15E-03	4.21E-05
Co-57	136.47	4.02E-03	2.37E-04	5.44E-03	2.27E-04		
Ce-139	165.86	3.71E-03	4.76E-05	5.17E-03	5.35E-05	2.06E-03	4.74E-05
Hg-203	279.20	2.78E-03	1.31E-04				
Sn-113	392.00	2.09E-03	3.25E-05	2.89E-03	4.22E-05	1.19E-03	2.89E-05
Cs-134	563.20	1.42E-03	2.62E-05	1.91E-03	3.30E-05	9.15E-04	2.78E-05
Cs-134	569.30	1.47E-03	1.75E-05	1.96E-03	2.18E-05	9.36E-04	1.60E-05
Cs-134	604.70	1.46E-03	5.84E-06	2.06E-03	6.74E-06	9.29E-04	4.30E-06
Cs-137	661.70	1.39E-03	1.17E-05	1.92E-03	1.41E-05	9.09E-04	9.69E-06
Cs-134	795.90	1.20E-03	5.14E-06	1.67E-03	5.92E-06	7.94E-04	4.07E-06
Cs-134	802.00	1.10E-03	1.97E-05	1.56E-03	2.27E-05	7.59E-04	1.70E-05
Mn-54	834.80	1.20E-03	7.69E-06	1.66E-03	8.94E-06	7.91E-04	5.99E-06
Y-88	898.00	1.10E-03	1.06E-05	1.58E-03	1.22E-05	7.62E-04	8.11E-06
Zn-65	1115.50	9.81E-04	6.21E-06	1.38E-03	7.31E-06	6.72E-04	5.00E-06
Cs-134	1365.00	8.44E-04	2.80E-05	1.02E-03	3.30E-05	5.29E-04	2.36E-05

Table 11. The same as Table 9 for the fat layer 4.

Nuclide	E (keV)	ε_{D_1}	$u(\varepsilon_{D_1})$	ε_{D_2}	$u(\varepsilon_{D_2})$	ε_{D_3}	$u(\varepsilon_{D_3})$
Am-241	59.54	2.35E-03	1.67E-05	2.88E-03	1.61E-05	1.16E-03	1.43E-05
Cd-109	88.03	2.81E-03	2.22E-05	3.52E-03	2.13E-05	1.32E-03	1.78E-05
Co-57	122.06	2.94E-03	3.93E-05	3.56E-03	4.08E-05	1.36E-03	3.20E-05
Co-57	136.47	2.88E-03	2.15E-04				
Ce-139	165.86	2.69E-03	4.88E-05	3.59E-03	5.18E-05	1.39E-03	3.75E-05
Sn-113	255.10						
Hg-203	279.20	2.08E-03	1.32E-04	1.90E-03	1.07E-04		
Sn-113	392.00	1.63E-03	3.17E-05	2.03E-03	3.55E-05		
Cs-134	563.20	1.09E-03	2.64E-05	1.52E-03	2.94E-05	6.70E-04	2.39E-05
Cs-134	569.30	1.16E-03	1.79E-05	1.48E-03	1.88E-05	7.43E-04	1.36E-05
Cs-134	604.70	1.14E-03	4.96E-06	1.50E-03	5.57E-06	7.22E-04	4.06E-06
Cs-137	661.70	1.08E-03	1.05E-05	1.43E-03	1.19E-05	7.08E-04	8.91E-06
Cs-134	795.90	9.49E-04	4.62E-06	1.25E-03	5.16E-06	6.16E-04	3.61E-06
Cs-134	802.00	9.16E-04	1.83E-05	1.24E-03	2.12E-05	5.74E-04	1.58E-05
Mn-54	834.80	9.47E-04	6.76E-06	1.27E-03	7.77E-06	6.14E-04	5.46E-06
Y-88	898.00	8.86E-04	9.40E-06	1.17E-03	1.07E-05	6.16E-04	7.63E-06
Zn-65	1115.50	7.95E-04	5.64E-06	1.08E-03	6.35E-06	5.32E-04	4.36E-06
Cs-134	1365.00	6.36E-04	2.47E-05	8.59E-04	3.24E-05	4.42E-04	2.03E-05

Figure 18 shows detector efficiency curves fitted to measured data.

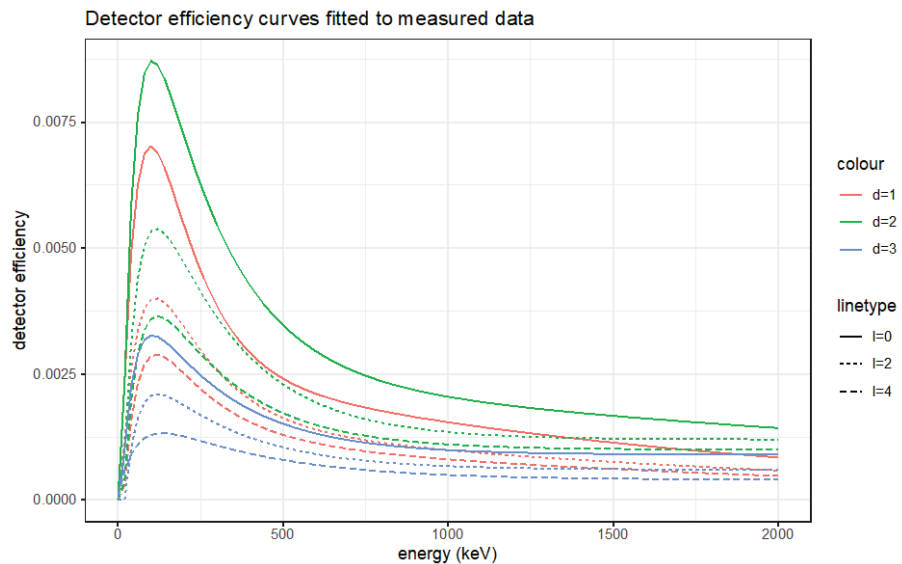


Figure 18. Detector efficiency [cps/y/s] curves fitted to data measured using the WBC system at Westinghouse for detectors $d = 1, 2, 3$ and anthropomorphic phantom with fat layers $l = 0, 2, 4$.

The curves have the form

$$\varepsilon(E) = \varepsilon_0 + \sum_{i=1}^3 a_i e^{-b_i E}, \quad (33)$$

where the coefficients ε_0 , a_i , and b_i are listed in Table 13.

Table 12. Efficiency [cps/g/s] for detector D_1 at energies [keV] of the peaks of ^{146}Gd and ^{153}Gd . Values were obtained using linear interpolation of values in Table 9–Table 11.

Energy (keV)	Eff0	Eff2	Eff4
97.4310	0.0068106	0.0039209	0.0028470
103.1801	0.0067890	0.0039300	0.0028697
154.5700	0.0062660	0.0037744	0.0027547

Table 13. Coefficients of the fit in equation (33).

Det.	Fat layer	ε_0	a_1	b_1	a_2	b_2	a_3	b_3
1	0	0	0.0158	0.0077	-0.0206	0.0195	0.0028	0.0006
1	2	0	0.0073	0.0059	-0.0099	0.0183	0.0016	0.0005
1	4	0	0.0042	0.0054	-0.0074	0.0219	0.0013	0.0005
2	0	0	-0.0188	0.0248	0.0123	0.0046	0.0026	0.0003
2	2	0.0012	-0.0012	0.4556	0.0081	0.0040	-0.0121	0.0223
2	4	0.0010	0.0059	0.0039	-0.0084	0.0228	-0.0008	0.0039
3	0	0.0009	0.0041	0.0038	-0.0027	0.4463	-0.0063	0.0266
3	2	0.0006	-0.0079	0.9172	0.0027	0.0036	-0.0052	0.0252
3	4	0.0004	0.0016	0.0028	-0.0019	0.0179	0	0

4.4. Simulation of the WBC system

Figure 19 and Figure 20 show the segmented anthropomorphic phantom. Air, soft tissue and bone was segmented using a threshold segmentation with CT number thresholds of 211 and 1225 HU, where HU stands for hounsfield unit. Threshold segmentation of lungs was problematic as some of the voxels on the soft tissue - air border were classified as lungs owing to the partial volume effect. For this reason, lungs were classified manually by drawing a polygonal region of interest for each slice.

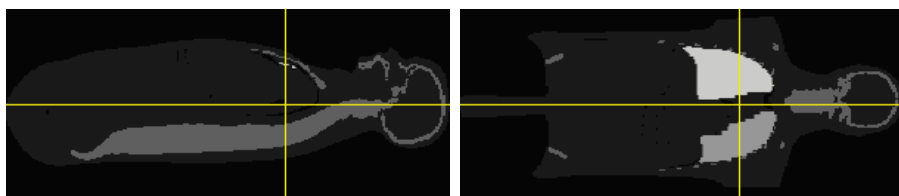


Figure 19. Sagittal and coronal views of the segmented anthropomorphic phantom. Voxel values were set to 0, 1, 2, 3 and 4 for the air, soft tissue, bone, left lung, and right lung, respectively.

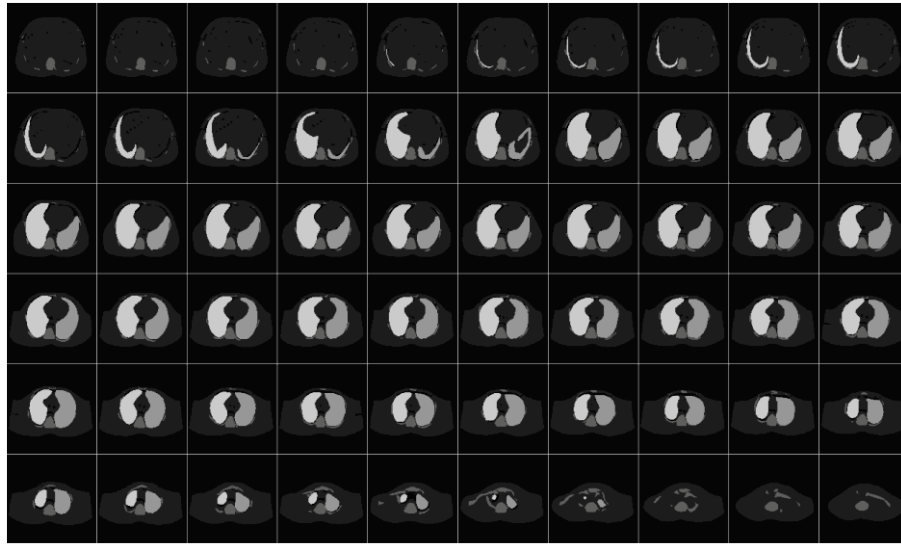


Figure 20. Slice-by slice axial view of the manually segmented lungs.

4.5. Comparison of measured and simulated calibration spectra

Measured spectra contain a larger fraction of the low-energy continuum owing to photons scattered inside the anthropomorphic phantom, see Figure 21. In the measured case, the source was more or less homogenously distributed in the lungs while in the simulated case, a point source located on the detector axis was used. The measured case had lower geometric efficiency and therefore the net peak areas are lower than in the simulated case.

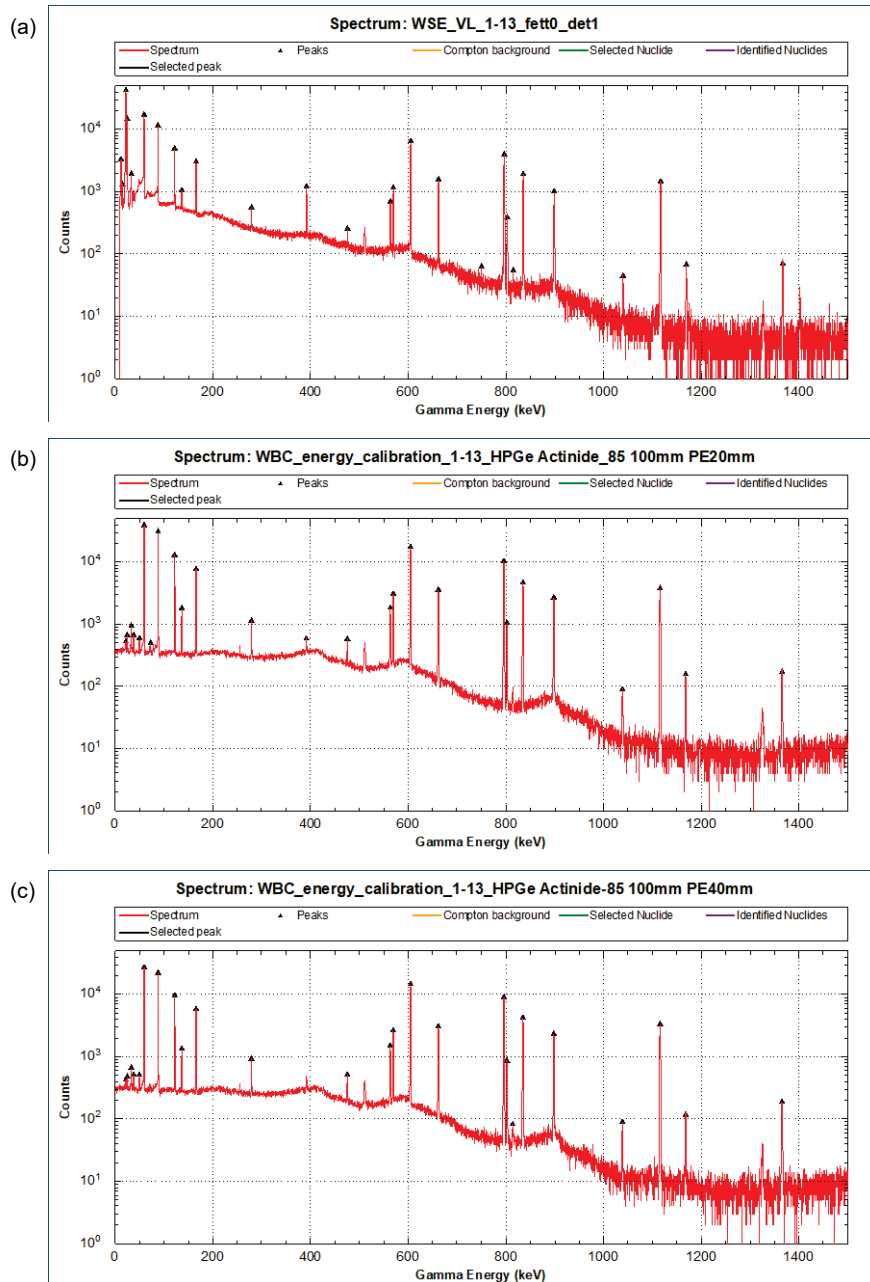


Figure 21. Comparison of measured and simulated calibration spectra. (a) Measured spectra for left lung. (b) Simulated spectra 20 mm PE. (c) Simulated spectra 40 mm PE.

4.6. Minimum detectable activity, MDA

MDA was calculated for 10 radionuclides chosen among the 16 radionuclides giving the highest CED from a release and having gamma-lines non-compromised with overlap from gamma-lines from other radionuclides, and (i) excluding radionuclides with non-measurable gamma-lines (e.g., ^{148}Gd , ^{179}Ta), and those with too low γ -emission probability (^{185}W , ^{186}Re , ^{175}Hf) or having short half-life (^{188}Re), (ii) including ^{146}Eu and ^{153}Gd since they are important for assessing ^{148}Gd . The 10 radionuclides selected (including ^{146}Gd) will represent about 81% of the expected inhalation

dose from the 49 most prominent radionuclides according to the release mixture [3]. The selection is shown in Table 14.

Table 14. Peaks for which the MDA was calculated.

Nuclide	Energy (keV)	Nuclide	Energy (keV)	Nuclide	Energy (keV)
W-187	685.8	Ta-183	107.9	Lu-172	1093.6
Hf-172	125.8	Ta-183	246.1	Gd-146	114.7
Ta-182	1189.0	Lu-173	172.2	Gd-146	115.5
Hf-178n	325.6	Yb-169	198.0	Eu-146	747.2
Hf-178n	426.4	Lu-171	739.8	Gd-153	103.2

4.6.1. Determination of MDA in lungs

The presented method for the calculation of MDA (section 3.5.4) uses the ratio of detector efficiencies for the real and computer-simulated detector systems, referred to as the detector efficiency correction factor in this report. The detector efficiency correction factor for the WBC detector system is shown in Figure 22. Note that the detector efficiency of the real WBC detectors was smaller than that of the computer-simulated detector for photon energies above 100 keV; their ratio was below 1 in this energy range.

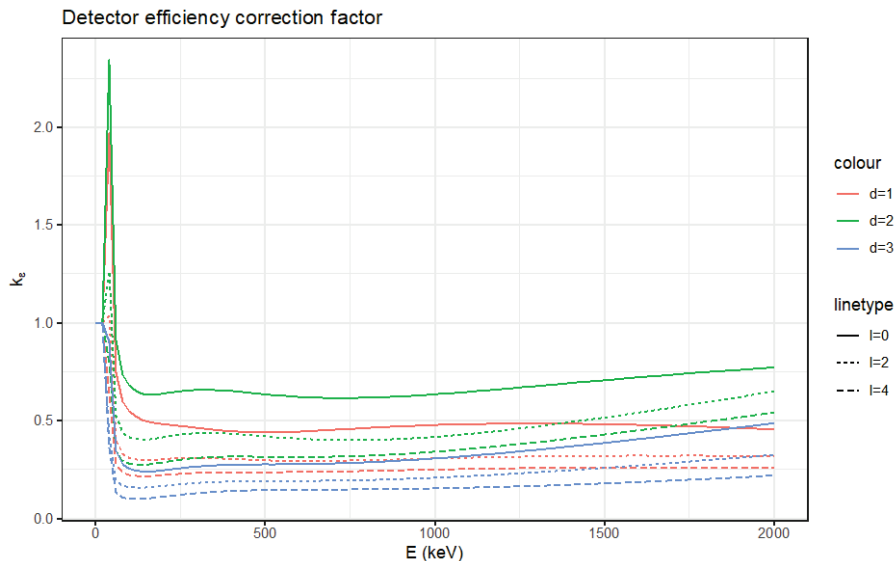


Figure 22. Detector efficiency correction factor for detectors $d = 1, 2, 3$ and anthropomorphic phantom with fat layers $l = 0, 2, 4$.

MDA in lungs as a function of time for the selected peaks, anthropomorphic phantom fat layer 0, detector 1, and CED of 1 mSv is plotted in Figure 23.

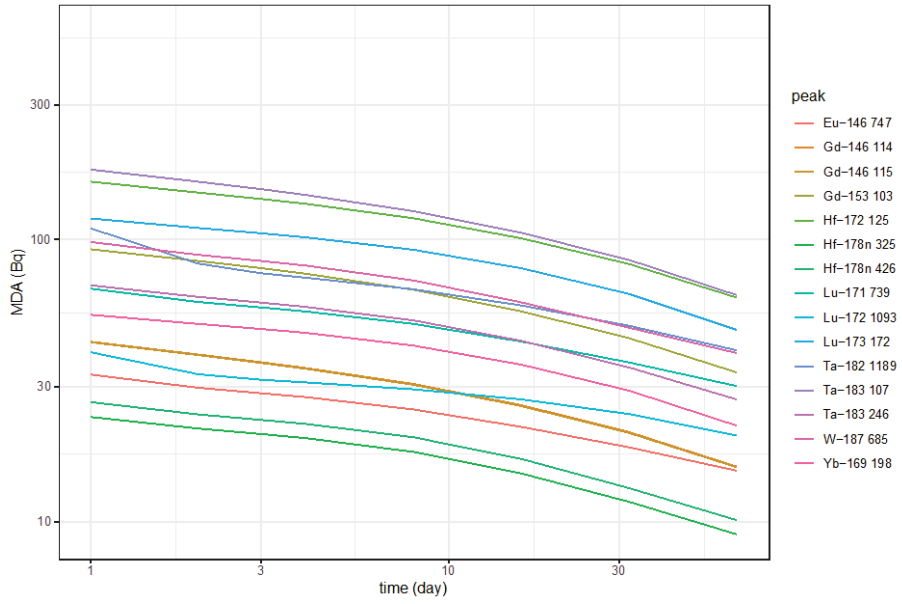


Figure 23. MDA in lungs as a function of time for considered peaks, fat layer 0, detector 1, and CED of 1 mSv.

The effects of the fat layer thickness and detector position are plotted in Figure 24 for ^{146}Eu at 747 keV, ^{146}Gd at 114 and 115 keV, and ^{153}Gd at 103 keV. The full set of data is available in the Appendix 8.5.2.

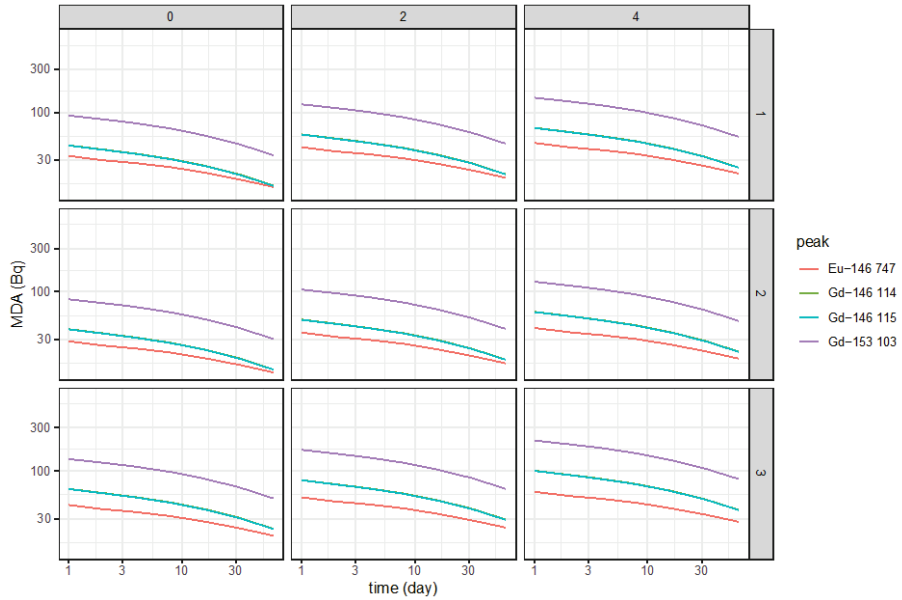


Figure 24. MDA in lungs as functions of time for ^{146}Eu at 747 keV, ^{146}Gd at 114 and 115 keV, ^{153}Gd at 103 keV, fat layers 0, 2, 4 (columns), detectors 1, 2, 3 (rows) at the CED of 1 mSv.

4.6.2. Determination of MDA in urine

The detector efficiency correction factor for the determination of MDA in urine is shown in Figure 25. The detector efficiency of the real detector was larger than that of the computer-simulated detector for photon energies above 100 keV; their ratio was above 1 in this energy range.

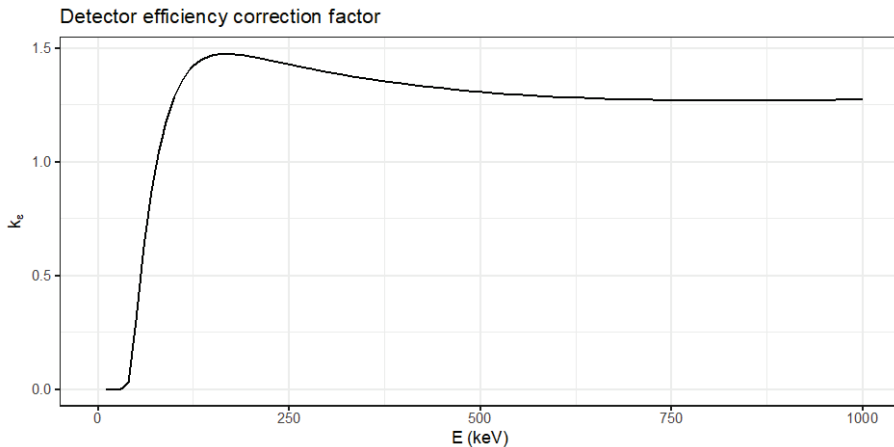


Figure 25. Detector efficiency corrector factor for the determination of MDA in urine.

MDA in urine as a function of time is plotted in Figure 26 and Figure 27, respectively, for all selected peaks and for ^{146}Eu at 747 keV, ^{146}Gd at 114 and 115 keV, and ^{153}Gd at 103 keV. The full set of data is available in the Appendix 8.5.1.

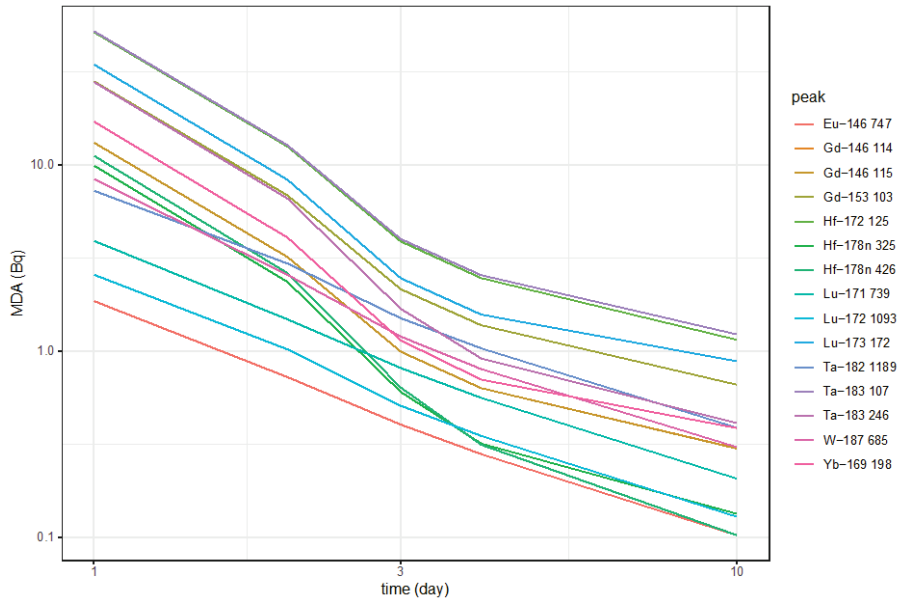


Figure 26. MDA in urine as a function of time for considered peaks and CED of 1 mSv.

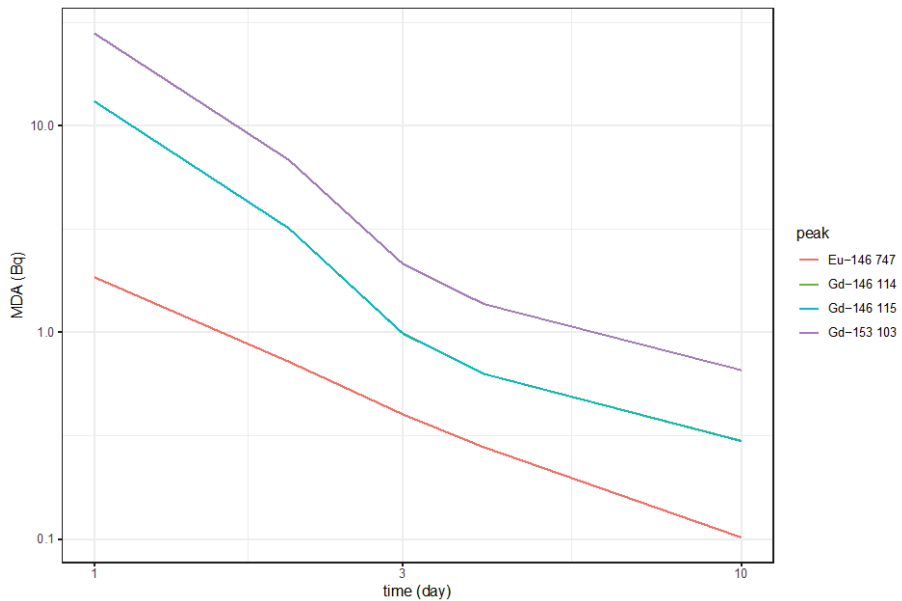


Figure 27. MDA in urine as a function of time for ^{146}Eu at 747 keV, ^{146}Gd at 114 and 115 keV, and ^{153}Gd at 103 keV.

4.7. Expected lung activity vs. MDA

Using the results of IMBA-calculations of time-dependent radionuclide retention in the lung a comparison of lung activity and MDA was made. This was done for (i) each of the 3 detectors, (ii) fat layers 0, 2 and 4, (iii) for 0, 1, 2, 3, 4, 8, 16, 32, 64 days after intake, (iv) and for committed effective doses of 1 and 20 mSv (for the mix of 49 radionuclides considered, SSM (2018) [3]. For the MDA calculations the 10 radionuclides described in chapter 4.1 were evaluated. A full set of results are given in Appendix 8.5.2. An excerpt is shown in Table 15.

Table 15. Comparison of expected lung activity and MDA for whole-body counting (30 min), detector 1, corresponding to 1 mSv CED. Fields with green color show favorable conditions for activity quantification.

Nuclide	γ -energy [keV]	Intensity [γ/decay]	Day 0		Day 2		Day 6		Day 32	
			Lung activity Bq	MDA Bq						
^{187}W	686	0,332	135400	188	0	88	0	72	0	49
^{172}Hf	126	0,113	829	552	576	147	526	119	384	82
^{182}Ta	1189	0,1649	1495	254	1286	82	1174	67	855	49
$^{178\text{n}}\text{Hf}$	326	0,941	51	116	35	21	32	18	24	12
$^{178\text{n}}\text{Hf}$	426	0,965	51	136	35	24	32	20	24	13
^{183}Ta	108	0,112	2223	550	1474	160	617	126	20	85
^{183}Ta	246	0,272	2223	311	1474	63	617	52	20	35
^{173}Lu	172	0,175	1354	404	988	110	875	92	635	64
^{169}Yb	198	0,3593	1415	200	991	50	777	42	347	29
^{171}Lu	740	0,487	1879	120	1161	60	625	50	62	37
^{172}Lu	1094	0,62	1051	81	625	33	300	29	19	24
^{146}Gd	115	0,443	196	141	139	39	114	31	61	21
^{146}Gd	116	0,443	196	140	139	39	114	31	61	21
^{146}Eu	747	0,98	0	59	36	30	80	25	60	18
^{153}Gd	103	0,211	166	290	121	84	106	66	74	45

4.8. Bioassay analysis; expected daily urine excretion activity vs. MDA

Using the results of IMBA-calculations of time-dependent daily excretion of radionuclides in urine a comparisons of urine activity and MDA were made. This was done for a committed effective doses of 1 and 20 mSv (for the mix of 49 radionuclides considered, SSM (2018) [3]. For the MDA calculations the 10 radionuclides described in chapter 4. were evaluated. Result for CED=1mSv is shown in Table 16.

Table 16. Comparison of expected daily urine excretion activity and MDA, corresponding to CED=1 mSv and CED=20 mSv. Calculations are made for a HPGe-detector of 42% relative efficiency and 1 litre urine samples in 1 litre sample plastic bottles and 24 h counting time. Fields with green color show favorable conditions for activity quantification, and fields with yellow color shows possible quantification with larger HPGe-detectors and/or evaporation of urine sample of about a factor of 10.

CED=1 mSv

Nuclide	γ -energy [keV]	Day 1		Day 2		Day 3		Day 4		Day 10	
		urine [Bq]	MDA [Bq]								
¹⁸⁷ W	686	49595	8.4	2604	2.6	114	1.2	17.8	0.80	0.11	0.30
¹⁷² Hf	126	1.4	51.5	3.5	12.5	3.6	3.9	3.3	2.5	2.1	1.1
¹⁸² Ta	1189	0.19	7.3	0.44	2.9	0.42	1.5	0.37	1.0	0.16	0.39
¹⁷⁸ⁿ Hf	326	0.09	9.9	0.21	2.3	0.22	0.60	0.20	0.32	0.13	0.13
¹⁷⁸ⁿ Hf	426	0.09	11.2	0.21	2.6	0.22	0.63	0.20	0.31	0.13	0.10
¹⁸³ Ta	108	0.25	52.2	0.51	12.7	0.43	4.0	0.32	2.5	0.07	1.22
¹⁸³ Ta	246	0.25	27.8	0.51	6.6	0.43	1.7	0.32	0.91	0.07	0.41
¹⁷³ Lu	172	20.0	34.5	16.1	8.3	6.9	2.5	3.1	1.6	0.85	0.88
¹⁶⁹ Yb	198	24.3	17.0	19.2	4.1	8.1	1.1	3.7	0.70	0.93	0.38
¹⁷¹ Lu	740	25.5	3.9	18.9	1.5	7.5	0.81	3.1	0.56	0.52	0.21
¹⁷² Lu	1094	14.0	2.6	10.2	1.0	3.9	0.51	1.6	0.35	0.24	0.13
¹⁴⁶ Gd	115	1.7	13.1	1.35	3.2	0.59	0.99	0.28	0.63	0.08	0.30
¹⁴⁶ Gd	116	1.7	13.1	1.35	3.2	0.59	0.99	0.28	0.63	0.08	0.30
¹⁴⁶ Eu	747	0.23	1.9	0.35	0.72	0.21	0.40	0.13	0.28	0.07	0.10
¹⁵³ Gd	103	1.4	28.0	1.2	6.8	0.52	2.1	0.25	1.4	0.08	0.66
¹⁴⁸ Gd	alpha	0.061		0.050		0.022		0.011		0.0035	

CED=20 mSv

Nuclide	γ -energy [keV]	Day 1		Day 2		Day 3		Day 4		Day 10	
		urine [Bq]	MDA [Bq]								
¹⁸⁷ W	686	991900	37.3	52080	11.3	2278	5.2	356	3.5	2.1	1.3
¹⁷² Hf	126	28.9	230	69.8	55.8	71.4	17.2	66.6	10.9	42.7	5.0
¹⁸² Ta	1189	3.87	32.2	8.9	12.9	8.5	6.5	7.3	4.4	3.3	1.5
¹⁷⁸ⁿ Hf	326	1.8	44.2	4.3	10.4	4.4	2.7	4.1	1.4	2.6	0.6
¹⁷⁸ⁿ Hf	426	1.8	49.9	4.3	11.7	4.4	2.8	4.1	1.4	2.6	0.4
¹⁸³ Ta	108	5.1	233	10.2	56.7	8.5	17.7	6.5	11.3	1.3	5.4
¹⁸³ Ta	246	5.1	124	10.2	29.3	8.5	7.5	6.5	4.0	1.3	1.8
¹⁷³ Lu	172	400	154	321	37.0	138	10.9	62.3	6.9	17.0	3.9
¹⁶⁹ Yb	198	486	76.1	384	18.1	163	5.0	73.1	3.1	18.5	1.7
¹⁷¹ Lu	740	511	17.4	378	6.5	149	3.6	62.1	2.4	10.3	0.9
¹⁷² Lu	1094	280	11.4	203	4.5	78.7	2.2	32.1	1.5	4.8	0.5
¹⁴⁶ Gd	115	33.6	58.7	27.0	14.2	11.8	4.4	5.6	2.8	1.7	1.3
¹⁴⁶ Gd	116	33.6	58.7	27.0	14.2	11.8	4.4	5.6	2.8	1.7	1.3
¹⁴⁶ Eu	747	4.7	8.2	7.0	3.2	4.3	1.8	2.5	1.2	1.3	0.4
¹⁵³ Gd	103	28.8	125	23.4	30.4	10.3	9.5	4.9	6.1	1.6	2.9
¹⁴⁸ Gd	alpha	1.23		1.00		0.44		0.21		0.07	

5. Discussion

5.1. Minimum detectable activity

MDA defined by equation (24) is affected by uncertainties in the time of measurement t , detector efficiency ε , and gamma line intensity P_γ . In gamma ray spectroscopy measuring samples in a laboratory, these uncertainties are typically negligible compared to the uncertainty in L_d . For this reason, they are often neglected in the calculation of MDA. In this work, we followed this approach even though the uncertainty in the detector efficiency ε due to the variability in person size may be quite large. More work is needed to estimate the uncertainties associated with body size variability and special distribution of inhaled activity.

The detection limit L_d depends on the mean number of counts for the background N_B when the signal S is not present. In this work, only the nuclides providing large contributions to the CED were considered, and thus the total continuum is somewhat underestimated. In practice, the value will be slightly larger and thus the L_d and consequently MDA will also be larger.

In principle, it is possible to perform the calculation for all 1000 released radionuclides. In practice, however, the main problem is that Nucleonica does not accept more than 20 radionuclides in the input file; the resulting XLSX files are already large (hundreds of MB). Owing to the web interface, the upload and download must be done manually, resulting in labor intensive calculation. Batch processing would require on-site version of Nucleonica, which was not available to the authors.

The determination of the net and background areas of a peak depends on the presence of other peaks in the considered energy region. In this work, we assumed that the user could determine these values for every input peak; the calculation was based on the spectrum continuum provided by Nucleonica. In practice, the determination of the peak background may be less straightforward.

Determination of the MDA, expressed for the major radionuclides and for different time periods following an intake, requires a realistic estimation of the amount of scattered radiation. Presented simulations using Nucleonica underestimate this amount. Accurate values would be obtained using the Monte Carlo simulations described above.

5.2. Accuracy of the CED measurement

The method for the determination of CED can be improved via (i) Monte Carlo simulations of the response of the whole-body counting detector system, and (ii) determination of the contaminated person's attenuation using two additional absorbing layers, for instance compact bone and soft tissue.

5.3. Strategy for lung and urine measurements

The results for lung measurements with the WBC system, Table 15 and Appendix 8.5, show that quantification of lung burden of 10 of the 16 most prominent radionuclides according to expected CED is possible for a CED of about 1 mSv and above. Those radionuclides, ^{148}Gd included, are expected to contribute to about 80% of the total CED from the full set of radionuclides released, being a good indicator of the total CED. Measurements can be made both early (days) and late (weeks) after exposure (quantification of ^{187}W requires lung measurements shortly after exposure). However, the body composition affects the MDA, and for obese persons, the

chances of detecting, e.g., Gd-isotopes would become more difficult, at least close in time after the exposure.

Efforts should be made to repeat WBC counting at least 1-2 times during the first weeks to follow the lung excretion rate for the different radionuclides. This should be done to verify the absorption types and parameters used in the dose calculations (IMBA/Taurus) based on ICRP data. If a significant deviation of lung clearance is observed for a particular radionuclide, the CED will be affected, and therefore revised IMBA/Taurus calculations need to be made. Quantification of lung burden at lower exposures, e.g., at CED of tenths of mSv would be challenging for any of the radionuclides in the release mixture. However, by prolonging the measurement times and by using spectral information from all 3 HPGe detectors, the MDA can be improved.

The data of urine excretion, Table 16, show that at moderate exposures, CED = 1 mSv or less, it will be difficult to assess the CED based on urine samples since the MDA for many of the important radionuclides is too high. E.g., ^{146}Gd and ^{153}Gd levels are too low, which makes predictions of ^{148}Gd impossible, thus would require radiochemical analysis. However, by using larger HPGe-detectors and/or preconcentration of urine before γ -spectrometric analysis, MDA can be improved and make quantification of more radionuclides possible. At larger exposure levels, e.g., CED of tens of mSv, quantification of most of the important radionuclides is possible, especially if the urine sampling is done a few days after exposure (see Table 16).

Urine sampling should be repeated in time to follow the urine excretion dynamics in order to compare with IMBA/Taurus model calculations.

The study shows that WBC is essential for estimating the CED at moderate exposure levels since urine excretion levels are too low for quantification. For screening purposes, i.e., screening of groups of individuals with expected low exposures ($>1\text{mSv}$), neither WBC nor urine measurements will be quantitative. However, by radiochemical analysis of ^{148}Gd in urine, considerably lower MDA can be achieved and could therefore be used as a proxy for evaluating the total CED from inhalation as soon as the nuclide vectors are established.

6. Conclusions

We have developed a method to determine the committed effective dose resulting from inhalation of radionuclides that can be released during an accident at the ESS. The method combines results from gamma spectrometry measurements using a whole-body counting (WBC) system and an analysis of bioassays. Using computer simulations, we demonstrated that peaks of, e.g., ^{153}Gd at 97.4 and 103.2 keV, the peak of ^{146}Gd at 154.6 keV, and the peak of ^{146}Eu at 747.2 keV are well-shaped and could be used for the determination of the activity of these radionuclides in lungs. The activity of ^{148}Gd in the lungs is then determined from fractions between activities of these radionuclides; these fractions, obtained by computer simulations, are described in ESS and SSM documents. In addition, radiochemical analysis of ^{148}Gd in selected urine samples may be needed to verify the Gd isotope relations. Biokinetics models in the IMBA and Taurus code are then used to calculate the resulting committed effective dose. Simulations were performed for a list of selected radionuclides in the activity release. It is assumed that the inclusion of all radionuclides in the activity release would somewhat increase the background radiation, but it would not affect the ability of the method to determine the net areas of well-shaped peaks of ^{146}Gd , ^{153}Gd , and ^{146}Eu .

An automated method for calculating the minimum detectable activity was developed, and results for the HPGe WBC system at Westinghouse (lung burden measurements) and a laboratory HPGe detector system (urine measurements) are presented. The method utilizes information about the theoretical number of counts for the continuum part of the spectrum calculated by Nucleonica. The results show that lung burden can be evaluated for a majority of the most prominent radionuclides in a release, at dose levels (CED) around 1 mSv and above, and by repeated WBC measurements over periods of weeks the excretion dynamics of the radionuclides in the lung can be obtained to provide more precise dose assessment.

Unfortunately, the simulations show that the levels of radionuclide excretion in urine are for most radionuclides low, and for corresponding dose levels (CED) of 1 mSv it will not be quantitative (<MDA). Therefore, urine analysis has a limited value at moderate exposures, i.e., it can complement lung burden measurements only at higher exposures.

The method developed here is designed for the WBC system at Westinghouse Electric AB in Västerås. However, it can be easily modified for other radionuclide mixtures and WBC lung burden systems, provided that the detector counting efficiencies are known.

7. Need for further research

7.1. Estimation of the size-related attenuation

The algorithm for the estimation of the size-related parameter h from net areas of two peaks produced by a single radionuclide (section 3.1.2) can be generalized to any number of peaks. For n peaks, $n - 1$ material layers can be considered. Equation (8) can be extended to a system of $n - 1$ equations

$$-\ln \left[\frac{N(E_2)}{N(E_1)} \frac{N^*(E_1)}{N^*(E_2)} \right] = [\mu_1(E_2) - \mu_1(E_1)]h_1 + \dots + [\mu_{n-1}(E_2) - \mu_{n-1}(E_1)]h_{n-1} \quad (34)$$

$$\dots$$

$$-\ln \left[\frac{N(E_n)}{N(E_1)} \frac{N^*(E_1)}{N^*(E_n)} \right] = [\mu_1(E_n) - \mu_1(E_1)]h_1 + \dots + [\mu_{n-1}(E_n) - \mu_{n-1}(E_1)]h_{n-1}, \quad (35)$$

which can be solved for h_1, \dots, h_{n-1} .

Equations (34)–(35) are like those used for material decomposition in computed tomography. A principal component analysis (PCA) of the system showed that the dimensionality of the problem is about 3–4 when statistical noise, biological materials with the atomic number less than 20, and the energy range 20–150 keV is considered [21]. In practical situations, however, the range of useful energies starts at about 35 keV. In this case the dimensionality is about 2 only [22]. It means that a linear combination of linear attenuation coefficients as functions of energy for two base materials, $v_1\mu_1(E) + v_2\mu_2(E)$ approximates any biological material well. Consequently, adding more base materials makes the system of equations ill conditioned. A material base commonly used in CT for the two-material decomposition is for instance the (compact bone, water) doublet. As an alternative to water, soft tissue can also be used.

An implementation of the two additional layers—for instance, compact bone and soft tissue or fat—has the potential to increase the accuracy of the size-specific correction.

7.2. Radiochemical method for ^{148}Gd analysis

Since the dose assessment from inhalation is much dependent on knowledge about the Gd isotopic ratios, where ^{148}Gd is an alpha emitter, a method to radiochemically isolate Gd for subsequent alpha spectrometric measurements is needed. Olszewski et al. 2021 [13] has developed a separation method, which needs to be further developed to handle different sample matrices, e.g., urine and air filters.

References

1. ESS-0051595 AA3.
2. ESS. Annex 1. Comparison ESS-JAERI-model. 2016. Report No.: ESS-0063736.
3. Blixt Buhr AM, Johansson J, Kock P, Boson J, Karlsson S, Lindgren J, et al. Underlag till beredskapsplaneringen kring ESS. Strålsäkerhets myndigheten; 2018 Sep. Report No.: 2018:22.
4. International Commission on Radiological Protection., Committee 2 on Permissible Dose for Internal Radiation. Dose coefficients for intakes of radionuclides by workers: replacement of ICRP publication 61. Oxford: Pergamon; 1995.
5. ICRP. The 2007 Recommendations of the International Commission on Radiological Protection. 2007;
6. ICRP. Human respiratory tract model for radiological protection. ICRP Publication 66. 1994. (Ann. ICRP 24(1-3)).
7. ICRP. Occupational intakes of radionuclides: Part 4. ICRP Publication 141. 2019. (Ann. ICRP 48(2/3)).
8. ICRP. Occupational intakes of radionuclides: Part 3. ICRP Publication 137. 2017. (Ann. ICRP 46(3/4)).
9. ICRP. Occupational intakes of radionuclides: Part 2. ICRP Publication 134. 2016. (Ann. ICRP 45(3/4)).
10. ICRP. Compendium of Dose Coefficients based on ICRP Publication 60. ICRP Publication 119. 2012. (Ann. ICRP 41(Suppl.)).
11. ICRP. Occupational intakes of radionuclides: Part 1. ICRP Publication 130. 2015. (Ann. ICRP 44(2)).
12. ICRP. Guide for the Practical Application of the ICRP Human Respiratory Tract Model. ICRP Supporting Guidance 3. 2002. (Ann. ICRP 32(1-2)).
13. Olszewski G, Lindahl P, Frisk P, Eriksson M, Pettersson HBL. Development of ¹⁴⁸Gd analysis method using stable Gd. *Talanta*. 2021 Jul;229:122295.
14. Barkauskas V, Stenström K. Prediction of the radionuclide inventory in the European Spallation Source target using FLUKA. *Nucl Instrum Methods Phys Res Sect B Beam Interact Mater At.* 2020 May;471:24–32.
15. ICRP. 1990 Recommendations of the International Commission on Radiological Protection. ICRP Publication 60. 1991. Report No.: Ann. ICRP 21 (1-3).
16. ICRP Publication 103 [Internet]. SAGE Publications Ltd. 2022 [cited 2022 May 2]. Available from: <https://uk.sagepub.com/en-gb/eur/icrp-publication-103/book243497>
17. White DR, Booz J, Griffith RV, Spokas JJ, Wilson IJ. Report 44. *J Int Comm Radiat Units Meas.* 1989 Jan 15;os23(1):NP-NP.

18. ISO. ISO 11929-4:2020 Determination of the characteristic limits (decision threshold, detection limit and limits of the coverage interval) for measurements of ionizing radiation — Fundamentals and application — Part 4: Guidelines to applications [Internet]. ISO. [cited 2022 Mar 12]. Available from: <https://www.iso.org/cms/render/live/en/sites/isoorg/contents/data/standard/07/18/71844.html>
19. Gilmore G. Practical gamma-ray spectrometry. Chichester, England ; Hoboken, NJ : Wiley; 2010.
20. Currie LA. Limits for qualitative detection and quantitative determination. Application to radiochemistry. *Anal Chem*. 1968 Mar 1;40(3):586–93.
21. Bornefalk H. XCOM intrinsic dimensionality for low-Z elements at diagnostic energies. *Med Phys*. 2012;39(2):654.
22. Magnusson M, Alm Carlsson G, Sandborg M, Carlsson Tedgren Å, Malusek A. Optimal selection of base materials for accurate dual-energy computed tomography: comparison between the Alvarez-Makovski method and DIRA. 2020.

8. Appendix

8.1. Decay radiation

8.1.1. Decay radiation for ^{146}Gd

Parent Nucleus	Parent E(level)	Parent Jπ	Parent T _{1/2}	Decay Mode	GS-GS Q-value (keV)	Daughter nucleus
$^{146}_{\text{Gd}} \text{ 64}$	0.0	0+	48.27 d 9	ε: 100 %	1032 7	$^{146}_{\text{Eu}} \text{ 63}$

Gamma and X-ray radiation:

Energy (keV)	Intensity (%)	Dose (MeV/Bq-s)
XR I	5.85	33.0 % 14
XR kα2	40.902	52.0 % 13
XR kα1	41.542	93.0 % 23
XR kβ3	46.905	9.30 % 23
XR kβ1	47.038	18.0 % 4
XR kβ2	48.249	5.96 % 14
	76.54 1	0.023 % 9
	114.71 2	44.3 % 8
	115.51 2	44.3 % 8
	154.57 2	46.9 % 8
	230.51 20	0.09 % 5
	267.8 2	0.038 % 19
	383.5 1	0.047 % 19
	421.6 1	0.082 % 9
	576.0 2	0.066 % 9
		1.8E-5 7
		0.0508 9
		0.0512 9
		0.0725 13
		2.1E-4 11
		1.0E-4 5
		1.8E-4 7
		3.4E-4 4
		3.8E-4 5

8.1.2. Decay radiation for ^{148}Gd

Parent Nucleus	Parent E(level)	Parent J π	Parent T _{1/2}	Decay Mode	GS-GS Q-value (keV)	Daughter Nucleus
$^{148}_{64}\text{Gd}$	0.0	0+	74.6 y 30	α : 100 %	3271.21 3	$^{144}_{62}\text{Sm}$

Alphas:

Energy (keV)	Intensity (%)	Dose (MeV/Bq-s)
--------------	---------------	-------------------

3182.690 24	100 %	3.182690
-------------	-------	----------

8.1.3. Decay radiation for ^{153}Gd

Parent Nucleus	Parent E(level)	Parent J π	Parent T _{1/2}	Decay Mode	GS-GS Q-value (keV)	Daughter Nucleus
$^{153}_{64}\text{Gd}$	0	3/2-	240.4 d 10	ϵ : 100 %	483.6 12	$^{153}_{63}\text{Eu}$

Gamma and X-ray radiation:

Energy (keV)	Intensity (%)	Dose (MeV/Bq-s)	
XR I	5.85	22.6 % 11	0.00132 6
	14.06383 20	0.018 % 3	2.5E-6 4
	19.81296 19	7E-5 %	1.4E-8
XR k α 2	40.902	34.9 % 12	0.0143 5
XR k α 1	41.542	62.4 % 20	0.0259 8
XR k β 3	46.905	6.24 % 20	0.00293 10
XR k β 1	47.038	12.1 % 4	0.00568 18
XR k β 2	48.249	4.00 % 13	0.00193 6
	69.67300 13	2.42 % 7	0.00169 5
	75.42213 23	0.078 % 3	5.91E-5 24
	83.36717 21	0.196 % 7	1.63E-4 6
	89.48595 22	0.069 % 4	6.2E-5 4
	97.43100 21	29.0 %	0.0283
	103.18012 17	21.1 % 6	0.0218 6
	172.85307 21	0.0360 % 20	6.2E-5 3

and

Decay radiation for ^{146}Eu

Parent Nucleus	Parent E(level)	Parent π	Parent $T_{1/2}$	Decay Mode	GS-GS Q-value (keV)	Daughter Nucleus
$^{146}_{63}\text{Eu}$	0.0	4-	4.61 d 3	ϵ : 100 %	3879 6	$^{146}_{62}\text{Sm}$

Gamma and X-ray radiation:

Energy (keV)	Intensity (%)	Dose (MeV/Bq-s)
XR I	5.64	13.1 % 6
XR $\kappa\alpha_2$	39.522	21.7 % 7
XR $\kappa\alpha_1$	40.118	39.0 % 12
XR $\kappa\beta_3$	45.293	3.89 % 12
XR $\kappa\beta_1$	45.414	7.52 % 23
XR $\kappa\beta_2$	46.578	2.48 % 7
	158.5 8	0.018 % 10
	202.2 4	0.0098 % 20
	210.5 5	0.0059 % 20
	222.33 10	0.0142 % 10
	224.05 3	0.042 % 3
	234.9 2	0.0216 % 11
	267.59 3	0.097 % 8
	271.683 21	0.869 % 24
	295.59 25	0.022 % 5
	372.67 23	0.070 % 23
	376.11 4	0.055 % 9
	380.91 7	0.10 % 4
	394.7 15	0.12 % 4
	397.31 6	0.18 % 7
	397.325 19	0.66 % 7
	399.81 10	0.014 % 4
	403.73 4	0.073 % 8
	410.766 19	0.644 % 19
	415.52 16	0.0058 % 20

	422.3 3	0.013 % 4	5.4E-5 17
	430.386 18	4.70 % 13	0.0202 6
	441.43 12	0.026 % 3	1.17E-4 13
	445.0 3	0.20 % 4	8.7E-4 18
	449.2 5	0.13 % 5	5.7E-4 22
	459.35 6	0.21 % 6	9E-4 3
	459.4 2	0.052 % 4	2.39E-4 19
	467.762 25	0.067 % 4	3.12E-4 19
	471.67 4	0.0358 % 19	1.69E-4 9
Annihil.	511.0	9.7 % 6	
	522.2 2	0.136 % 5	7.12E-4 25
	532.87 7	0.130 % 8	7.0E-4 4
	534.1 2	0.082 % 5	4.4E-4 3
	534.26 9	0.13 % 4	6.8E-4 21
	544.32 13	0.14 % 6	7E-4 3
	548.4 10	0.014 % 4	7.5E-5 22
	549.1 10	0.14 % 3	7.5E-4 16
	550.4 3	0.034 % 6	1.9E-4 3
	553.35 11	0.37 % 7	0.0021 4
	553.8 10	0.026 % 8	1.4E-4 4
	569.11 10	0.020 % 6	1.1E-4 3
	569.53 5	0.116 % 7	6.6E-4 4
	575.64 16	0.021 % 6	1.2E-4 3
	583.76 3	0.112 % 6	6.5E-4 4
	600.4 10	0.20 % 4	0.00118 24
	606.22 22	0.017 % 4	1.01E-4 24
	611.46 25	0.015 % 4	9.0E-5 24
	621.85 3	0.544 % 18	0.00339 11
	624.75 14	0.080 % 10	5.0E-4 6
	632.888 40	1.28 % 3	0.00807 20
	633.083 23	35.7 % 10	0.226 7
	634.137 21	44.8 % 13	0.284 8
	636.22 13	0.19 % 8	0.0012 5
	653.0 3	0.024 % 8	1.5E-4 5

664.65 14	0.5 % 4	0.003 3
665.424 15	10.32 % 25	0.0687 17
686.54 10	0.0316 % 24	2.17E-4 17
702.099 19	3.81 % 13	0.0267 9
703.089 22	3.73 % 13	0.0262 9
703.46 6	0.106 % 20	7.5E-4 14
704.774 19	1.87 % 5	0.0132 4
721.24 8	0.053 % 4	3.8E-4 3
733.97 13	0.047 % 6	3.5E-4 4
736.55 11	0.078 % 8	5.8E-4 6
742.65 15	0.71 % 10	0.0052 7
747.159 16	98 % 3	0.733 20
749.8 15	0.049 % 5	3.7E-4 4
753.80 8 ?	0.026 % 3	2.00E-4 23
760.963 23	0.092 % 3	7.0E-4 3
766.838 23	0.090 % 3	6.94E-4 23
775.533 25	0.095 % 3	7.4E-4 3
783.96 3	0.0471 % 22	3.69E-4 17
791.107 19	0.454 % 13	0.00359 10
804.67 6	0.093 % 3	7.5E-4 3
812.21 3	0.079 % 3	6.39E-4 23
814.70 25	0.0086 % 16	7.0E-5 13
823.21 3	0.0551 % 22	4.54E-4 18
826.32 12	0.0135 % 20	1.12E-4 16
833.1 2	0.0118 % 10	9.8E-5 8
833.11 9	0.0120 % 13	1.00E-4 11
837.72 8	0.0060 % 8	5.0E-5 7
838.02 15	0.0048 % 10	4.0E-5 8
840.94 10	0.0201 % 11	1.69E-4 10
843.72 9	0.0032 % 7	2.7E-5 6
844.72 15	0.054 % 20	4.6E-4 17
845.81 10	0.036 % 8	3.1E-4 7
848.84 9	0.14 % 3	0.0012 3
848.85 30	0.018 % 7	1.5E-4 6

850.49 10	0.232 % 14	0.00197 11
852.28 12	0.038 % 9	3.3E-4 8
865.353 23	0.136 % 4	0.00118 3
870.55 6	0.011 % 4	9E-5 3
881.5 2	0.0353 % 21	3.11E-4 18
881.55 3	0.0348 % 17	3.07E-4 15
888.46 15	1.08 % 25	0.0096 22
889.44 15	0.58 % 17	0.0051 15
891.29 20	0.12 % 3	0.0010 3
899.486 22	1.35 % 10	0.0122 9
900.797 18	2.93 % 21	0.0264 19
903.98 25	0.050 % 13	4.5E-4 12
914.031 16	0.618 % 18	0.00565 17
918.94 6	0.070 % 3	6.4E-4 3
930.39 11	0.020 % 5	1.8E-4 5
937.29 4	0.033 % 4	3.1E-4 4
937.33 8	0.0022 % 4	2.0E-5 4
937.68 8	0.043 % 16	4.0E-4 15
941.30 3	0.158 % 6	0.00149 5
948.14 15	0.0080 % 13	7.6E-5 12
968.83 9	0.046 % 3	4.5E-4 3
974.77 8	0.146 % 22	0.00142 21
974.9 1	0.098 % 5	9.6E-4 5
976.51 5	0.19 % 7	0.0018 7
979.09 10	0.044 % 3	4.3E-4 3
989.49 4	0.0648 % 25	6.42E-4 25
998.7 3	0.0045 % 13	4.5E-5 13
1004.3 4	0.010 % 3	1.0E-4 3
1009.27 11	0.0117 % 12	1.18E-4 12
1017.08 16	0.0172 % 21	1.75E-4 21
1022.05 9	0.023 % 7	2.3E-4 7
1027.26 5	0.072 % 3	7.4E-4 3
1028.10 5	0.021 % 3	2.1E-4 3
1030.274 37	0.0168 % 14	1.73E-4 15

1036.71 10	0.051 % 3	5.3E-4 3
1038.35 20	0.024 % 3	2.4E-4 3
1047.36 5	0.0488 % 17	5.11E-4 18
1057.62 10	2.3 % 4	0.024 4
1058.71 10	3.9 % 4	0.042 4
1063.6 7	0.009 % 3	9E-5 3
1068.32 7	0.0336 % 18	3.59E-4 19
1078.29 7	0.0373 % 15	4.02E-4 16
1086.637 15	0.562 % 16	0.00611 17
1088.83 8	0.031 % 3	3.4E-4 3
1090.844 21	0.214 % 6	0.00233 7
1094.10 11	0.0270 % 24	3.0E-4 3
1094.10 4	0.058 % 22	6.3E-4 24
1110.03 16	0.022 % 3	2.4E-4 3
1110.79 5	0.013 % 3	1.4E-4 3
1116.566 15	0.421 % 12	0.00470 13
1120.79 9	0.0261 % 16	2.92E-4 17
1132.05 7	0.12 % 3	0.0013 3
1133.11 7	0.69 % 3	0.0078 4
1137.66 13	0.042 % 3	4.8E-4 3
1137.8 3	0.042 % 3	4.8E-4 3
1150.626 15	2.11 % 6	0.0243 7
1155.08 4	0.188 % 7	0.00218 8
1161.75 14	0.0124 % 15	1.44E-4 17
1166.67 10	0.017 % 3	1.9E-4 3
1175.09 11	0.109 % 19	0.00128 22
1175.09 11	0.14 % 3	0.0016 3
1176.522 23	1.61 % 5	0.0189 6
1184.93 3	0.130 % 4	0.00155 5
1186.98 10	0.0309 % 19	3.67E-4 22
1190.1 3	0.0629 % 24	7.5E-4 3
1191.01 10	0.013 % 4	1.5E-4 5
1198.3 10	0.008 % 7	9E-5 8
1208.82 8	0.0291 % 19	3.52E-4 24

1214.209 21	0.313 % 9	0.00380 11
1225.39 11	0.0133 % 14	1.63E-4 17
1231.03 10	0.0164 % 16	2.02E-4 20
1239.86 20	0.0080 % 19	1.00E-4 23
1255.72 6	0.029 % 4	3.7E-4 5
1260.89 9	0.0234 % 18	2.96E-4 23
1277.55 6	0.0425 % 20	5.4E-4 3
1293.48 13	0.114 % 11	0.00147 14
1297.028 16	5.37 % 15	0.0696 19
1303.46 4	0.077 % 4	0.00101 5
1325.35 4	0.088 % 3	0.00117 5
1330.33 20	0.029 % 4	3.9E-4 5
1332.74 4	0.189 % 8	0.00252 10
1335.52 9	0.131 % 6	0.00176 9
1336.01 9	0.043 % 3	5.8E-4 4
1345.176 22	0.154 % 5	0.00207 7
1347.79 6	0.0425 % 20	5.7E-4 3
1356.145 17	0.315 % 9	0.00427 12
1366.69 8	0.0344 % 24	4.7E-4 3
1371.33 10	0.008 % 3	1.1E-4 4
1373.29 15	0.014 % 5	1.9E-4 7
1378.135 19	0.532 % 16	0.00733 22
1385.60 6	0.12 % 7	0.0016 10
1385.6 3	0.0579 % 23	8.0E-4 3
1406.98 3	1.72 % 5	0.0242 7
1408.66 3	1.23 % 4	0.0173 5
1415.859 21	0.215 % 6	0.00304 9
1419.70 3	0.129 % 6	0.00182 8
1445.136 23	0.364 % 12	0.00526 17
1447.12 9	0.091 % 18	0.0013 3
1448.1 2	0.18 % 7	0.0026 10
1448.21 6	0.091 % 3	0.00132 5
1469.86 7	0.096 % 4	0.00141 6
1470.21 4	0.020 % 6	2.9E-4 9

1471.64 9	0.068 % 3	1.00E-3 5
1475.3 3	0.011 % 3	1.6E-4 4
1477.83 17	0.029 % 10	4.3E-4 15
1484.72 8	0.080 % 4	0.00119 6
1488.48 13	0.034 % 4	5.1E-4 6
1491.16 3	0.026 % 3	3.8E-4 4
1496.39 10	0.010 % 3	1.5E-4 4
1498.35 14	0.0078 % 23	1.2E-4 3
1500.44 3	0.126 % 5	0.00188 7
1517.000 20	0.667 % 19	0.0101 3
1522.712 19	0.88 % 3	0.0134 4
1533.711 18	6.05 % 19	0.093 3
1535.93 5	0.173 % 15	0.00265 23
1542.56 3	0.104 % 4	0.00160 6
1550.98 11	0.15 % 3	0.0023 4
1551.99 11	0.10 % 3	0.0015 5
1565.02 20	0.006 % 6	9E-5 9
1568.93 10	0.037 % 5	5.8E-4 8
1580.16 18	0.0126 % 17	2.0E-4 3
1587.53 8	0.011 % 7	1.7E-4 11
1588.53 8	0.014 % 7	2.2E-4 11
1592.04 6	0.17 % 3	0.0027 5
1593.05 6	0.17 % 3	0.0027 5
1596.66 7	0.097 % 4	0.00155 7
1633.30 3	0.410 % 12	0.00670 19
1648.00 3	0.572 % 21	0.0094 3
1649.76 10	0.132 % 17	0.0022 3
1653.72 8	0.0562 % 22	9.3E-4 4
1663.42 6	0.0645 % 23	0.00107 4
1667.0 7	0.014 % 6	2.3E-4 10
1681.94 13	0.0214 % 17	3.6E-4 3
1686.397 21	0.625 % 18	0.0105 3
1691.643 22	0.411 % 12	0.00695 20
1711.844 22	0.207 % 6	0.00354 11

1724.07 6	0.069 % 10	0.00118 17
1725.08 6	0.059 % 10	0.00102 17
1728.76 7	0.012 % 3	2.0E-4 5
1743.69 3	0.0371 % 19	6.5E-4 3
1756.08 3	0.91 % 3	0.0160 6
1766.277 21	0.665 % 19	0.0117 3
1784.762 13	0.708 % 21	0.0126 4
1796.89 8	0.0341 % 19	6.1E-4 3
1802.76 7	0.153 % 8	0.00276 15
1804.79 24	0.036 % 11	6.6E-4 20
1818.78 3	0.123 % 4	0.00223 7
1823.90 10	0.0085 % 19	1.6E-4 3
1840.52 6	0.020 % 8	3.6E-4 14
1857.33 5	0.051 % 10	9.5E-4 18
1857.92 5	0.091 % 10	0.00170 19
1858.34 5	0.058 % 10	0.00108 18
1863.29 17	0.0141 % 13	2.63E-4 24
1869.86 25	0.0072 % 16	1.3E-4 3
1878.62 3	0.147 % 10	0.00276 19
1879.63 3	0.078 % 10	0.00148 19
1896.85 19	0.008 % 4	1.5E-4 7
1897.85 19	0.008 % 4	1.5E-4 7
1898.17 8	0.015 % 4	2.8E-4 7
1902.45 6	0.0385 % 18	7.3E-4 3
1931.087 20	1.19 % 4	0.0229 7
1937.57 11	0.075 % 5	0.00144 10
1944.3 3	0.0079 % 19	1.5E-4 4
1948.65 6	0.074 % 3	0.00143 6
1956.97 4	0.122 % 4	0.00238 7
1978.20 6	0.0502 % 20	9.9E-4 4
1980.79 3	0.145 % 7	0.00288 13
1987.44 15	0.012 % 7	2.3E-4 14
1988.45 15	0.017 % 7	3.3E-4 14
1994.0 10	0.014 % 4	2.7E-4 8

1995.75 9	0.285 % 12	0.00570 24
1998.00 15	0.087 % 12	0.00174 24
2004.25 11	0.0291 % 24	5.8E-4 5
2010.37 4	0.059 % 10	0.00118 20
2011.38 4	0.137 % 10	0.00276 20
2017.40 13	0.0229 % 17	4.6E-4 3
2037.86 7	0.071 % 3	0.00146 6
2049.96 8	0.027 % 4	5.6E-4 8
2050.97 8	0.114 % 15	0.0023 3
2052.71 5	0.66 % 3	0.0136 5
2072.50 15	0.0075 % 9	1.55E-4 19
2080.02 15	0.6 % 3	0.013 5
2081.11 15	1.5 % 3	0.031 5
2081.7 3	0.098 % 10	0.00204 21
2095.64 20	0.023 % 3	4.7E-4 6
2096.64 20	0.023 % 3	4.7E-4 6
2103.16 5	0.074 % 3	0.00155 7
2132.09 10	0.0233 % 12	4.98E-4 25
2137.08 4	0.118 % 4	0.00252 8
2149.2 3	0.029 % 10	6.3E-4 21
2155.76 3	0.519 % 15	0.0112 3
2158.92 13	0.0051 % 22	1.1E-4 5
2164.86 5	0.0542 % 19	0.00117 4
2203.73 3	0.171 % 5	0.00376 11
2210.35 6	0.0588 % 24	0.00130 5
2221.64 5	0.092 % 4	0.00205 10
2224.98 15	0.051 % 3	0.00114 7
2227.2 4	0.0098 % 10	2.18E-4 22
2244.71 4	0.158 % 5	0.00355 11
2267.49 4	0.436 % 14	0.0099 3
2273.4 15	0.047 % 5	0.00107 11
2310.81 8	0.0204 % 11	4.72E-4 24
2320.54 4	0.095 % 3	0.00221 7
2345.91 30	0.392 % 12	0.0092 3

2358.17 13	0.0299 % 19	7.1E-4 4
2360.49 14	0.0293 % 19	6.9E-4 4
2368.93 22	0.0077 % 9	1.81E-4 21
2389.00 17	0.0559 % 15	0.00134 3
2389.13 4	0.153 % 7	0.00366 16
2400.94 4	0.240 % 9	0.00577 22
2404.74 22	0.0124 % 11	3.0E-4 3
2436.74 4	0.93 % 3	0.0226 6
2484.39 8	0.0198 % 9	4.92E-4 22
2491.51 4	0.179 % 6	0.00445 15
2497.46 5	0.0620 % 21	0.00155 5
2544.21 6	0.0483 % 17	0.00123 4
2582.51 11	0.0097 % 7	2.51E-4 18
2591.11 8	0.0188 % 7	4.88E-4 18
2621.56 11	0.0095 % 6	2.49E-4 16
2629.50 5	0.0652 % 21	0.00172 6
2644.43 5	0.106 % 4	0.00280 9
2650.35 17	0.0077 % 6	2.03E-4 16
2650.35 17 ?	0.0077 % 6	2.03E-4 16
2671.65 5	0.0389 % 13	0.00104 4
2680.57 7	0.0175 % 7	4.68E-4 18
2724.70 6	0.0302 % 11	8.2E-4 3
2762.04 8	0.0143 % 7	3.96E-4 18
2770.12 8	0.0188 % 8	5.22E-4 22
2798.97 6	0.0350 % 13	9.8E-4 4
2845.0 3	1.0E-3 % 3	2.8E-5 8
2858.2 3	0.0020 % 5	5.6E-5 14
2878.76 10	0.0064 % 5	1.84E-4 15
2904.87 9	0.0386 % 25	0.00112 7
2906.99 13	0.0151 % 22	4.4E-4 6
2946.10 10	0.0080 % 9	2.4E-4 3
2968.41 18	0.00284 % 20	8.4E-5 6
2973.3 4	7.8E-4 % 20	2.3E-5 6
2993.61 24	0.00196 % 20	5.9E-5 6

3002.24 12	0.0061 % 3	1.83E-4 10
3038.50 23	8.8E-4 % 10	2.7E-5 3
3042.85 8	0.0026 % 5	7.8E-5 15

8.2. Simulated gamma spectra

Simulated gamma spectra are in Figure 28-33. These spectra include peaks from daughter products; the acquisition time of 1 h is too short for a noticeable build-up of such products.

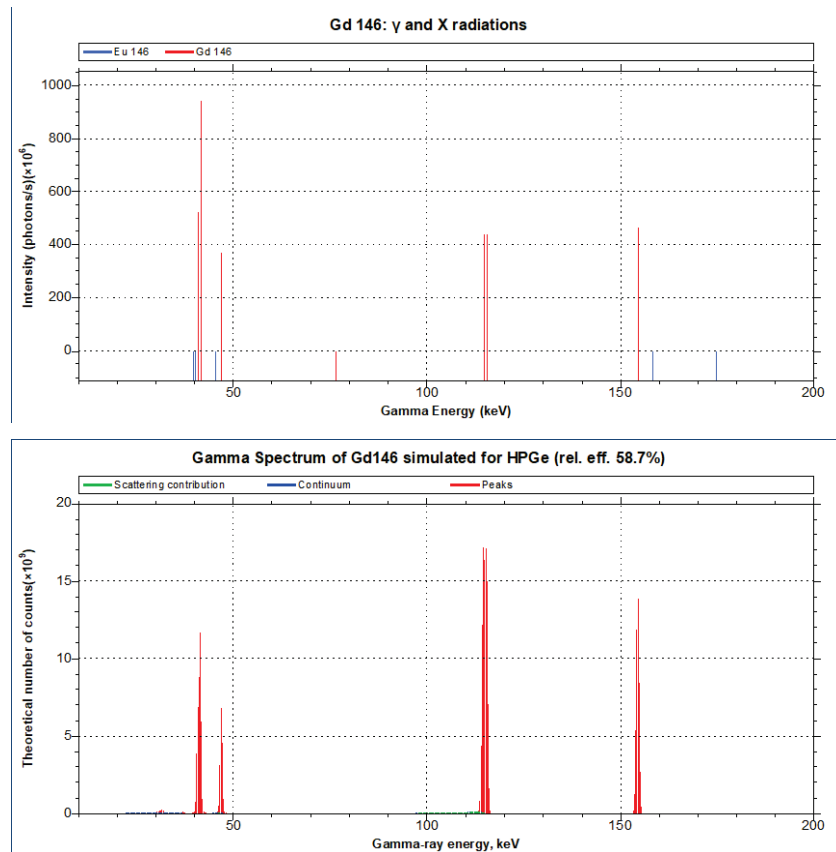


Figure 28. Gamma spectrum of ^{146}Gd for the activity of 1GBq. (a) Theoretical energy lines. (b) Detector response simulation for the acquisition time of 1h.

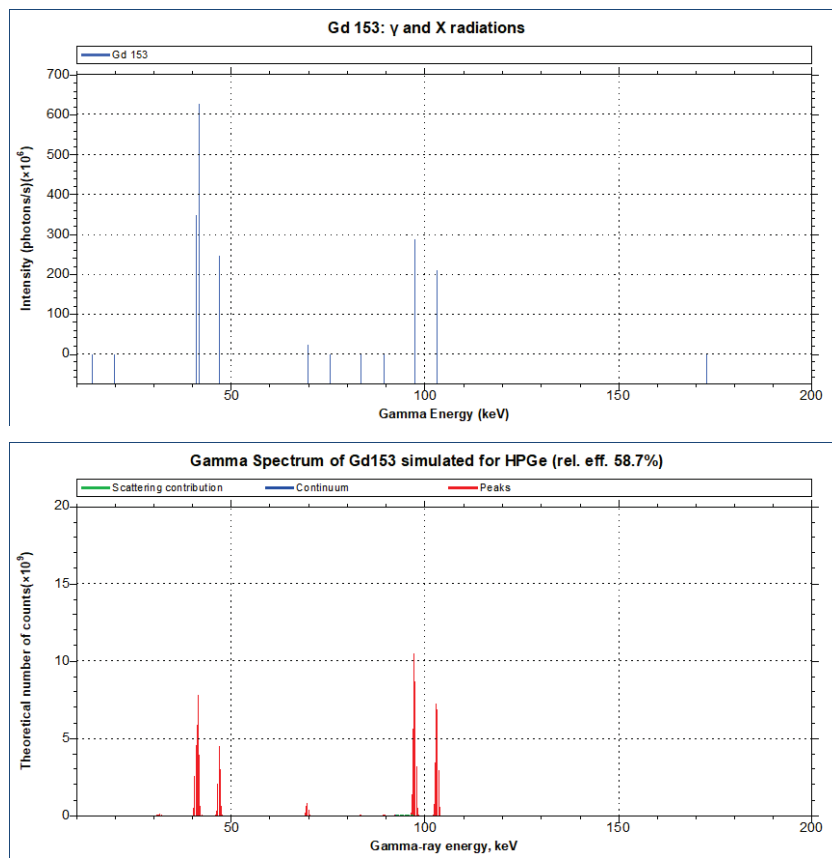


Figure 29. Gamma spectrum of ^{153}Gd for the activity of 1GBq. (a) Theoretical energy lines. (b) Detector response simulation for the acquisition time of 1h.

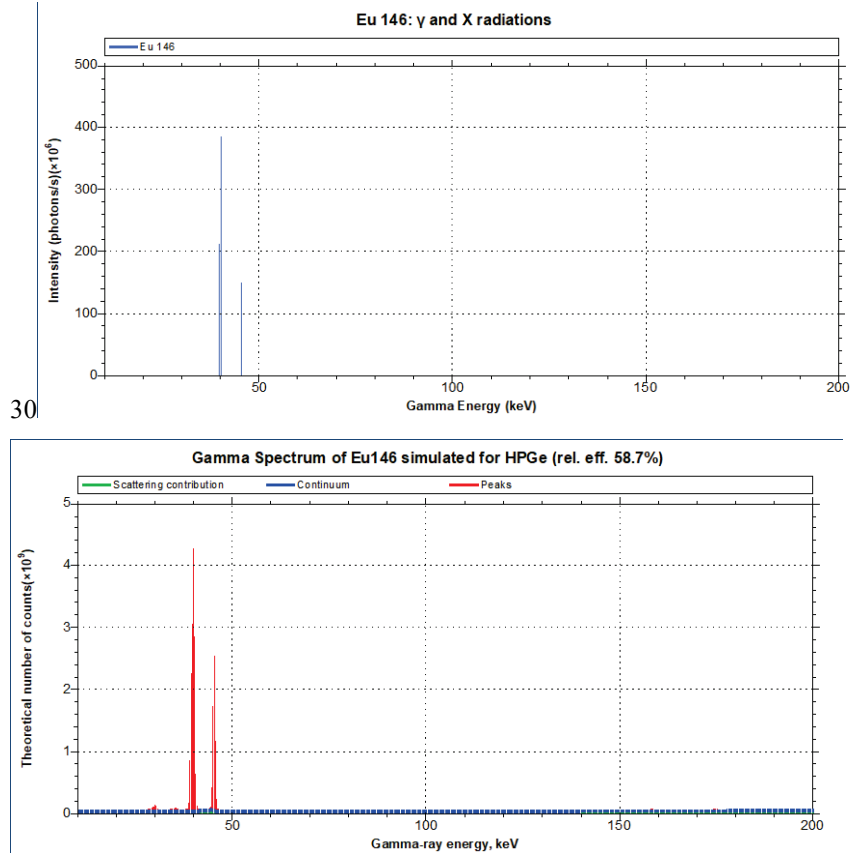


Figure 30. Gamma spectrum of ^{146}Eu for the activity of 1GBq. (a) Theoretical energy lines. (b) Detector response simulation for the acquisition time of 1h.

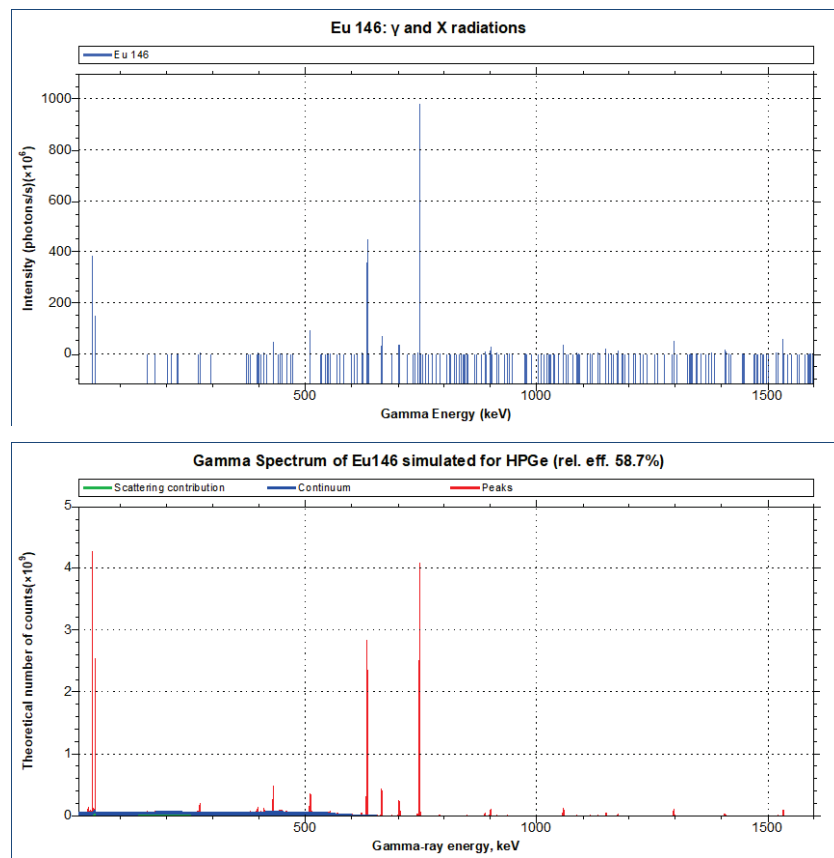


Figure 31. The same as in Figure 30 for the energy range 10 – 1600 keV.

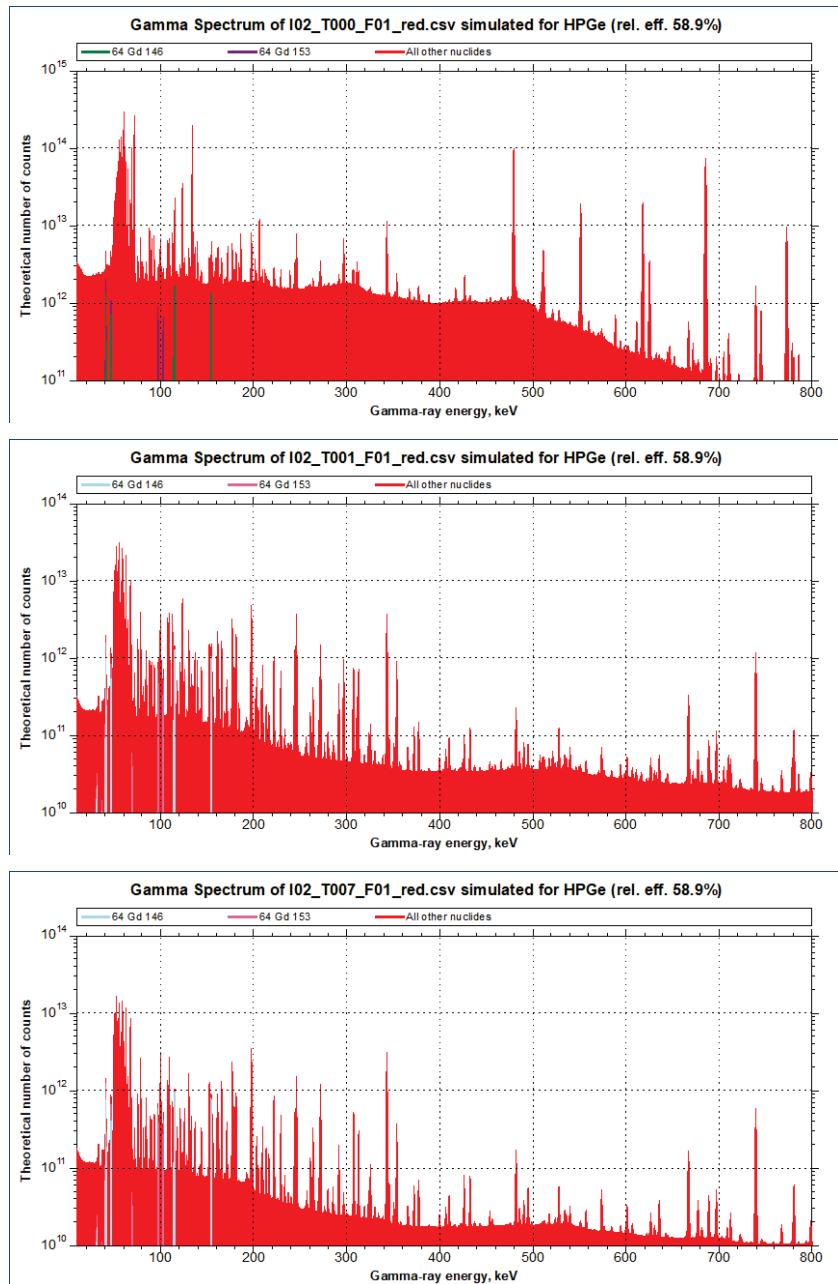


Figure 32. Simulated gamma spectra for ESS activity intake 02 at 0, 1, and 7 days after inhalation. Energy range 10-800keV.

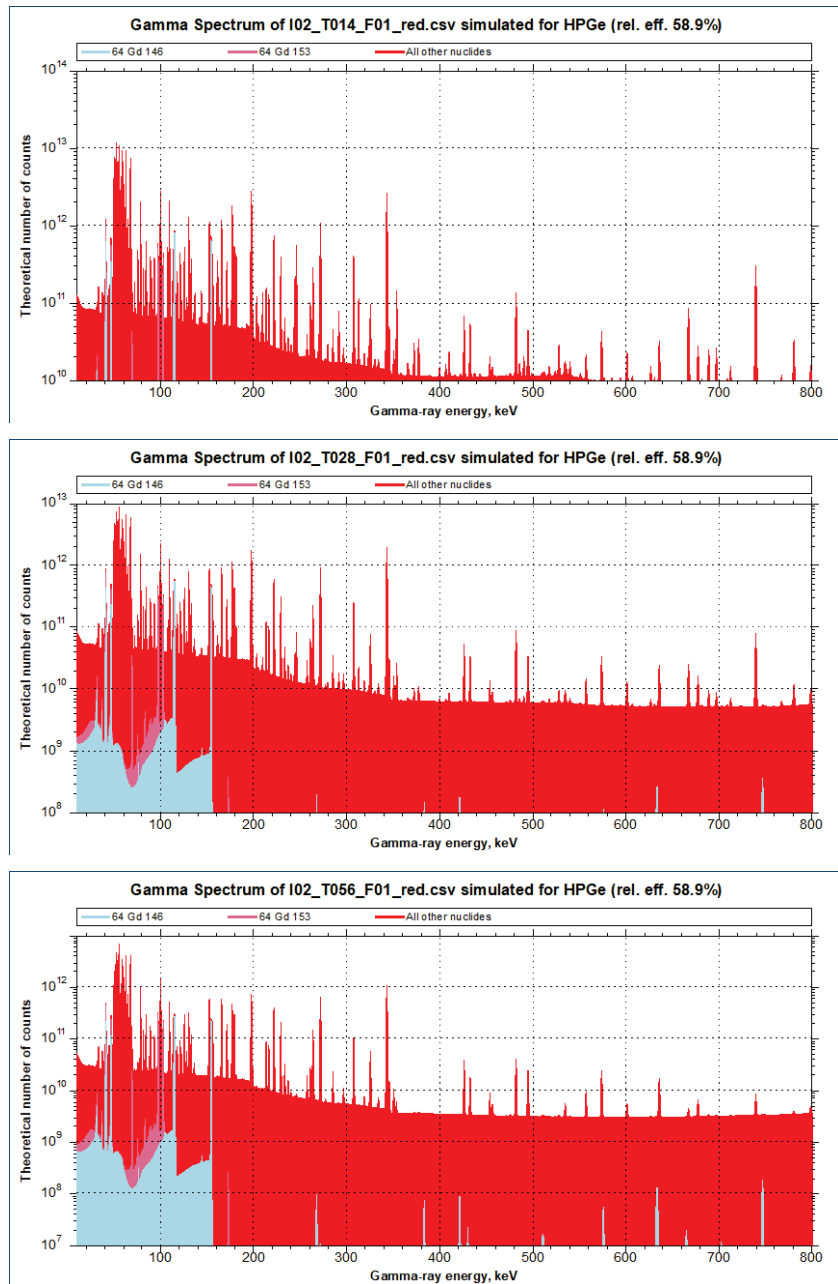


Figure 33. The same as Figure 32 for 14, 28, and 56 days after inhalation.

8.3. IMBA

The software IMBA is available in three standard versions (lite, plus and pro). IMBA bases its calculations on parameters from ICRP 68 and 72. Users can specify their own parameter values. The new internal dosimetry software, Taurus, uses the latest data from ICRP². Main screen of IMBA is shown in Figure 34.

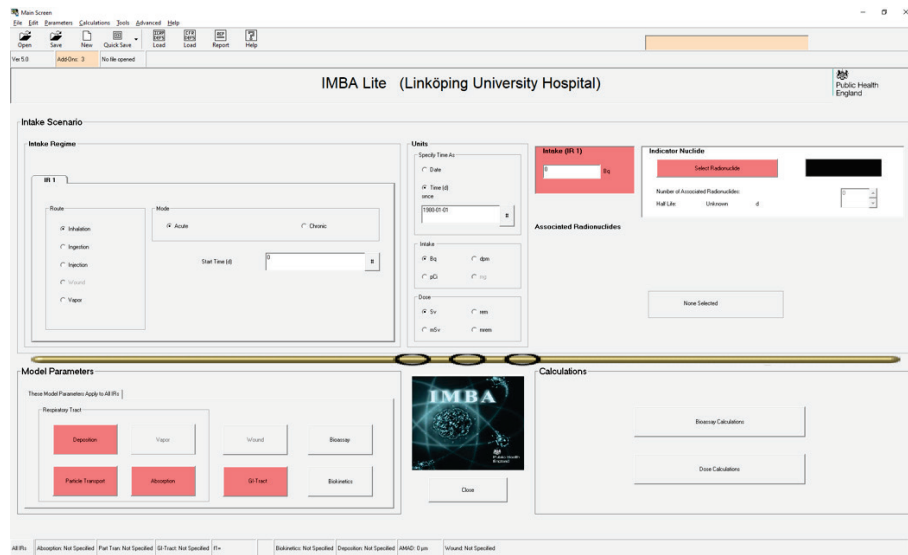


Figure 34. The main screen

The main screen is divided into Intake scenario and Model parameters. Intake scenario (top main panel) is divided into Intake regime, units, radionuclide, and Intake.

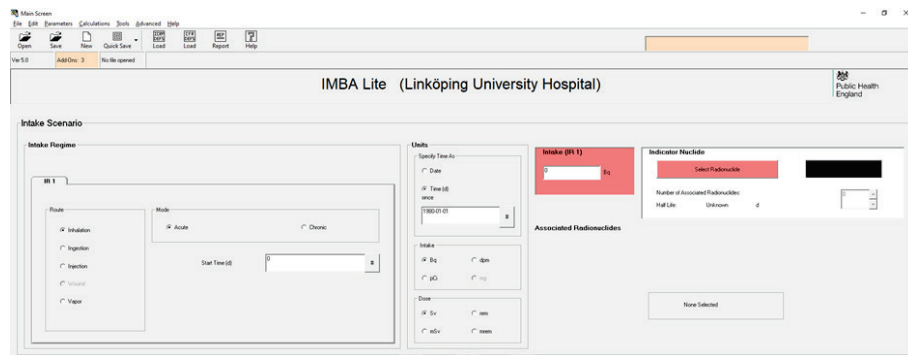


Figure 35. Intake scenario panel

² <https://www.phe-protectionservices.org.uk/imba/>

Intake Scenario

Intake Regimes

Enter Number of Intake Regimes (1-10)

IR 1

Route	Mode
<input checked="" type="radio"/> Inhalation	<input checked="" type="radio"/> Acute
<input type="radio"/> Ingestion	<input type="radio"/> Chronic
<input type="radio"/> Injection	
<input type="radio"/> Wound	
<input type="radio"/> Vapor	

Start Time(d) #

Units

Specify Time As

Date

Time (d)

since #

Intake

Bq dpm

pCi mg

Dose

Sv rem

mSv mrem

Figure 36. Intake regimes sub-panel and units sub-panel

In the intake regimes sub-panel, you can select:

- the route of intake: inhalation, ingestion, injection, or vapor.
- the mode of intake: acute or chronological
- the start time of intake.

In the units sub-panel, you can specify:

- date - to select start and end times
- time - to display start and end as a fraction of a day
- intake - the unit of activity
- dose – the unit of dose

Intake (IR 1) Bq/d

Indicator Nuclide [Redacted]

Number of Associated Radionuclides: #

Half Life: Unknown #

Associated Radionuclides

Figure 37. The intake and radionuclide sub-panel

If you know the intake you can enter it in the Intake sub-panel. In the radionuclide sub-panel, select the indicator nuclide and then select the isotope from the drop-down list.

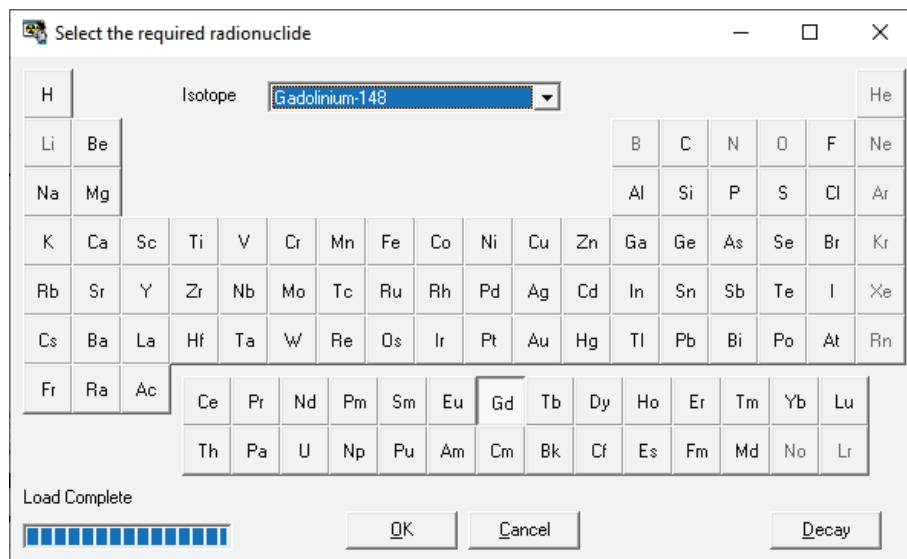


Figure 38. The periodic table from where you select the radionuclide of interest.



Figure 39. In the lower part of the main screen there are two sub-panels, model parameters and calculations.

Model parameters sub-panel

If the buttons are highlighted it means that it is necessary for you to select the parameters before making calculations.

If inhalation is selected as the route of intake the parameters for

- Deposition
- Particle transport
- Absorption
- GI-tract

will be highlighted.

In the sub-panels you can use ICRP 66 parameters values by clicking on the “load icrp defaults”-button or define our own (user defined).

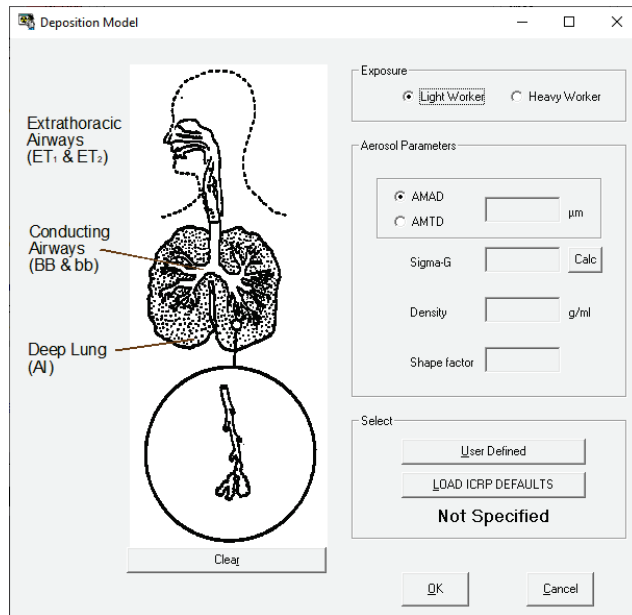


Figure 40. The deposition model.

In the deposition model you must define the aerosol parameters and the worker category, light or heavy worker.

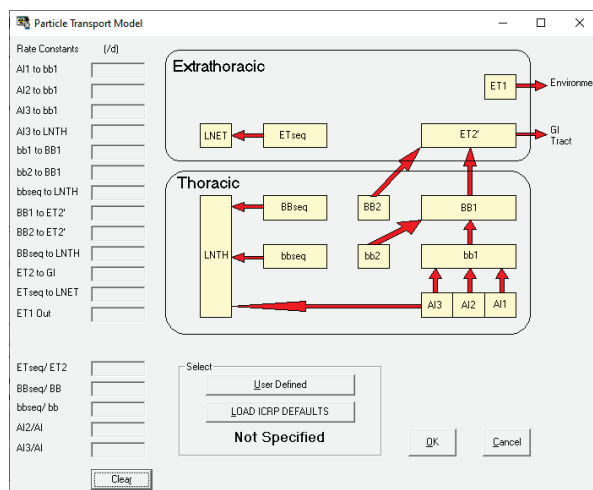


Figure 41. Particle transport model

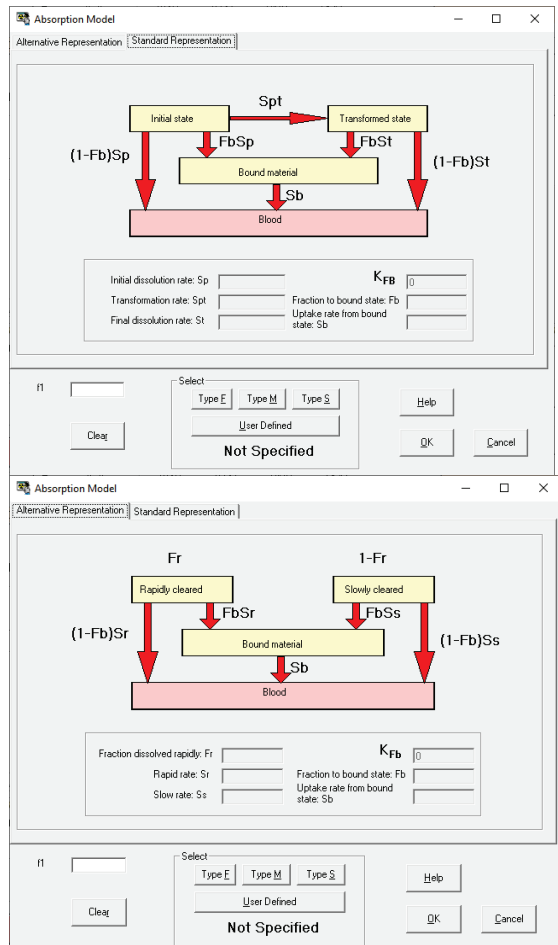


Figure 42. Absorption model.

In the absorption model you can use standard representation or alternative representation.

The standard representation is useful in cases where the overall absorption rate increases with time. Type in the gut absorption fraction (f_1) or click the button “help” to get information about chemical forms and absorption type (from ICRP). You can then choose ICRP default or use your own parameter values.

Parameters:

- S_p - initial dissolution rate [d^{-1}]
- S_{pt} - transformation rate [d^{-1}]
- S_t - final dissolution rate [d^{-1}]
- F_b – Fraction to bound state
- S_b - uptake rate from bound state

The alternative representation is useful for general situation where the overall absorption rate decreases with time. Type in the gut absorption fraction (f_1) or click the button “help” to get information about chemical forms and absorption type (from ICRP). You can then choose ICRP default or use your own parameter values.

Parameters:

- f_1 – fraction dissolved rapidly
- s_r – rapid rate [d^{-1}]
- s_s – slow rate [d^{-1}]
- f_b – fraction to bound state
- s_b – uptake rate from bound state [d^{-1}]

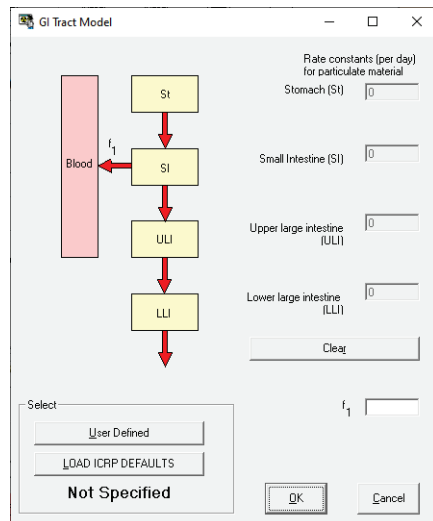


Figure 43. GI-tract model

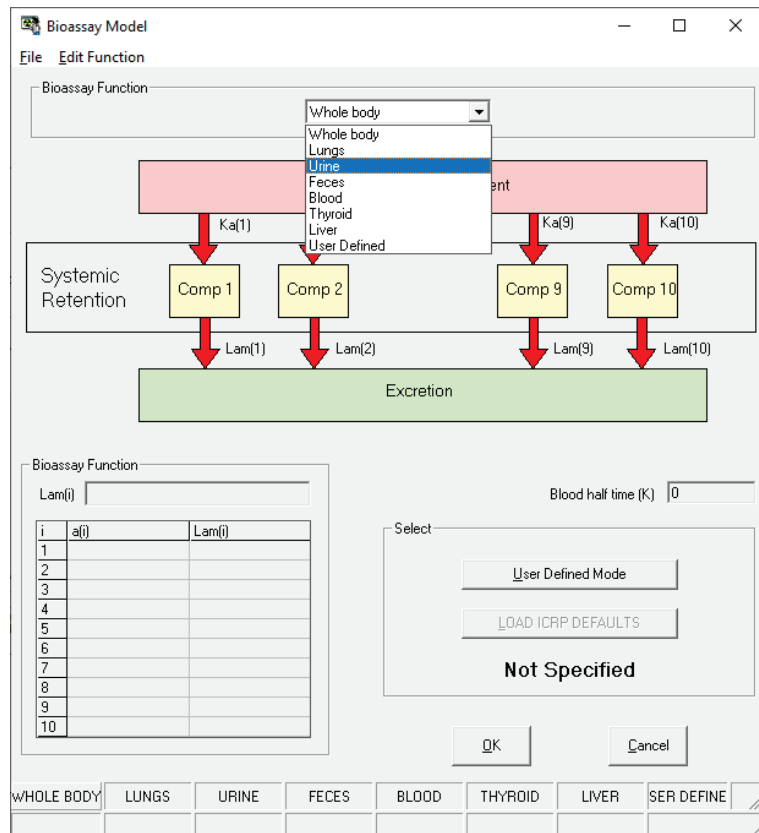


Figure 44. The bioassay model panel.

Select the bioassay function from the drop-down list and then click on “Load ICRP defaults” or “user defined” button. If you choose “lungs” the sentence “No systemic model is required for the lungs” will show up, because lung retention is calculated automatically by using the ICRP 66 respiratory tract model HRTM).

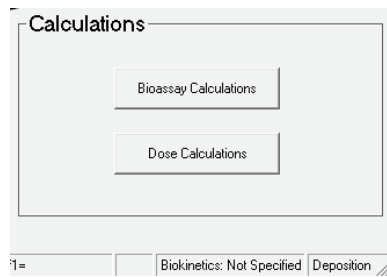


Figure 45. Calculations sub-panel

If you click at the bioassay calculations button you can estimate the amount of intake and/or predict bioassay quantities. The dose calculation button opens the dose calculation screen, and you can calculate doses.

Bioassay calculations

The arrow on the screen indicates whether the bioassay data shown in the table (to the right) are measured (blue arrow) or predicted (green arrow). The same colour codes are used in the table.

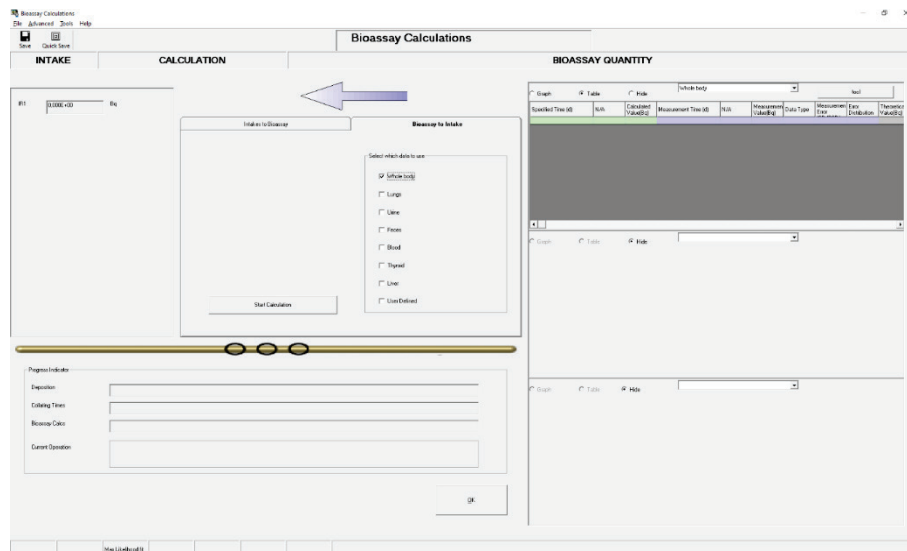


Figure 46 Bioassay calculation screen and the tab bioassay to intake (blue arrow).

Under the tab bioassay to intakes choose bioassay from the list and fill in the bioassay measurement values in the blue column in the table. Perform a calculation and then create a graph.

Figure 47. Bioassay calculations screen and the tab intake to bioassay (green arrow).

Under the tab Intake to bioassay:

Fill in the number of times you want to predict the bioassay quantity (max 200 times), specify start and end time/day.

If the bioassays are urine or faeces, you must also fill in sample collection period.

Figure 48. The dose calculation screen

Figure 49. The dose calculation sub-panel

The highlighted tab indicates that you must fill in data.

Figure 50. The WR tab

In the WR tab you must select the radiation weighting factors.

Figure 51. The WT tab (left side). Options for tissue weight factors (right side).

In the tab WT you must select the tissue weighting factors. Click on the button and fill in values according to latest ICRP-data. To start the calculations, return to calculation tabs and click on calculation button. The effective dose shown in the calculation tab and equivalent dose or effective dos (depending on choice) in the table to the right.

The screenshot shows a software window titled "DOSE". At the top, there are three radio buttons: "Equiv" (selected), "Eff", and "Indicator Nuclide". Below this is a table with columns: "Target Organs", "Equivalent Dose (Sv) IR(1)", "Equivalent Dose (Sv) Total", and two empty columns. The rows list various organs with their corresponding calculated doses. The entire table has a light orange background.

Target Organs	Equivalent Dose (Sv) IR(1)	Equivalent Dose (Sv) Total		
Adrenals	9,91E-06	9,91E-06		
Urinary Bladder	9,93E-06	9,93E-06		
Brain	9,91E-06	9,91E-06		
Breast	9,91E-06	9,91E-06		
Gall Bladder	9,91E-06	9,91E-06		
Heart Wall	9,91E-06	9,91E-06		

Figure 52. The results of the dose calculations

A report can be created that contains all or a selection of the results.

Choose what the report should show from the report panel.

The screenshot shows a "Report" dialog box. At the top, it says "Report will be saved in: e:\Append\Default RPT" with a "Browse" button. The main area is divided into sections:

- Administrative Details:** Fields for Name (First: Etan, Middle: , Last: Etson), Personal Details (Date of Birth: 1911-11-11, Sex: Male, Employee ID: 11, Employee SSN:), and Case Details (Case ID: 1, File Name Prefix: , Case Flag:).
- Other Details:** Description of Case (Intake of Po-210) and Date of Assessment (2006-12-20).
- Include in Report:** A dropdown menu set to "Complete Details" with buttons for "Select All" and "Clear All". Other checkboxes include "Administrative Details", "Software Version", and "Parameter Filename".
- Input Information:** Includes checkboxes for "Indicator Radionuclide", "Associated Radionuclides", "Intake Regimes", "Model Parameters", "Measurement Data", "Radia'n Weighting Factors", and "Tissue Weighting Factors".
- Results of Calculations:** Includes checkboxes for "Intakes", "Bioassay Results", "Indicator Radionuclide", "Equivalent Doses", "Associated Radionuclides", "Equivalent Doses", "Effective Doses", "Calendar Year Doses", and "Effective Doses".
- Actions:** Buttons for "Create Report", "View Report", and "Print Report".

Figure 53. The report panel.

8.4. CT scans

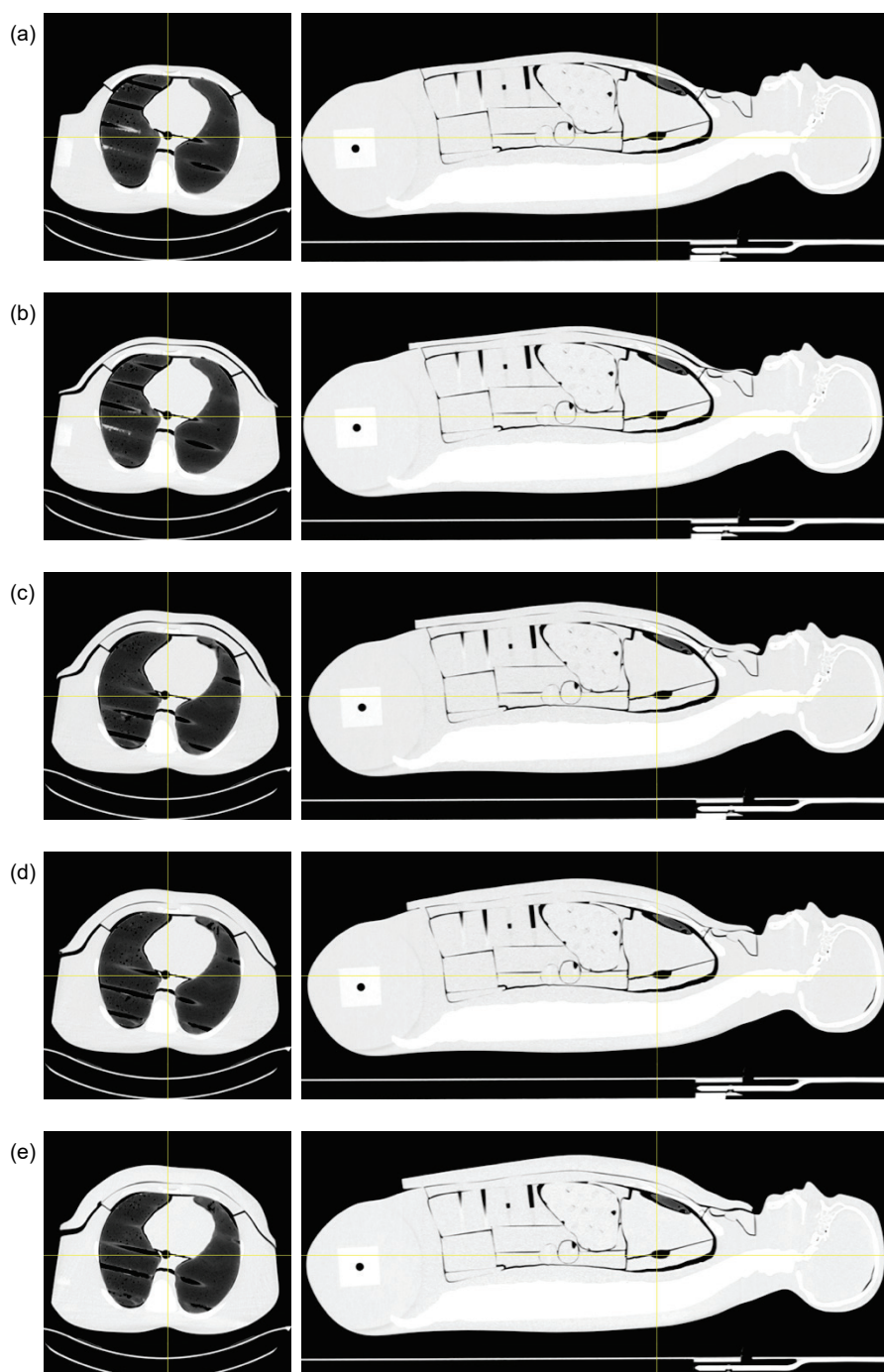


Figure 54. Axial and sagittal views of the phantom reconstructed at 70 keV. Fat layer (a) 0, (b) 1, (c) 2, (d) 3, (e) 4 was positioned on top of the phantom.

8.5. Minimum detectable activity

8.5.1. Urine

CED=1 mSv									
Nuclide	γ -energy [keV]	Day 1		Day 2		Day 3		Day 4	
		urine [Bq]	MDA [Bq]						
^{89}W	686	49595	8.4	2604	2.6	114	1.2	17.8	0.80
^{87}Rb	126	1.4	51.5	3.5	12.5	3.6	3.9	2.5	2.1
^{87}La	1189	0.19	7.3	0.44	2.9	0.42	1.5	0.37	1.0
^{89}Yb	326	0.09	9.9	0.21	2.3	0.22	0.60	0.20	0.32
^{87}Lu	426	0.09	11.2	0.21	2.6	0.22	0.63	0.20	0.13
^{87}Ta	108	0.25	52.2	0.51	12.7	0.43	4.0	0.32	0.10
^{87}Ta	246	0.25	27.8	0.51	6.6	0.43	1.7	0.32	0.11
^{87}Lu	172	20.0	34.5	16.1	8.3	6.9	2.5	3.1	1.6
^{89}Yb	198	24.3	17.0	19.2	4.1	8.1	1.1	3.7	0.70
^{87}Lu	740	25.5	3.9	18.9	1.5	7.5	0.81	3.1	0.56
^{87}Lu	1094	14.0	2.6	10.2	1.0	3.9	0.51	1.6	0.35
^{144}Gd	115	1.7	13.1	1.35	3.2	0.59	0.99	0.28	0.63
^{144}Gd	116	1.7	13.1	1.35	3.2	0.59	0.99	0.28	0.63
^{144}Eu	747	0.23	1.9	0.35	0.72	0.21	0.40	0.13	0.07
^{144}Gd	103	1.4	26.0	1.2	6.8	0.52	2.1	0.25	0.66
CED=20 mSv									
Nuclide	γ -energy [keV]	Day 1		Day 2		Day 3		Day 4	
		urine [Bq]	MDA [Bq]						
^{89}W	686	99183	27.3	52081	11.3	2278	5.2	356	3.5
^{87}Rb	126	28.9	230	69.8	55.8	71.4	17.2	66.6	10.9
^{87}La	1189	3.87	32.2	8.9	12.9	8.5	6.5	7.3	4.4
^{89}Yb	326	1.8	44.2	4.3	10.4	4.4	2.7	4.1	2.6
^{87}Lu	426	1.8	49.9	4.3	11.7	4.4	2.8	4.1	2.6
^{87}Ta	108	5.1	233	10.2	56.7	8.5	17.7	6.5	11.3
^{87}Ta	246	5.1	124	10.2	29.3	8.5	7.5	6.5	4.0
^{87}Lu	172	400	154	321	138	10.9	62.3	6.9	42.7
^{89}Yb	198	486	76.1	384	18.1	163	5.0	73.1	5.0
^{87}Lu	740	511	17.4	378	6.5	149	3.6	62.1	2.4
^{87}Lu	1094	280	11.4	203	4.5	78.7	2.2	32.1	1.5
^{144}Gd	115	33.6	58.7	27.0	14.2	11.8	4.4	5.6	4.8
^{144}Gd	116	33.6	58.7	27.0	14.2	11.8	4.4	5.6	4.8
^{144}Eu	747	4.7	8.2	7.0	3.2	4.3	1.8	2.5	1.3
^{144}Gd	103	28.8	125	23.4	30.4	10.3	9.5	4.9	6.1

CHD-20 mSv, D1, P2									
Nuclide	γ -energy [keV]	Day 0	Day 1	Day 2	Day 3	Day 4	Day 5	Day 6	Day 7
^{89}W	696	2.7E-06	1.1E-07	4.1E-07	4.6E-07	5.2E-07	4.1E-07	1.1E-07	4.1E-07
^{75}Fe	126	1.7E-04	1.2E-03	9.1E-03	7.7E-02	5.2E-02	4.8E-02	4.1E-02	3.9E-02
^{71}Hf	1189	3.0E-04	1.4E-03	2.1E-03	2.6E-03	5.0E-02	1.1E-04	7.7E-02	5.1E-02
^{89}Ta	126	1.0E-03	6.3E-02	7.3E-02	1.3E-02	6.9E-02	1.1E-02	6.5E-02	1.1E-02
^{89}Yb	426	1.0E-03	7.4E-02	7.3E-02	1.4E-02	7.0E-02	1.2E-02	6.8E-02	1.1E-02
^{71}Ta	98	4.4E-04	3.2E-03	3.4E-03	1.0E-03	2.9E-04	5.0E-02	8.0E-02	4.8E-02
^{89}Ta	246	4.4E-04	1.7E-03	3.4E-03	3.8E-02	2.9E-04	3.4E-02	2.2E-04	1.2E-04
^{73}Lu	172	2.7E-04	2.3E-03	2.1E-03	6.2E-02	2.0E-04	1.9E-03	6.1E-02	1.7E-02
^{89}Yb	98	2.0E-04	1.1E-03	2.2E-03	3.0E-02	2.0E-04	2.8E-02	2.7E-02	1.6E-04
^{71}Lu	740	3.0E-04	6.1E-02	2.7E-02	3.7E-02	2.3E-04	2.1E-02	1.9E-02	2.7E-02
^{71}Lu	1094	2.1E-04	4.5E-02	1.5E-02	1.1E-02	7.0E-02	1.1E-04	1.1E-02	1.1E-02
^{89}Cd	115	3.9E-03	8.3E-02	2.0E-02	2.0E-03	5.5E-02	2.1E-02	2.6E-03	1.0E-02
^{89}Yb	116	3.9E-03	8.2E-02	2.0E-02	2.0E-03	5.5E-02	2.1E-02	2.6E-03	1.0E-02
^{89}Lu	747	0.0E+00	3.3E-02	4.2E-02	1.9E-02	7.2E-02	1.6E-02	1.2E-02	1.2E-02
^{89}Cd	913	3.3E-03	1.7E-03	2.6E-03	5.4E-02	2.4E-03	4.6E-02	2.8E-02	1.0E-03
CHD-20 mSv, D2, P2									
^{89}W	696	2.7E-06	8.3E-02	1.4E-07	4.6E-02	5.2E-21	4.1E-02	2.4E-34	3.9E-02
^{71}Hf	126	1.7E-04	2.8E-03	1.2E-04	8.0E-02	1.2E-04	7.3E-02	1.1E-04	1.1E-02
^{89}Ta	1189	3.0E-04	5.2E-03	2.6E-04	4.9E-02	7.0E-02	5.6E-02	5.2E-02	5.0E-02
^{89}Yb	126	1.0E-03	5.3E-02	7.3E-02	1.4E-02	7.0E-02	9.2E-01	6.4E-02	6.1E-01
^{71}Ta	426	1.0E-03	6.2E-02	7.3E-02	1.2E-02	7.0E-02	6.9E-02	6.5E-02	6.2E-02
^{89}Ta	98	4.4E-04	2.8E-03	3.4E-03	9.0E-02	2.5E-04	7.6E-02	1.2E-04	1.2E-04
^{73}Lu	246	4.4E-04	1.5E-03	3.4E-03	2.5E-02	2.9E-04	2.0E-02	2.2E-02	4.4E-02
^{71}Lu	172	2.7E-04	2.0E-03	2.1E-04	5.8E-02	2.0E-03	5.3E-02	1.7E-04	1.7E-04
^{89}Yb	98	2.0E-04	3.0E-02	2.0E-02	6.2E-02	2.0E-04	2.4E-02	1.9E-02	2.5E-03
^{71}Lu	740	3.0E-04	5.6E-02	2.2E-02	2.3E-03	1.9E-04	2.3E-02	1.7E-04	1.7E-02
^{71}Lu	1094	2.1E-04	3.7E-02	2.0E-02	1.0E-02	7.0E-02	1.1E-04	1.1E-02	1.1E-02
^{89}Cd	115	3.9E-03	8.3E-02	2.0E-02	2.0E-03	5.5E-02	2.1E-02	2.6E-03	1.0E-02
^{89}Yb	116	3.9E-03	8.2E-02	2.0E-02	2.0E-03	5.5E-02	2.1E-02	2.6E-03	1.0E-02
^{89}Lu	747	0.0E+00	3.3E-02	4.2E-02	1.9E-02	7.2E-02	1.6E-02	1.2E-02	1.2E-02
^{89}Cd	913	3.3E-03	1.5E-03	2.6E-03	5.4E-02	2.4E-03	4.6E-02	2.8E-02	1.0E-03
CHD-20 mSv, D3, P2									
^{89}W	696	2.7E-06	8.3E-02	1.4E-07	4.6E-02	5.2E-21	4.1E-02	2.4E-34	3.9E-02
^{71}Hf	126	1.7E-04	2.8E-03	1.2E-04	8.0E-02	1.2E-04	7.3E-02	1.1E-04	1.1E-02
^{89}Ta	1189	3.0E-04	5.2E-03	2.6E-04	4.9E-02	7.0E-02	5.6E-02	5.2E-02	5.0E-02
^{89}Yb	126	1.0E-03	5.3E-02	7.3E-02	1.4E-02	7.0E-02	9.2E-01	6.4E-02	6.1E-01
^{71}Ta	426	1.0E-03	6.2E-02	7.3E-02	1.2E-02	7.0E-02	6.9E-02	6.5E-02	6.2E-02
^{89}Ta	98	4.4E-04	2.8E-03	3.4E-03	9.0E-02	2.5E-04	7.6E-02	1.2E-04	1.2E-04
^{73}Lu	246	4.4E-04	1.5E-03	3.4E-03	2.5E-02	2.9E-04	2.0E-02	2.2E-02	4.4E-02
^{71}Lu	172	2.7E-04	2.0E-03	2.1E-04	5.8E-02	2.0E-03	5.3E-02	1.7E-04	1.7E-04
^{89}Yb	98	2.0E-04	3.0E-02	2.0E-02	6.2E-02	2.0E-04	2.4E-02	1.9E-02	2.5E-03
^{71}Lu	740	3.0E-04	5.6E-02	2.2E-02	2.3E-03	1.9E-04	2.3E-02	1.7E-04	1.7E-02
^{71}Lu	1094	2.1E-04	3.7E-02	2.0E-02	1.0E-02	7.0E-02	1.1E-04	1.1E-02	1.1E-02
^{89}Cd	115	3.9E-03	8.3E-02	2.0E-02	2.0E-03	5.5E-02	2.1E-02	2.6E-03	1.0E-02
^{89}Yb	116	3.9E-03	8.2E-02	2.0E-02	2.0E-03	5.5E-02	2.1E-02	2.6E-03	1.0E-02
^{89}Lu	747	0.0E+00	3.3E-02	4.2E-02	1.9E-02	7.2E-02	1.6E-02	1.2E-02	1.2E-02
^{89}Cd	913	3.3E-03	1.5E-03	2.6E-03	5.4E-02	2.4E-03	4.6E-02	2.8E-02	1.0E-03
CHD-20 mSv, D4, P2									
^{89}W	696	2.7E-06	1.1E-06	4.1E-07	4.6E-02	5.2E-21	4.1E-02	2.4E-34	3.9E-02
^{71}Hf	126	1.7E-04	1.6E-03	1.2E-04	8.0E-02	1.2E-04	7.3E-02	1.1E-04	1.1E-02
^{89}Ta	1189	3.0E-04	1.6E-03	1.2E-04	4.9E-02	7.0E-02	5.6E-02	5.2E-02	5.0E-02
^{89}Yb	126	1.0E-03	8.2E-02	7.3E-02	1.6E-02	7.0E-02	9.2E-01	6.4E-02	6.1E-01
^{71}Ta	426	1.0E-03	9.3E-03	7.3E-02	1.8E-02	7.0E-02	6.9E-02	6.5E-02	6.2E-02
^{89}Ta	98	4.4E-04	4.5E-03	3.4E-04	1.3E-03	2.5E-04	1.2E-03	1.2E-04	1.2E-04
^{73}Lu	246	4.4E-04	2.3E-03	3.4E-04	5.0E-02	2.9E-04	4.3E-02	2.2E-04	1.2E-04
^{71}Lu	172	2.7E-04	3.1E-03	2.1E-04	9.2E-02	2.0E-04	8.1E-02	1.7E-04	1.7E-02
^{89}Yb	98	2.0E-04	1.5E-03	2.2E-04	6.9E-02	1.1E-04	3.6E-02	2.1E-04	2.1E-04
^{71}Lu	740	3.0E-04	3.0E-02	2.0E-02	4.0E-02	2.1E-04	3.7E-02	1.8E-02	1.8E-02
^{89}Yb	740	3.0E-04	2.2E-02	2.7E-02	7.0E-02	1.1E-04	3.7E-02	1.8E-02	1.8E-02
^{89}Lu	747	0.0E+00	4.0E-02	4.2E-02	2.2E-02	7.0E-02	2.0E-02	1.7E-02	1.7E-02
^{89}Cd	913	3.3E-03	2.4E-03	3.0E-03	5.3E-02	2.0E-03	3.1E-02	2.0E-02	1.0E-03
^{89}Yb	913	3.3E-03	2.4E-03	3.0E-03	5.3E-02	2.0E-03	3.1E-02	2.0E-02	1.0E-03



The Swedish Radiation Safety Authority has a comprehensive responsibility to ensure that society is safe from the effects of radiation. The Authority works from the effects of radiation. The Authority works to achieve radiation safety in a number of areas: nuclear power, medical care as well as commercial products and services. The Authority also works to achieve protection from natural radiation and to increase the level of radiation safety internationally.

The Swedish Radiation Safety Authority works proactively and presentively to protect people and the environment from the harmful effects of radiation, now and in the future. The Authority issues regulations and supervises compliance, while also supporting research, providing training and information, and issuing advice. Often, activities involving radiation require licences issued by the Authority. The Swedish Radiation Safety Authority maintains emergency preparedness around the clock with the aim of limiting the aftermath of radiation accidents and the unintentional spreading of radioactive substances. The Authority participates in international co-operation in order to promote radiation safety and finances projects aiming to raise the level of radiation safety in certain Eastern European countries.

The Authority reports to the Ministry of the Environment and has around 300 employees with competencies in the fields of engineering, natural and behavioral sciences, law, economics and communications. We have received quality, environmental and working environment certification.

Publikationer utgivna av Strålsäkerhetsmyndigheten kan laddas ned via strålsäkerhetsmyndigheten.se eller beställas genom att skicka e-post till registrator@ssm.se om du vill ha broschyren i alternativt format, som punktskrift eller daisy.

Strålsäkerhetsmyndigheten
Swedish Radiation Safety Authority
SE-171 16 Stockholm
Phone: 08-799 40 00
Web: ssm.se
E-mail: registrator@ssm.se